NANYANG TECHNOLOGICAL UNIVERSITY

COPPER INCORPORATED TITANIUM DIOXIDE PHOTOCATALYST FOR HYDROGEN PRODUCTION

XU SHIPING

SCHOOL OF CIVIL AND ENVIRONMENTAL ENGINEERING

2012

COPPER INCORPORATED TITANIUM DIOXIDE PHOTOCATALYST FOR HYDROGEN PRODUCTION

XU SHIPING

School of Civil and Environmental Engineering

A thesis submitted to the Nanyang Technological University in partial fulfillment of the requirement for the degree of Doctor of Philosophy

2012

ACKNOWLEDGEMENTS

First of all, I would like to express my sincere gratitude to my supervisor, Associate Professor Darren Delai Sun, for his guidance, support, patience and encouragement. Without his prudent guidance and invaluable advice, this thesis could not be completed smoothly.

My special thanks to all Sun's group members for their constant guidance, encouragement and valuable opinions. I am also grateful to all fellow graduate students from School of Civil and Environmental Engineering for their companionship, discussion and fun that made my research life meaningful and colorful.

My great thanks to the technicians in the Environmental Laboratory, especially Mrs. Phang-Tay Beng Choo and Mr. Tan Han Khiang, for their valuable advice, technical knowledge and kind assistance in the experiment preparation and instrument operation.

I am most grateful to School of Civil and Environmental Engineering, Nanyang Technological University, by providing the PhD scholarship, facilities and heartfelt assistance.

Last but not least, I dedicate all my achievements to my family members, whom I know I can always fall back on during both good and bad time. Their love, support and encouragement are the most important motivation in all my pursuits.

TABLE OF CONTENTS

ACKNOWLEDGEMENTS I
TABLE OF CONTENTS II
ABSTRACT VI
LIST OF TABLES VIII
LIST OF FIGURES IX
LIST OF PUBLICATIONS XIV

CHAPTER 1
INTRODUCTION 1

1.1 Motivation 1
1.2 Objectives and Significance 4
1.3 Organization of Thesis 6

CHAPTER 2
LITERATURE REVIEW 8

2.1 Principles, Mechanisms of Photocatalysis 8
2.1.1 Electronic processes 8
2.1.2 Photocatalysis on TiO_2 17
2.2 H_2 Production Using TiO_2 27
2.2.1 Methods to promote H_2 production 28
2.2.2 Cu incorporated TiO_2 49
2.2.3 Factors influencing photocatalytic H_2 production 54
2.2.4 Summary 56

CHAPTER 3
OPTIMAL OPERATION CONDITIONS AND ACTIVITY MAINTENANCE OF Cu-TiO_2 IN PHOTOCATALYTIC H_2 PRODUCTION 57

3.1 Introduction 57

3.2 Experimental 58

3.2.1 Preparation of Cu-TiO_2 photocatalyst 58

3.2.2 Characterization of Cu-TiO_2 photocatalyst 58

3.2.3 Photocatalytic reaction system 59

3.2.4 Optimization of operation conditions 60

3.2.5 H_2 detection 61

3.3 Results and Discussion 62

3.3.1 Characterization of as-prepared Cu-TiO_2 62

3.3.2 Photocatalytic activity of as-prepared Cu-TiO_2 65

3.3.3 Optimization of operation conditions for Cu-TiO_2 73

3.3.4 Maintenance of H_2 generation activity of Cu-TiO_2 80

3.3.5 Characterization of Cu-TiO_2 after H_2 generation 83

3.4 Conclusion 86

CHAPTER 4

EFFECT OF FABRICATION METHOD OF Cu-TiO_2 ON PHOTOCATALYTIC H_2 PRODUCTION 88

4.1 Introduction 88

4.2 Experimental 89

4.2.1 Preparation of Cu-TiO_2 photocatalysts 89

4.2.2 Characterization of Cu-TiO_2 photocatalysts 91

4.2.3 Photocatalytic reaction 92

4.3 Results and Discussion 92

4.3.1 Characterization of Cu-TiO_2 92

4.3.2 Photocatalytic H_2 production over Cu-TiO_2 102

4.4 Conclusion 109

CHAPTER 5

STUDY OF HIGHLY EFFICIENT TiO_2 NANOTUBE BASED Cu-TiO_2 PHOTOCATALYST FOR H_2 PRODUCTION 111

5.1 Introduction 111

5.2 Experimental 113

5.2.1 Preparation of TNT and Cu-TNT 113

5.2.2 Characterization of TNT and Cu-TNT 114

5.2.3 Photocatalytic reaction 115

5.3 Results and Discussion 115

5.3.1 Characterization of photocatalysts 115

5.3.2 Photocatalytic H_2 production 129

5.4 Conclusion 133

CHAPTER 6

SIMULTANEOUS Cu^{2+} REMOVAL AND H_2 PRODUCTION OVER TiO_2 NANOTUBE FROM WATER 134

6.1 Introduction 134

6.2 Experimental 137

6.2.1 Synthesis and characterization of TNT 137

6.2.2 Photocatalytic reaction 137

6.3 Results and Discussion 138

6.3.1 Reactions under various initial Cu^{2+} concentrations 138

6.3.2 Effect of co-existing ions on photocatalytic reactions 146

6.3.3 Characterization of photocatalyst after reaction 151

6.4 Conclusion 155

CHAPTER 7

CONCLUSIONS AND RECOMMENDATIONS 157

7.1 Conclusions 157

7.2 Recommendations 160

REFERENCES 162

ABSTRACT

Recently, copper (Cu) incorporated TiO_2 (Cu-TiO_2) was reported to be a cost-effective photocatalyst which possessed H_2 generation activity using sacrificial reagents in water. Nevertheless, very few studies have been conducted to investigate the utilization of Cu-TiO_2 for H_2 production while the mechanisms remained unclear, even the reported H_2 evolution rates were low for practical application. Therefore, this study aims to fabricate the highly efficient Cu-TiO_2 photocatalyst for H_2 production and investigate the optimal H_2 generation conditions.

In the first phase of this study, Cu-TiO_2 prepared with well recognized P25 as TiO_2 support was confirmed with big potential for photocatalytic H_2 production. Effect of operation conditions on H_2 generation and maintenance of Cu-TiO_2 activity level in intensive photocatalytic reaction were investigated as well. It was found that Cu content in the photocatalyst was crucial for photocatalytic H_2 generation, and an optimum Cu content at 9.1 mol% was discovered. Moreover, H_2 generation rate could be accelerated by increasing sacrificial reagent concentration, and high activity of Cu-TiO_2 could be maintained over a pH range of 5.8-10.0. However, photocatalytic H_2 generation activity was suppressed under long irradiation time.

Fabrication method is very important to achieve high activity of the Cu-TiO_2 photocatalyst, as it determines the morphology, crystal structure, crystal size, BET surface area etc., of the final product. Based on the optimal operation conditions obtained in the first phase of this study, effects of Cu-TiO_2 fabrication method were further investigated by highlighting four well established metallization methods. It was found that the four fabrication methods led to different chemical states of Cu, as well as different distribution ratio of Cu between surface and bulk phases of the

photocatalyst. Both factors were proved to affect photocatalytic H_2 generation rate.

To further enhance the activity of P25 based Cu-TiO_2, the novel TiO_2 nanotube (TNT) was employed as TiO_2 support to form a new Cu-TNT photocatalyst. It was found that TNT significantly improved the activity of Cu-TiO_2; as a result, the H_2 generation rate of Cu-TNT was much higher than the benchmark P25 based photocatalysts, and even superior to some Pt/Ni incorporated TNT. The high activity of Cu-TNT was mainly attributed to the unique one-dimensional (1-D) tubular structure, large BET surface area and high dispersion of Cu component. In addition, compared to wet impregnation method, adsorption-calcination process, which was exclusive for TNT sample, was superior for the fabrication of active Cu-TNT, since it was favorable to produce photocatalyst with large quantity of highly dispersed Cu components.

In view of the fabrication mechanisms of Cu-TiO_2, Cu^{2+} removal from wastewater with simultaneous H_2 production was investigated to explore its potential applications especially for the benefit of concurrent wastewater treatment and energy production. It was found that, under UV irradiation, Cu^{2+} over a wide concentration range of 8-800 ppm, could be removed rapidly from water with the presence of TNT. The removed Cu^{2+} was then combined with TiO_2 to produce efficient Cu-TiO_2 photocatalyst for H_2 production. Initial Cu^{2+}/Ti ratio in solution was a main factor affecting H_2 generation rate of the in-situ fabricated Cu-TiO_2. In addition, reduction process of Cu^{2+} was also a critical factor in governing H_2 evolution, while the effects became more complicated under higher initial Cu^{2+}/Ti ratio conditions.

LIST OF TABLES

Table 2.1 Band gap energies and corresponding wavelengths of light for various semiconductors (Stumm, 1992). 10

Table 2.2 General mechanism for heterogeneous photocatalysis on TiO_2 (Hoffmann et al., 1995). 22

Table 2.3 Frequently used dyes and absorption wavelength maxima λ_{max} (Jana, 2000). 47

Table 3.1 Comparison of H_2 production over various Metal-TiO_2 69

Table 4.1 Summary of surface elemental composition, Cu content and BET specific surface area of as-prepared Cu-TiO_2 photocatalyst. 97

Table 5.1 Summary of elemental compositions detected by EDS and BET surface area of photocatalysts. 117

Table 5.2 Summary of surface elemental compositions of photocatalysts detected by XPS. 126

LIST OF FIGURES

Figure 2.1 Diagram of electronic band structure of metal, semiconductor and insulator. 8

Figure 2.2 Schematic de-excitation pathways for electrons and holes in photocatalyst (Linsebigler et al., 1995). 11

Figure 2.3 Band edge positions for various semiconductors in aqueous electrolyte at pH=1 (Wu, 2005). 13

Figure 2.4 Band positions of TiO_2 (anatase) together with the redox potentials of certain metal ions (1 M) at different pH (Chen et al., 2001). 14

Figure 2.5 Electronic states in semiconductor with different particle size (LUMO: lowest unoccupied molecular orbital, HOMO: highest occupied molecular orbital) (Hoffmann et al., 1995). 15

Figure 2.6 Schematics of electric charges redistribution in semiconductor-metal interface (Linsebigler et al., 1995). 17

Figure 2.7 Crystal structure of anatase and rutile. 18

Figure 2.8 Comparison of band gap and band edge positions of anatase and rutile (Wu, 2005). 19

Figure 2.9 Secondary reactions in photocatalysis process over TiO_2 (Hoffmann et al. 1995). 24

Figure 2.10 Schematic diagram of inner and outer-irradiation photocatalytic reactor 25

Figure 2.11 Conceptual scheme of water splitting systems: (a) two-step system and (b) one-step system (Abe et al., 2005). 31

Figure 2.12 Forward and backward reactions in the two-step water-splitting system (Abe et al., 2005). 32

Figure 2.13 Schematics of the photocatalytic reaction cell employing Fe^{3+}/Br^{-} as redox mediators (Fujihara et al., 1998). 33

Figure 2.14 Schematics of charge separation in composite semiconductors (Ni et al., 2007). 40

Figure 2.15 Schematic charge transfer in Pt-$TiO_{2-x}N_x$-WO_3 composite photocatalyst (Yang et al., 2006)..... 44

Figure 2.16 Schematic diagram of band gap structure of CM-n-TiO_2 (Xu et al., 2007). 45

Figure 2.17 Mechanism of dye-sensitized photocatalytic H_2 generation under visible light irradiation (Ni et al., 2007). 46

Figure 3.1 Schematic diagram of setup for photocatalytic reaction..... 60

Figure 3.2 GC spectrum of gas produced from the photocatalytic reaction. 61

Figure 3.3 XRD patterns of Cu-TiO_2 with variation of Cu content (a-l: 0, 0.1, 0.5, 1.0, 4.8, 7.0, 9.1, 11.1, 13.0, 28.6, 60.0, and 100 mol%). 63

Figure 3.4 TEM image of 9.1 mol% Cu-TiO_2..... 64

Figure 3.5 SEM image and elemental mapping of 9.1 mol% Cu-TiO_2. 64

Figure 3.6 Effect of Cu content (mol%) in Cu-TiO_2 photocatalyst on H_2 generation (photocatalyst: 1 g L^{-1}; methanol: 10 volume%). 65

Figure 3.7 Dependence of H_2 generation rate on Cu content (photocatalyst: 1 g L^{-1}; methanol: 10 volume%). 66

Figure 3.8 Effect of combination mode between Cu component and TiO_2 on H_2 generation (photocatalyst: 1 g L^{-1}; methanol: 10 volume%). 72

Figure 3.9 Effect of initial methanol concentration (volume%) on H_2 generation (photocatalyst: 9.1 mol% Cu-TiO_2, 1 g/L). 74

Figure 3.10 Dependence of H_2 generation rate on initial methanol concentration (photocatalyst: 9.1 mol% Cu-TiO_2, 1 g L^{-1}). Inset: log r~log C, r: rate, C: concentration. 74

Figure 3.11 Effect of solution pH on H_2 generation (photocatalyst: 9.1 mol% Cu-TiO_2, 1 g L^{-1}; methanol: 10 volume%). 76

Figure 3.12 Cu leaching (%) over pH range of 1-13 in 5 h soak (photocatalyst: 9.1 mol% Cu-TiO_2, 1 g L^{-1}). 77

Figure 3.13 Effect of photocatalyst dosage (g L^{-1}) on H_2 generation (photocatalyst: 9.1 mol% Cu-TiO_2; methanol: 10 volume%)..... 79

Figure 3.14 Dependence of H_2 evolution rate on photocatalyst dosage (photocatalyst: 9.1 mol% Cu-TiO_2; methanol: 10 volume%). 79

Figure 3.15 Time course of H_2 evolution under 10 h irradiation. 81

Figure 3.16 Recovery of H_2 generation activity. 81

Figure 3.17 XRD patterns of Cu-TiO_2 after H_2 generation (a: 9.1 mol% for 1 h; b: 9.1 mol% for 10 h; c: 28.6 mol% for 1 h). 84

Figure 3.18 SEM image and elemental mapping of 9.1 mol% Cu-TiO_2 after H_2 generation for 1 h. 85

Figure 3.19 TEM image of 9.1 mol% Cu-TiO_2 after H_2 generation for 1 h..... 86

Figure 4.1 XRD patterns of as-prepared Cu-TiO_2 photocatalysts. (Pattern of PD sample was obtained after reaction due to the limitation of in-situ fabrication.) ... 93

Figure 4.2 (a) XPS survey spectrum of SG photocatalyst; (b) High-resolution Cu 2p spectrum; (c) High-resolution Ti 2p spectrum. 94

Figure 4.3 TEM images of Cu-TiO_2 photocatalysts (a: WI; b: SG). 96

Figure 4.4 SEM images of Cu-TiO_2 photocatalysts (a: SG; b: NR; c: P25). 99

Figure 4.5 Pore size distribution of Cu-TiO_2 photocatalysts. 100

Figure 4.6 UV-visible absorption spectra of Cu-TiO_2 photocatalysts (a: WI; b: PD; c: NR; d: SG; e: SG-TiO_2; f: P25)..... 102

Figure 4.7 Time courses of H_2 evolution over Cu-TiO_2. 103

Figure 4.8 Changes of H_2 evolution rates over Cu-TiO_2. 103

Figure 4.9 Cu leaching from Cu-TiO_2 into the aqueous phase corresponding to pH

decline across the 5 h reaction. (For PD sample, Cu^{2+} reduction occurred in the first 30 min of reaction.) 106

Figure 4.10 XRD patterns of Cu-TiO_2 photocatalysts after 5 h reaction. (Pattern of PD sample was given in Figure 4.1.) 108

Figure 5.1 Schematic diagram of charge transfer in Cu-TNT photocatalyst under irradiation. 112

Figure 5.2 XRD patterns of photocatalysts (a: TNT; b: TNT-A-C; c: TNT-WI; d: P25; e: P25-A-C; f: P25-WI). 115

Figure 5.3 EDS spectra of photocatalysts (a: TNT; b: TNT-A-C; c: TNT-WI). .. 117

Figure 5.4 (a) FESEM and (b) TEM images of TNT. 119

Figure 5.5 TEM images of (a) TNT-A-C and (b) TNT-WI. 120

Figure 5.6 Isotherm of N_2 adsorption/desorption on the surface of TNT. 122

Figure 5.7 Pore size distributions of photocatalysts..... 122

Figure 5.8 XPS survey spectra of photocatalysts (a: TNT; b: TNT-A-C; c: TNT-WI). 124

Figure 5.9 High-resolution XPS spectra of (a) Cu 2p, (b) Ti 2p and (c) O 1s. 125

Figure 5.10 UV-visible absorption spectra of photocatalysts (a: P25-WI; b: P25-A-C; c: TNT-WI; d: TNT-A-C; e: P25; f: TNT). 129

Figure 5.11 Time courses of H_2 evolution over photocatalysts under irradiation. 130

Figure 5.12 Changes of H_2 evolution rates over photocatalysts in 5 h reactions. 130

Figure 6.1 Schematic diagram of simultaneous Cu^{2+} removal and H_2 production over TNT under irradiation. 135

Figure 6.2 Variation of Cu^{2+} concentration during photocatalytic reaction. 139

Figure 6.3 Changes of Cu^{2+} removal efficiency across 4 h reaction. 139

Figure 6.4 Time courses of H_2 evolution simultaneous with Cu^{2+} removal.....142

Figure 6.5 Changes of H_2 evolution rate during photocatalytic reaction. 142

Figure 6.6 Changes of (a) H_2 evolution rate and (b) Cu^{2+} concentration when Cu-TNT (TNT-10%) is applied to fresh reaction solution with (or without) presence of Cu^{2+} (Cu^{2+}/Ti=10 atom%). 145

Figure 6.7 Variation of Cu^{2+} concentration during photocatalytic reaction with presence of co-existing (a) anions and (b) cations. 147

Figure 6.8 Time courses of H_2 evolution during photocatalytic reaction with presence of co-existing (a) anions and (b) cations. 148

Figure 6.9 Zeta potential of TNT under various pH conditions. 149

Figure 6.10 EDS spectra of Cu-TNT (a: TNT-1%; b: TNT-10%; c: TNT-50%; d: TNT-100%). 152

Figure 6.11 XRD patterns of Cu-TNT (a: TNT-1%; b: TNT-10%; c: TNT-50%; d: TNT-100%). 153

Figure 6.12 High resolution XPS spectra of Cu 2p in Cu-TNT (a: TNT-1%; b: TNT-10%; c: TNT-50%; d: TNT-100%). 154

LIST OF PUBLICATIONS

Journal papers:

1. **Xu, S.**, Ng, J., Wang, Y., Du, A. J. and Sun, D. D. (2012). "Simultaneous copper ions removal and hydrogen production from water over TiO_2 nanotube photocatalyst." Water Science and Technology 65(3): 533-538.

2. Liu, Z., Bai, H., **Xu, S.** and Sun, D. D. (2011). "Hiararchical CuO/ZnO 'corn-like' architecture for photocatalytic hydrogen generation." International Journal of Hydrogen Energy 36(21): 13743-13480.

3. **Xu, S.**, Du, A. J., Liu, J., Ng, J. and Sun, D. D. (2011). "Highly efficient CuO incorporated TiO_2 nanotube photocatalyst for hydrogen production from water." International Journal of Hydrogen Energy 36(11): 6560-6568.

4. **Xu, S.**, Ng, J., Du, A. J., Liu, J. and Sun, D. D. (2011). "Highly efficient TiO_2 nanotube photocatalyst for simultaneous hydrogen production and copper removal from water." International Journal of Hydrogen Energy 36(11): 6538-6545.

5. **Xu, S.**, Ng, J., Zhang, X., Bai, H. and Sun, D. D. (2011). "Adsorption and photocatalytic degradation of Acid Orange 7 over hydrothermally synthesized mesoporous TiO_2 nanotube." Colloids and Surfaces A: Physicochemical and Engineering Aspects 379 (1-3): 169-175.

6. **Xu, S.**, Ng, J., Zhang, X., Bai, H. and Sun, D. D. (2010). "Fabrication and comparison of highly efficient Cu incorporated TiO_2 photocatalyst for hydrogen generation from water." International Journal of Hydrogen Energy 35(11): 5254-5261.

7. Ng, J., **Xu, S.**, Zhang, X., Yang, H. Y. and Sun, D. D. (2010). "Hybridized nanowires and cubes: a novel architecture of a heterojunctioned $TiO_2/SrTiO_3$ thin film for efficient water splitting." Advanced Functional Materials 20(24): 4287-4294.

8. Liu, J., Wang, Y., **Xu, S.** and Sun, D. D. (2010). "Synthesis of graphene soluble in organic solvents by simultaneous ether-functionalization with octadecane groups and reduction." Materials Letters 64(20): 2236-2239.

9. **Xu, S.** and Sun, D. D. (2009). "Significant improvement of photocatalytic hydrogen generation rate over TiO_2 with deposited CuO." International Journal of Hydrogen Energy 34(15): 6096-6104.

10. Zhang, X., Pan, J. H., Du, A. J., **Xu, S.** and Sun, D. D. (2009). "Room-temperature fabrication of anatase TiO_2 submicrospheres with nanothornlike shell for photocatalytic degradation of methylene blue." Journal of Photochemistry and Photobiology A: Chemistry 204(2-3): 154-160.

11. **Xu, S.**, Zhang, X., Ng, J. and Sun, D. D. (2009). "Preparation and application of TiO_2/Al_2O_3 microspherical photocatalyst for water treatment." Water Science and Technology: Water Supply 9(1): 39-44.

Conference presentations:

1. **Xu, S.**, Ng, J., Zhang, X., Bai, H. and Sun, D. D. (2010). "Adsorption and photocatalytic degradation of Acid Orange 7 over hydrothermally synthesized mesoporous TiO_2 nanotube." The 6th International Conference on Interfaces against Pollution, Beijing, China, 15-19 May.

2. Wang, Y., **Xu, S.**, Zhang, X. and Sun, D. D. (2010). "Enhanced photocatalytic oxidation by anatase nanotubes for water treatment." 7th IWA Leading Edge Conference on Water and Wastewater Technologies, Phoenix, Arizona, USA, 2-4 June.

3. **Xu, S.**, Zhang, X., Ng, J. and Sun, D. D. (2009). "Preparation and application of TiO_2/Al_2O_3 microspherical photocatalyst for water treatment." IWA Chemical Industries 2008 International Conference, Beijing, China, 9-11 November, second Place Award.

4. **Xu, S.**, Sun, D. D., Gao, B. and Zhang, X. (2007). "Effect of Coagulation Floc Structure on Membrane Fouling for the Removal of Natural Organic Matter in Water." 4th IWA Leading Edge Conference and Exhibition on Water and Wastewater Technologies, Singapore, 3-6 June.

CHAPTER 1

INTRODUCTION

1.1 Motivation

Nowadays living quality of human beings and development of the world economy rely heavily on the energy availability. Among most of the energy sources, fossil fuels remain as the most popular and economical energy source for the past few decades as they possess very useful properties, not shared by non-conventional energy sources. Unfortunately, fossil fuels are limited and non-renewable, and will be depleted in the near future; furthermore, global consumption of fossil fuels does create critical environmental problems (green-house effect, air pollution, and oil spills etc.) throughout the world, both of which require a major restructuring of the global energy system.

Since the first oil crisis in 1973, many efforts have been devoted in searching alternative and renewable energy sources. Comparing with wind, hydropower, motion of tides, heat of the Earth's magma, and ocean temperature gradients etc., solar energy harvesting attracts more attention since the amount of solar energy reaching the Earth is sufficient to supply mankind with many thousand times the energy it presently requires (Zhang et al., 2010); moreover, solar energy stored in the form of electricity and H_2 etc., can be utilised regardless of time and locations.

Among solar fuel candidates, H_2 plays an important role because of its high energy content, environmental compatibility, ease of storage and distribution, and many common applications including spacecraft, vehicles powered by internal combustion engine or fuel cell electric motor, and domestic heating applications

etc. However, solar H_2 contributes little to the entire H_2 production outside the laboratory. In the United States, approximate 95% of total H_2 demand are sourced from the steam reforming of natural gas, followed by off-gas cleanup and electrolysis processes (Manivel et al., 2010). These processes do not reduce the dependence on fossil fuels, and even aggravate global warming since H_2 production from fossil fuel feedstock leads to carbon dioxide emissions even greater than those from simply using fossil fuel directly.

Renewable, environment-friendly H_2 production from photo-processes with abundant sunlight as energy source has been studied by many researchers. There are several broad categories of photo-processes, namely, photoelectrochemical (PEC) (Fujishima et al., 1972; Nozik, 1975; Hodes et al., 1976; O'Regan et al., 1991; El Zayat et al., 1998; Stanley et al., 1998; Bak et al., 2002), photocatalytic (Lehn et al., 1980; Bard et al., 1995; Zou et al., 2001; Ni et al., 2007), and photobiological (Weaver et al., 1980; Miyake et al., 1987; Singh et al., 1990; Melis et al., 2000) processes. Compared with the complicated configurations and limited material choices of PEC, as well as relatively strict reaction conditions for bacteria in photobiological system, photocatalytic H_2 production from a simple water splitting using fine powder photocatalyst has been regarded as a feasible and promising option (Korzhak et al., 2008; Kudo et al., 2009; Zhu et al., 2009; Abe, 2010; Chen et al., 2010; Leung et al., 2010; Shimura et al., 2011).

Photocatalytic water splitting process initiates from photo-excitation of semiconductor by photons with energy equal to or higher than its band gap energy level, resulting in excited electrons promoted into conduction band (CB) and holes left in valance band (VB). Water is then reduced/oxidized by excited electron/hole to produce H_2/O_2, when CB/VB level is more negative/positive than H_2/O_2 production level.

Compared with other photocatalysts, TiO_2 is more favourable and widely studied owing to its high activity, chemical stability, wide availability and environmental-friendly properties. However, H_2 generation efficiency over commonly used TiO_2 from water is still low, mainly due to the fast recombination of electron/hole pairs, and rapid backward reaction (Ni et al., 2007). Many efforts have been made to overcome this hindrance, including noble metal loading (Bamwenda et al., 1995; Kim et al., 2002; Sakthivel et al., 2004; Subramanian et al., 2004), addition of electron donors (Sayama et al., 1997; Li et al., 2001; Galinska et al., 2005; Patsoura et al., 2006), metal ion doping (Martin et al., 1994a; Wilke et al., 1999; Xu et al., 2002), semiconductor composition (So et al., 2004) etc. Both noble metal loading and addition of electron donors have been widely studied for H_2 production, and proved to be very effective in enhancing photocatalytic activity of TiO_2 since both methods contribute to efficient electron/hole separation (Ni et al., 2007). However, considering high cost incurred by the use of noble metal and sacrificial reagents, it is urgently needed to fabricate a highly efficient, cost-effective photocatalyst, at the same time, utilizing organic wastes or pollutants as sacrificial reagents by converting them into environmental-friendly products.

Cu incorporated TiO_2 (Cu-TiO_2) is a cost-effective photocatalyst compared to noble metal loaded TiO_2, and has been proved to possess high photocatalytic activity for air pollution treatment (Boccuzzi et al., 1994; Larsson et al., 1998). Recently, some researchers found that, compared to Pt/Au loaded TiO_2, Cu-TiO_2 possessed satisfactory photocatalytic activity for reduction of water under sacrificial conditions to produce H_2 (Bandara et al., 2005; Sreethawong et al., 2005; Choi et al., 2007), since Cu compounds facilitated the charge separation and provided reduction sites for H_2 formation. Moreover, several Cu compounds (Cu/Cu_2O/CuO) have been proved to be active (Sakata et al., 1998; Wu et al., 2004;

Wu et al., 2009), which further affirms the huge potential of Cu-TiO_2 in photocatalytic H_2 production. However, the reported H_2 evolution rates were still low for practical applications, and few studies have been conducted to investigate and improve the H_2 generation activity of Cu-TiO_2; meanwhile, knowledge about the preparation methods for highly efficient Cu-TiO_2 photocatalyst and effect of operation conditions on H_2 generation is not available. All of these require further systematic studies to explore the potential of novel Cu-TiO_2 in photocatalytic H_2 production for energy harvesting.

In addition, Cu is a natural resource that is heavily employed in industrial application. However wastewater containing Cu generated from industrial activities poses major environmental concern which is needed to be addressed urgently. If Cu from wastewater could be recovered and reused by TiO_2 photocatalyst, it could simultaneously provide multiple solutions for wastewater purification and concurrent formation of highly efficient Cu-TiO_2 photocatalyst for H_2 (clean energy) production. This study is aimed to investigate these mentioned hypotheses with results presented in four main chapters.

1.2 Objectives and Significance

The main objective of this study is to fabricate a highly efficient Cu-TiO_2 photocatalyst for H_2 production from water. The specific aims of this research are as follows:

- To synthesize and characterize Cu-TiO_2 with well recognized P25 as TiO_2 support via wet impregnation method, to confirm the potential of Cu-TiO_2 in photocatalytic H_2 production;

- To optimize the operation conditions of Cu-TiO_2, for example, sacrificial reagent concentration, pH of reaction solution and photocatalyst dosage, to improve H_2 generation;

- To investigate the fabrication methods of a highly active Cu-TiO_2 photocatalyst for H_2 generation;

- To further improve the photocatalytic activity of Cu-TiO_2 via employing highly efficient TiO_2 nanotube as support;

- To investigate the formation of Cu-TiO_2 by utilizing Cu^{2+} present in wastewater, and explore the potential application of Cu-TiO_2 in concurrent Cu^{2+} removal and H_2 production.

Significance and benefits of this research are as follows:

These fundamental studies of energy harvesting from H_2 using Cu-TiO_2 photocatalyst will provide insights that can be employed to help in searching for alternative and cost-effective energy sources in view of the energy crisis and climate changes. In particular, this research can contribute to the novel fabrication method of Cu-TiO_2 photocatalyst including the use of TiO_2 nanotubes for the improvement of H_2 production based on the studies of its mechanisms. The removal of Cu^{2+} from wastewater by utilizing it to form Cu-TiO_2 photocatalyst and simultaneous production of H_2 from wastewater would provide great potentials by not only harvesting energy but also tackling heavy metal pollution problem from wastewater.

1.3 Organization of Thesis

This thesis is divided into seven chapters:

Chapter 1 provides a brief introduction, while Chapter 2 presents the literature review encompassing principles and mechanisms of photocatalysis, and outlines the attempts in improving H_2 generation activity of TiO_2. A brief review on Cu-TiO_2 and TiO_2 nanotubes are discussed as well.

Chapter 3 provides a systematic study of utilizing Cu-TiO_2 fabricated via wet impregnation method for H_2 production. Effect of Cu content in the photocatalyst, sacrificial reagent concentration, pH of reaction solution and photocatalyst dosage on H_2 generation was studied, and optimal operation conditions for further studies were determined. Changes of Cu-TiO_2 and maintenance of Cu-TiO_2 activity in intensive photocatalytic reaction were investigated as well.

Based on the optimal operation conditions obtained in Chapter 3, Chapter 4 discusses the effect of fabrication methods of Cu-TiO_2 on H_2 generation activity. Four methods, namely, in-situ sol-gel, wet impregnation, chemical reduction of Cu salt, and in-situ photo-deposition were highlighted. After structure and component characterization, the activities of all products were tested and compared; factors influencing H_2 generation activity induced by different fabrication methods were discussed.

To further improve the H_2 generation activity, highly efficient TiO_2 nanotube was synthesized and employed as TiO_2 support for Cu-TiO_2, and the results were reported in Chapter 5. Factors contributing to high activity were also investigated and presented in this chapter.

Chapter 6 presents an interesting and valuable novel approach of Cu-TiO_2 in simultaneous Cu^{2+} removal and H_2 production from water. Effect of Cu^{2+} reduction with various Cu^{2+} concentrations on H_2 generation, and chemical states of Cu after reaction were comprehensively studied and discussed.

The major findings of this study and some recommendations for the future investigations are summarized in Chapter 7.

CHAPTER 2

LITERATURE REVIEW

2.1 Principles, Mechanisms of Photocatalysis

2.1.1 Electronic processes

2.1.1.1 Band gap

Different from metal which possesses continuous electronic states, semiconductor and insulator have a band gap (E_g) existed in their electronic band structure, which is a void energy region (Figure 2.1). This region extends from the bottom of the vacant conduction band (CB) to the top of the filled valence band (VB), and no energy level is available in this region.

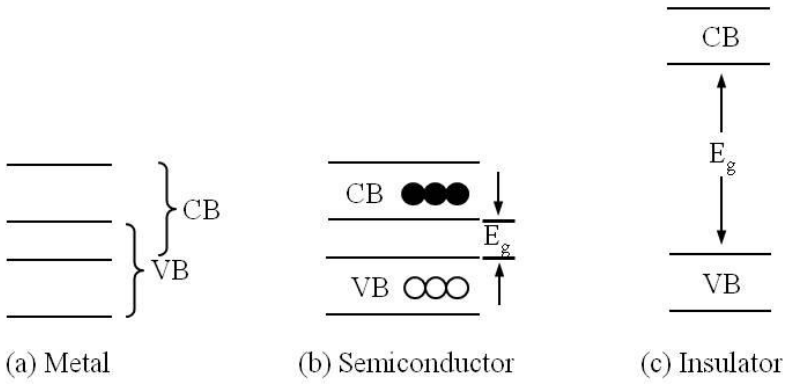

Figure 2.1 Diagram of electronic band structure of metal, semiconductor and insulator.

Band gap can be calculated by following equation:

$$E_g=E_c-E_v \quad (2\text{-}1)$$

where E_c is the lowest energy level of CB (CB edge), E_v is the highest energy level of VB (VB edge).

Table 2.1 gives band gap energies and corresponding wavelengths of light for a variety of semiconductors. The required wavelength of light that possesses sufficient energy to excite the electron could be calculated from Planck's equation:

$$E = h\nu = \frac{hc}{\lambda} \quad (2\text{-}2)$$

where E is the energy (J) required to overcome the band gap, h is Planck's constant (6.626×10^{-34} J s), ν is frequency of wavelength, c is the speed of light in vacuum (2.998×10^{8} m s^{-1}), and λ is wavelength of light (m).

Generally, band gap energy of semiconductor is less than 5 eV; while for insulator, gap is much larger, and it is hardly possible for electrons to be excited across the band gap to endow the insulator working as an effective catalyst.

Table 2.1 Band gap energies and corresponding wavelengths of light for various semiconductors (Stumm, 1992).

Photocatalyst	E_g (eV)	Wavelength (nm)	Photocatalyst	E_g (eV)	Wavelength (nm)
ZrO_2	5.0	248	α-Fe_2O_3	2.34	516
Ta_2O_5	4.0	310	ZnTe	2.3	530
SnO_2	3.5	354	$PdFe_{12}O_{19}$	2.3	539
$KTaO_3$	3.5	354	GaP	2.3	539
$SrTiO_3$	3.4	365	$CdFe_2O_4$	2.3	539
Nb_2O_5	3.4	365	CdO	2.2	539
ZnO	3.35	370	$Hg_2Nb_2O_7$	1.8	689
$BaTiO_3$	3.3	376	$Hg_2Ta_2O_7$	1.8	689
TiO_2	3.0-3.3	376-413	CuO	1.7	729
SiC	3.0	376	PbO_2	1.7	729
V_2O_5	2.8	443	CdTe	1.4	885
Bi_2O_3	2.8	443	GaAs	1.4	885
$FeTi_3$	2.8	443	InP	1.3	954
PbO	2.76	449	Si	1.1	1127
WO_3	2.7	459	β-HgS	0.54	2296
CdS	2.4	516	β-MnO_2	0.26	4768

2.1.1.2 Photo-excitation

Photocatalysis process initiates from generation of electron/hole pairs in the semiconductor particles. Upon light absorption with energy equal to or greater than E_g, a band to band electron transition occurs. Electron in the filled VB is excited to

the vacant CB leaving behind a hole in VB. As a result, the strongly reducing electron and strongly oxidizing hole are formed.

Linsebigler et al. (1995) proposed four possible pathways for the separated electrons and holes upon excitation (Figure 2.2). The photo-induced electrons could undergo charge transfer to adsorbed species on the semiconductor surface from solution or gas phase contact, and reduce the electron acceptors (Figure 2.2C). Meanwhile, holes could migrate to the surface to oxidize the electron donor species (Figure 2.2D). In competition with charges transfer to adsorbed species, electrons and holes could recombine either on the surface or in the bulk of the semiconductor particle (Figures 2.2A & B) with the release of heat.

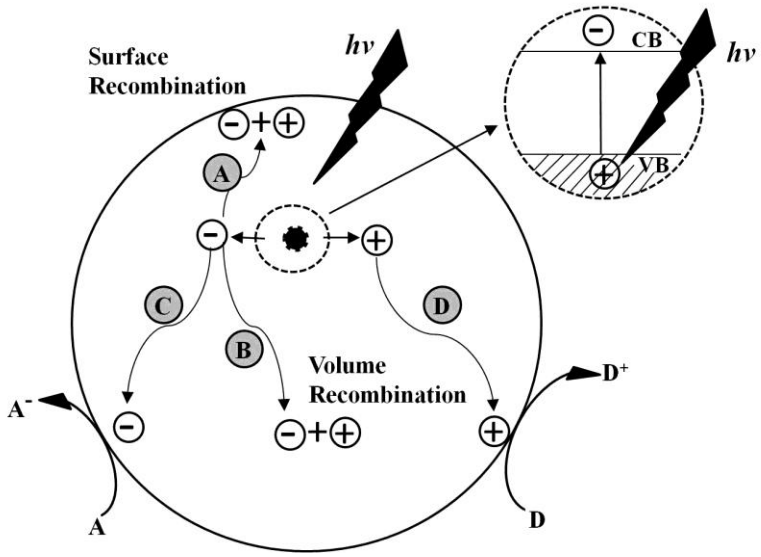

Figure 2.2 Schematic de-excitation pathways for electrons and holes in photocatalyst (Linsebigler et al., 1995).

Photocatalytic efficiency usually depends on how rapidly the minor charge carriers (holes in n-type semiconductor and electrons in p-type semiconductor) reach the surface of the solid and how fast they are captured via interfacial charge transfer.

Recombination is detrimental to the efficiency of semiconductor photocatalysts since it reduces the effective number of electrons and holes for photoreaction. Modification to semiconductor, aiming at reducing recombination, is necessary to increase the quantum yield of photocatalytic process.

2.1.1.3 Band edge position

The ability and rate of charge transfer processes for electrons and holes are determined by respective positions of CB and VB edge of the semiconductor and the redox potential levels of the adsorbate species. The prerequisite for an effective charge transfer is that, the relevant potential levels of the electron acceptors should be more positive than the conduction band potential of the semiconductor to accept electron; meanwhile, potential levels of the electron donors are required to be more negative than the valence band to donate electrons.

Figure 2.3 shows band edge positions of several common semiconductors. The energy scale is given for comparison with the normal hydrogen electrode (NHE). The positions are obtained in contact with aqueous electrolyte at pH=1.

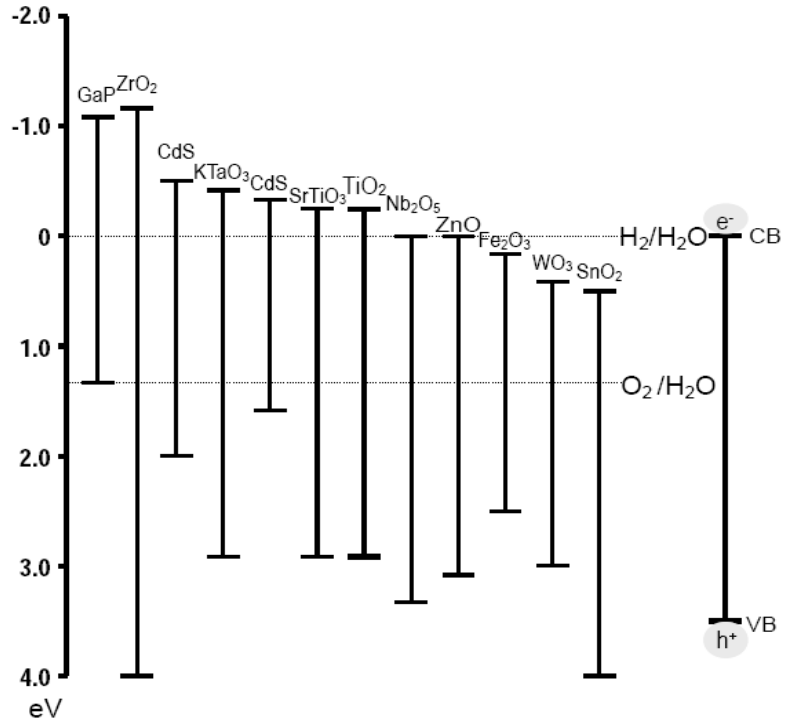

Figure 2.3 Band edge positions for various semiconductors in aqueous electrolyte at pH=1 (Wu, 2005).

It is worthy to note that band edge positions of both CB and VB are pH dependent like redox potentials of some adsorbates. Take TiO_2 as example, both CB and VB positions decrease by 59 mV for ΔpH=+1 (25°C) (Ward et al., 1983).

Figure 2.4 clearly illustrates the positions of conduction and valence band of TiO_2 in contact with aqueous electrolyte solution at different pH, comparing with the redox potentials of several environmentally important metal ions.

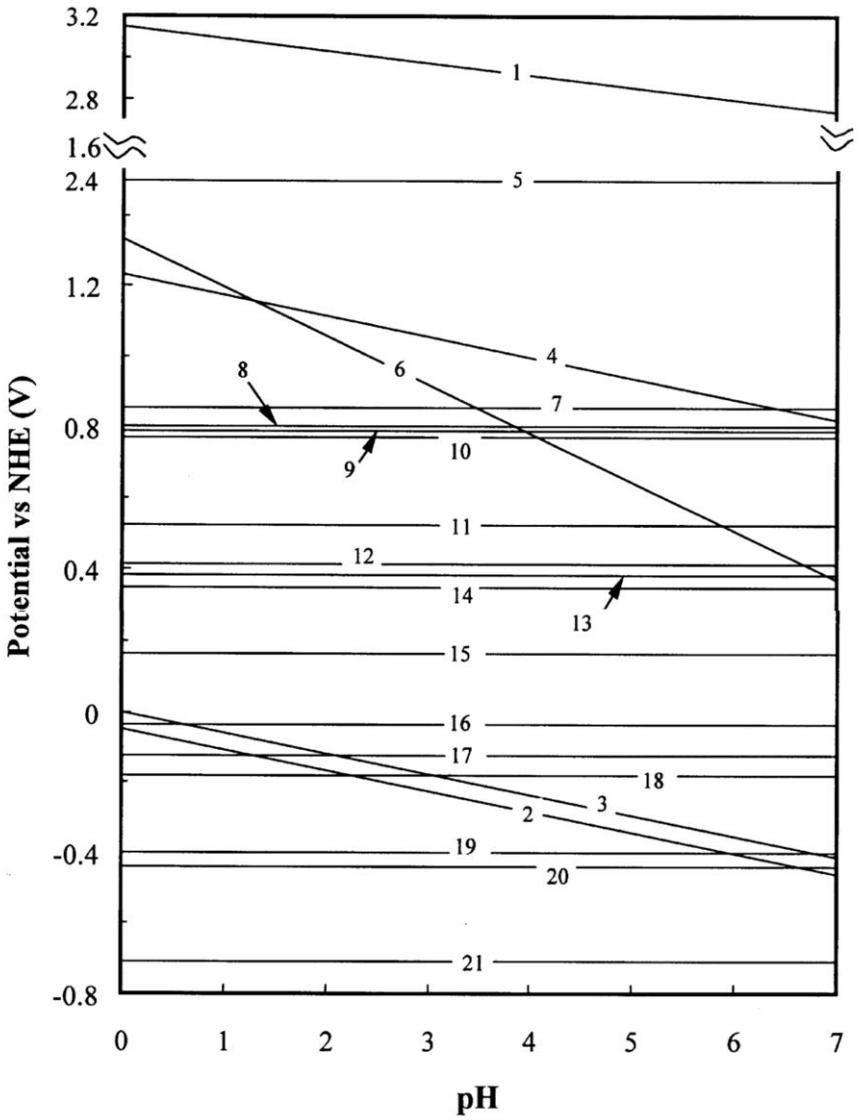

1 E_{VB}; 2 E_{CB}; 3 H^+/H_2; 4 O_2/H_2O; 5 Au^{3+}/Au; 6 Cr^{6+}/Cr^{3+}; 7 Hg^{2+}/Hg; 8 Ag^+/Ag; 9 Hg_2^{2+}/Hg; 10 Fe^{3+}/Fe^{2+}; 11 Cu^+/Cu; 12 $HgCl_2/Hg$; 13 $HgCl_4^{2-}/Hg$; 14 Cu^{2+}/Cu; 15 Cu^{2+}/Cu^+; 16 Fe^{3+}/Fe; 17 Pb^{2+}/Pb; 18 Ni^{2+}/Ni; 19 Cd^{2+}/Cd; 20 Fe^{2+}/Fe; 21 Cr^{3+}/Cr

Figure 2.4 Band positions of TiO_2 (anatase) together with the redox potentials of certain metal ions (1 M) at different pH (Chen et al., 2001).

It can be seen that, electrons in the CB are stronger reductants in the basic pH range, while holes in VB are stronger oxidants in low pH ranges. Hence, with the right choice of semiconductors and pH conditions, many electron transfer reactions

are feasible (Figures 2.3 & 2.4).

2.1.1.4 Quantum size effect

Band gap and band edge positions of semiconductor should undergo changes if particle size of the semiconductor decreases to nanometer scale. When the size of semiconductor particles becomes comparable to the de Broglie wavelength of charge carriers (photo-induced electrons and holes) in the semiconductor, on the order of 1-10 nm, quantum size effects (QSE) is expected to occur (Figure 2.5).

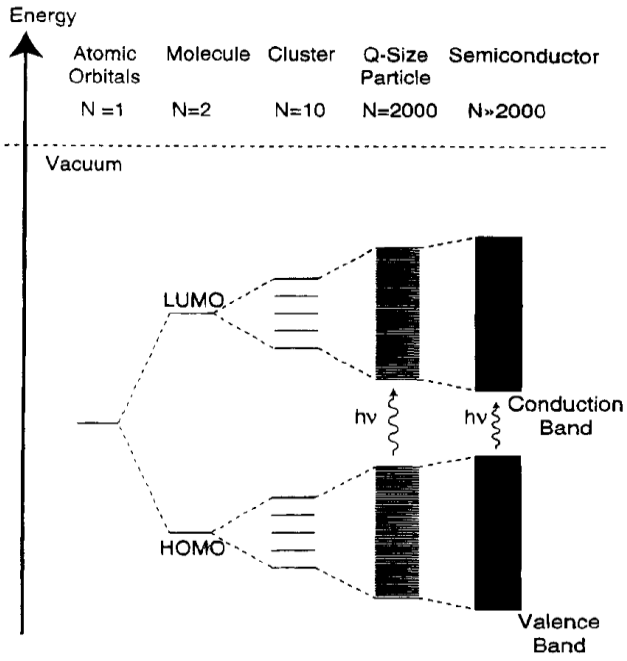

Figure 2.5 Electronic states in semiconductor with different particle size (LUMO: lowest unoccupied molecular orbital, HOMO: highest occupied molecular orbital) (Hoffmann et al., 1995).

Charge carriers in quantum size particles (Q-particles) are confined in a potential well with small geometrical dimensions, and do not experience the electronic

delocalization like in a bulk semiconductor which possesses conduction and valence band. Instead, the confinement creates a quantization of discrete electronic states, and increases the effective band gap of the semiconductor (Linsebigler et al. 1995), which is experimentally observed as a blue shift in the absorption and emission spectra of the semiconductor. Larger effective band gap definitely improves the ability of semiconductor working as reductant or oxidant; hence, it attracts many researchers focusing on the fabrication of nanosized TiO_2.

2.1.1.5 Band bending

Charge carriers' recombination could be suppressed if the carriers transfer from the semiconductor to contact phase, or be trapped at surface states at the interface, namely, forming a space charge layer. Generally, contact between a semiconductor and another phase (liquid, gas, or metal) involves a redistribution of electric charges, leading to band bending of the semiconductor, and formation of space charge layer (Linsebigler et al., 1995). Take semiconductor-metal system as an example (illustrated in Figure 2.6), when isolated from each other, metal possesses lower Fermi level position than n-type semiconductor (Rhoderick et al., 1988), that is to say, metal has a higher work function than the semiconductor. Once the two materials are connected electrically, electrons migration from the semiconductor to the metal side occurs until the two Fermi levels are aligned. On the semiconductor side, space charge layer forms, and bands bend upward toward the surface as a result of excess positive charge accumulation since electrons migrate away from the space charge layer. On the contrary, surface of the metal acquires excess negative charges. Therefore, a barrier forms at the semiconductor-metal interface, which is called the Schottky barrier. This barrier can serve as an effective electron trap to prevent electron/hole recombination in photocatalysis.

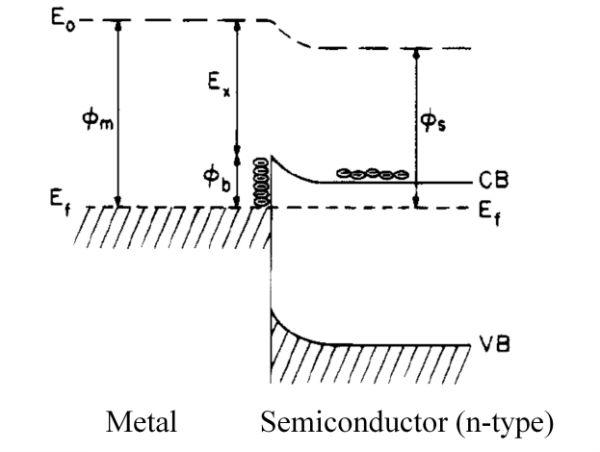

Figure 2.6 Schematics of electric charges redistribution in semiconductor-metal interface (Linsebigler et al., 1995).

2.1.2 Photocatalysis on TiO_2

2.1.2.1 Introduction of TiO_2 photocatalyst

TiO_2 is an n-type semiconductor, and is the most popular photocatalyst in heterogeneous photocatalysis, due to its highly efficient, cost-effective and environment-friendly properties; in addition, TiO_2 is biologically and chemically inert, stable with respect to photo-corrosion and chemical corrosion (Zhu et al., 2009). Many efforts have been devoted into research by employing TiO_2 for environmental purification and energy production. For instance, TiO_2 has been widely tested and used in photo-degradation of various organic and inorganic pollutants, destruction of bacteria and viruses (Sjogren et al., 1994; Kikuchi et al., 1997), inactivation of cancer cells (Blake et al., 1999), odor control, and cleanup of oil spills (Gerischer et al., 1992). It is also widely used in solar cells for the production of H_2 and electric energy, as gas sensor, white pigment (e.g. in paints and cosmetics products), optical coating and corrosion-protective coating.

TiO_2 composes of three crystal structures, anatase, rutile, and brookite, and the first

two components are commonly used as active photocatalyst. Crystal structure of anatase and rutile can be described in terms of chains of TiO_6 octahedra, but the two crystal structures are different in distortion and assembly patterns of the octahedral (Figure 2.7).

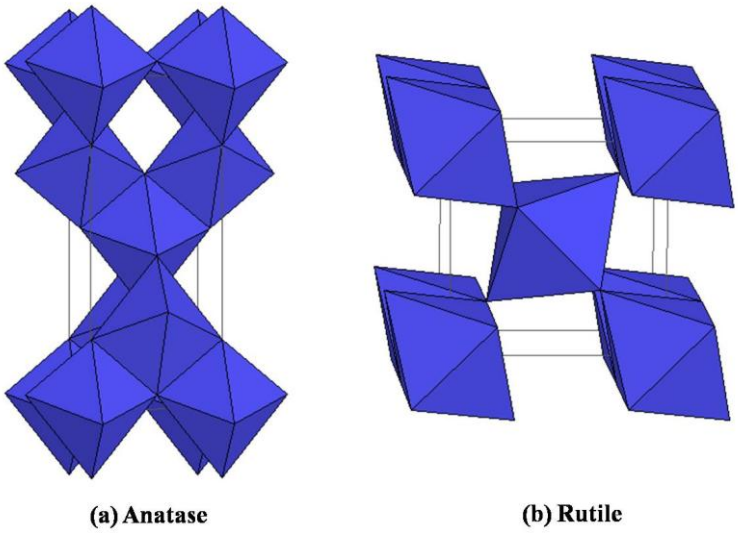

Figure 2.7 Crystal structure of anatase and rutile.

This structure difference causes different band gap energies (anatase: 3.2 eV/388 nm, rutile: 3.0 eV/413 nm), and different band edges (Figure 2.8). Compared to rutile, anatase possesses higher CB and lower VB, determining the higher photocatalytic reduction and oxidation ability of anatase (Fox et al., 1993). Nevertheless, rutile is the most thermodynamically stable, and other crystal structures would reconstruct to produce rutile upon heating to high temperature.

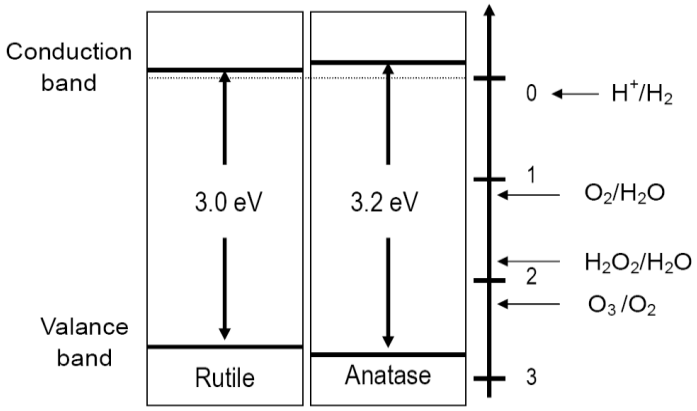

Figure 2.8 Comparison of band gap and band edge positions of anatase and rutile (Wu, 2005).

It is appreciated that physicochemical properties of nanomaterials are significantly different from bulk materials, and the most popular commercial TiO_2, is Degussa P25, average particle size of which is 30 nm and BET surface area is 50 m^2 g^{-1}. P25 is usually used as benchmark for research purpose. Recently, 1-D nanostructured TiO_2 (nanotube, nanosheet and nanofiber) has attracted considerable attention due to its unique, layered nanostructure and ability to combine properties and applications of conventional TiO_2 nanoparticles. Among them, TiO_2 nanotube (TNT) is of great interest owing to it unique combination of morphological and physicochemical properties, such as large specific surface area, mesoporous structure, high aspect ratio, and efficient electron conductivity (Bavykin et al., 2009).

TNT was first successfully synthesized by Kasuga et al. in 1998 (Kasuga et al., 1998). To date, there are three general approaches in preparing TNT, namely, alkaline hydrothermal route, anodization techniques, and chemical (template) synthesis. Among them, the hydrothermal synthesis is recognized as a facile and low cost method, which allows convenient scale-up for mass-production (Bavykin

et al., 2009). Much effort has been devoted to understand the formation mechanisms of TNT during hydrothermal treatment (Chen et al., 2002b), and to optimize fabrication conditions (Bavykin et al., 2004; Menzel et al., 2006), as well as to study its properties (Yuan et al., 2004). In addition, TNT has exhibited immense potential in a wide variety of applications, ranging from environmental purification (Liu et al., 2008), photocatalysis (Lin et al., 2004), energy storage (Armstrong et al., 2005), and gas sensing (Mor et al., 2004) etc.

2.1.2.2 Surface chemistry of TiO_2

The interaction of electron donors and acceptors with metal oxide semiconductors partially depends on surface chemistry of these compounds. Metal oxide particles are known to be amphoteric, when they are suspended in water. In the case of TiO_2, hydroxyl groups on the TiO_2 surface undergo the following acid-base equilibria:

$$>TiOH_2^+ \overset{pK_{a1}}{\longleftrightarrow} >TiOH + H^+ \quad (2\text{-}3)$$

$$>TiOH \overset{pK_{a2}}{\longleftrightarrow} >TiO^- + H^+ \quad (2\text{-}4)$$

where >TiOH represents the "titanol" surface group, pK_{a1} is the negative log of the microscopic acidity constant for the first acid dissociation of equation 2-3, and pK_{a2} is that for the second acid dissociation of equation 2-4 (Lachheb et al., 2002). The point of zero charge, pH_{zpc}, is given by one half of the sum of the two surface pK_a as follows, as in the case of amphoteric amino acids (Wikipedia):

$$pH_{zpc} = (pK_{a1} + pK_{a2})/2 \quad (2\text{-}5)$$

In the case of Degussa P25, surface acidity constants, pK_{a1} and pK_{a2}, were detected

to be 4.5 and 8, respectively, and pH_{zpc} was 6.25 (Kormann et al., 1991). This implies that interactions between TiO_2 with cationic electron donors and acceptors are favored at high pH (> pH_{zpc}), while anionic reagents will be favored at low pH (< pH_{zpc}). Study of Kormann et al. supported this inference, where enhanced rates of oxidation of many cations were observed at alkaline pH conditions (Kormann et al., 1991). This could not be explained by the shift of band edges of TiO_2 in aqueous solution, since if the shifting of band edges was the dominating factor, lower rates of substrate oxidation should be observed at high pH, as VB edge decreases by 59 mV with each increasing unit of pH. Therefore, they supposed that the adsorption of the reagents to TiO_2 particles surface played a more important role in determining the photoactivity than shifts in redox potential of the band edges.

Numerous researchers reported that adsorption of substrates onto the semiconductor surfaces followed most often Langmuir adsorption isotherm, and photo-degradation rate of chemical compounds on semiconductor surfaces followed the classical Langmuir- Hinshelwood expression.

2.1.2.3 Mechanism for heterogeneous photocatalysis on TiO_2

Martin et al. and Hoffmann et al. proposed general mechanism for heterogeneous photocatalysis on TiO_2, based on laser flash photolysis measurements. They also presented characteristic time for different steps in the mechanism (Martin et al., 1994a; Martin et al., 1994b; Hoffmann et al., 1995), which is shown in Table 2.2.

Table 2.2 General mechanism for heterogeneous photocatalysis on TiO_2 (Hoffmann et al., 1995).

Primary Process	Characteristic Time	
Charge-carrier generation		
$TiO_2 + h\nu \rightarrow h_{vb}^+ + e_{cb}^-$	(fs)	(2-6)
Charge-carrier trapping		
$h_{vb}^+ + >Ti^{IV}OH \rightarrow \{>Ti^{IV}OH\cdot\}^+$	Fast (10 ns)	(2-7)
$e_{cb}^- + >Ti^{IV}OH \leftrightarrow \{>Ti^{III}OH\}$	Shallow trap (100 ps) dynamic equilibrium	(2-8a)
$e_{cb}^- + >Ti^{IV} \rightarrow >Ti^{III}$	Deep trap (10 ns) irreversible	(2-8b)
Charge-carrier recombination		
$e_{cb}^- + \{>Ti^{IV}OH\cdot\}^+ \rightarrow >Ti^{IV}OH$	Slow (100 ns)	(2-9)
$h_{vb}^+ + \{>Ti^{III}OH\} \rightarrow >Ti^{IV}OH$	Fast (10 ns)	(2-10)
Interfacial charge transfer		
$\{>Ti^{IV}OH\cdot\}^+ + Red \rightarrow >Ti^{IV}OH + Red\cdot^+$	Slow (100 ns)	(2-11)
$e_{tr}^- + Ox \rightarrow >Ti^{IV}OH + Ox\cdot^-$	Very slow (ms)	(2-12)

where h_{vb}^+ represents a VB hole, e_{cb}^- is a CB electron, e_{tr}^- is a trapped CB electron, $>Ti^{IV}OH$ is the primary hydrated surface functionality of TiO_2, $\{>Ti^{IV}OH\cdot\}^+$ is the surface-trapped VB hole (i.e. surface-bound hydroxyl radical), $\{>Ti^{III}OH\}$ is the surface trapped CB electron, "Red" is an electron donor (i.e. reductant), and "Ox" is an electron acceptor (i.e. oxidant).

During preparation process of photocatalysts, surface and bulk irregularities commonly occur. These irregularities are associated with surface electron states which possess different energy level from bands in the bulk semiconductor. These electron states serve as charge carrier traps and help to suppress the recombination of electrons and holes. Equation 2-8a shows the reversible trapping of a CB electron in a shallow trap (defect sites) below CB edge, and there is a finite probability that the trapped electron can be transferred back into the CB at room temperature.

The overall quantum efficiency of interfacial charge transfer is determined by two crucial processes: competition between charge carriers recombination and trapping (ps vs. ns), followed by the competition between trapped carriers recombination and interfacial charge transfer (μs vs. ms). An increase in either the lifetime of charge carriers or the interfacial electron transfer rate constant is supposed to achieve higher quantum efficiency for photocatalytic reaction.

Secondary reactions with photo-induced e_{cb}^-/h_{vb}^+ are summarized and illustrated in Figure 2.9.

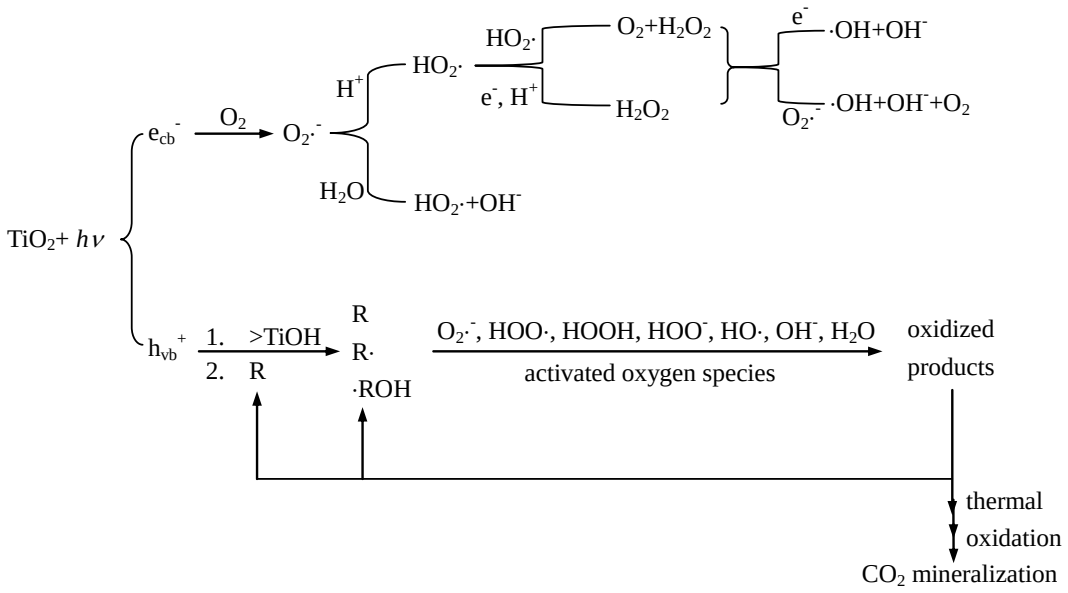

Figure 2.9 Secondary reactions in photocatalysis process over TiO_2 (Hoffmann et al. 1995).

In most circumstances, O_2 is present to serve as the primary electron acceptor. Gerischer et al. suggested that electron transfer to O_2 might be the rate-limiting step in photocatalytic reaction (Gerischer et al., 1991, 1992; Wang et al., 1992). When O_2 was not reduced at a sufficiently high rate, electrons accumulated on the photocatalyst particles, and accelerated the rate of radiationless recombination until the electron transfer to O_2 was equal to the hole generation rate. Following a two-electron reduction of O_2, H_2O_2 is formed via mechanism as shown in Figure 2.9. H_2O_2 would also contribute to the degradation of organic or inorganic electron donors by serving as a direct electron acceptor (i.e. oxidant) or as a source of hydroxyl radical ($H_2O_2 \rightarrow 2{\cdot}OH$).

Hydroxyl radicals are mainly formed on the surface of TiO_2 by reaction of VB hole with adsorbed H_2O, hydroxide, or surface titanol groups (>TiOH), and serve as a strong oxidant. In the above general mechanism, hole transfer is assumed not to

progress directly, and oxidation occurs exclusively through a surface-bound hydroxyl radical or trapped hole species. However, many researchers deem that the oxidation might occur by either indirect oxidation via hydroxyl radical (i.e. a trapped hole at particle surface), or directly through the VB hole before it was trapped within the particle or at the particle surface (Draper et al., 1990; Mao et al., 1991; Richard, 1993; Carraway et al., 1994). For the indirect oxidation, the oxidative radicals could react with substrates in solution to yield oxidized products; while, for direct oxidation, the substrates should first be adsorbed onto the photocatalyst surface and then react with VB holes to produce the final products.

2.1.2.4 Photocatalytic experimental system

There are several types of apparatus for photocatalytic reaction. From the view point of irradiation, both inner and outer-irradiation types of reactors, shown in Figure 2.10, are found to be employed in photocatalytic reaction.

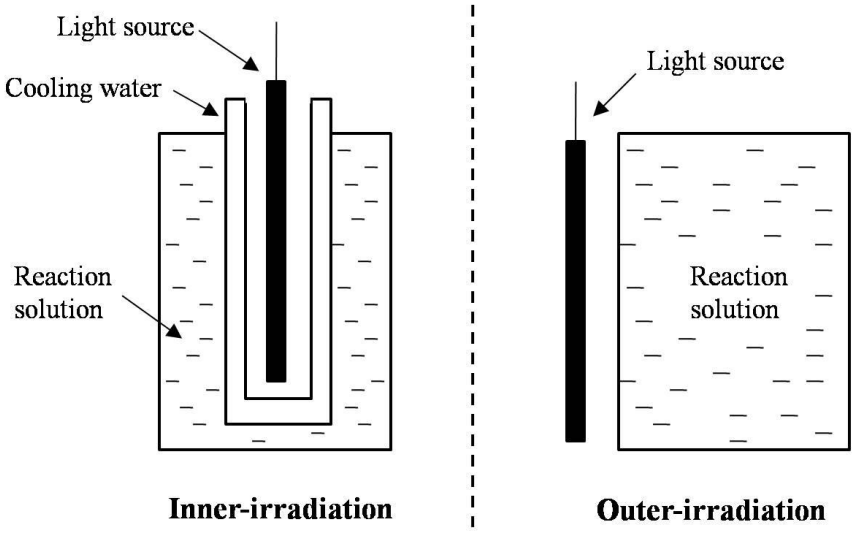

Figure 2.10 Schematic diagram of inner and outer-irradiation photocatalytic reactor

In general, inner-irradiation reaction cell is more efficient (Galinska et al., 2005; Kudo et al., 2009), since the light source is surrounded by the reaction solution, and most of the light with suitable wavelength can be utilized during the photocatalytic reaction. For out-irradiation type of reaction cell, the photo reactor is placed at a distance to the light source (Jin et al., 2007), and only partial light would reach the reactor, therefore utilization efficiency of light is lower. Nevertheless, out-irradiation reaction cell is advantageous in adapting to various light sources with different shapes and sizes etc.; whereas, modification of reactor may be needed for inner-irradiation reactor when different light source is being utilized due to cooling water tube configuration or airtight seal requirement of the reactor.

Many photocatalytic experiments are investigated with the use of fine photocatalyst particles, making full use of the surface area of photocatalyst, and requiring only a simple reaction setup. But this type of suspended photocatalyst system limits practical applications due to engineering difficulty in the recovery and recycling of the highly dispersed photocatalyst from reaction solution by means of filtration or centrifugation (Skorb et al., 2008). To overcome this drawback, many approaches are proposed, such as, immobilization of photocatalyst, fabrication of magnetic photocatalysts (Shchukin et al., 2002), combination of nano-crystalline TiO_2 with the organic mesophases (Shchukin et al., 2004), etc. Among them, immobilization of photocatalyst to form a photocatalytic film is regarded as an efficient approach to resolve the separation problem (Dang et al., 2009). However, the immobilized photocatalysts lose the effective surface area to a certain extent, and hence decrease the photocatalytic activity as compared to a suspended photocatalyst system. Therefore, effective photocatalyst configuration with a good balance between photocatalytic activity and ease of catalyst separation for engineering applications may require more detailed

investigation.

2.2 H_2 Production Using TiO_2

Unlike photocatalytic oxidation of pollutants, in photocatalytic H_2 generation process, photo-induced CB electrons are the key elements to reduce protons to H_2 molecules, instead of VB holes serving as strong efficient oxidant. To initiate H_2 generation, CB level of photocatalyst should be more negative than H_2 evolution level (E_{H_2/H_2O}).

Since the first discovery of photocatalytic water splitting on a TiO_2 electrode (Fujishima et al., 1972) just before oil shock of 1973, TiO_2 photocatalytic H_2 production from water has attracted enormous research effort to make H_2 produced by this way to be a clean, inexpensive and sustainable energy source. However, H_2 generation rate by TiO_2 photocatalytic water splitting is still very low, owning to the fast recombination of photo-induced electron/hole pairs, fast backward reaction (recombination of H_2 and O_2 to produce water), undesirable side-reactions, and inability to utilize visible light (UV light that can be utilized by TiO_2 only accounts for about 4% of the solar radiation). In order to address above problems, continuous efforts have been made to promote the photocatalytic activity and expand visible light response range. Among them, addition of chemical additives, metal loading, metal ion doping, semiconductor composition, anion doping, dye sensitization, and suitable coupling of these modification methods, have been investigated, and proved to be effective to enhance H_2 generation or expand visible light response. Fundamental mechanisms, current research and development of these techniques are discussed in the following sections.

In most of the studies for photocatalytic H_2 production, activity of photocatalyst

was measured by H_2 evolution rate normalized by photocatalyst amount or reaction solution volume, with unit of μmol h^{-1} $g^{-1}_{catalyst}$ or μmol h^{-1} $ml^{-1}_{solution}$ (Choi et al., 2007; Wu et al., 2009; Gombac et al., 2010). For convenience, mmol or ml could also be used to describe H_2 evolution amount or volume, while unit of time could be in min, hence mmol h^{-1} $g^{-1}_{catalyst}$ and ml min^{-1} $g^{-1}_{catalyst}$ may also be seen in some studies to represent H_2 evolution rate (Galinska et al., 2005; Xu et al., 2009).

2.2.1 Methods to promote H_2 production

2.2.1.1 Addition of chemical additives

To improve the photocatalytic H_2 generation efficiency over TiO_2, many types of chemical additives have been studied aiming to suppress the rapid recombination of photo-induced electron/hole pairs. Among them, many kinds of electron donors, redox mediators, and carbonate salts were proved to be effective to enhance the H_2 generation efficiency over TiO_2.

Addition of electron donors (sacrificial reagents or hole scavengers) has been proven to be very useful since electron donors react irreversibly with photo-generated VB holes, leaving behind the strong reducing CB electrons to reduce protons into H_2 molecules (Shimura et al., 2011).

Various organic compounds (hydrocarbons) have been used as electron donors, such as common alcohol, aldehyde, organic acid, ketone, EDTA, etc. Since electron donors are consumed during reaction, continual addition of electron donors is required to sustain the H_2 generation. It would be highly benificial if the undesired organic pollutants can serve as electron donors, which means that photocatalytic decomposition of organic pollutants and H_2 production can take

place simultaneously. This process possesses great value since it is both environment-friendly and economy-friendly; it not only saves extra electron donors, but also decomposes pollutants, in addition, provides clean H_2 fuel. Some efforts have been put in this field: CN^- (Lee et al., 2001), Chloro-organics (Li et al., 2003; Li et al., 2006), azo-dye (Patsoura et al., 2006), fossil fuel (Hashimoto et al., 1984), biomass (Kondarides et al., 2008) and sewage sludge (Kida et al., 2004) have been tried as electron donors, and encouraging results have been found.

Several factors with regard to electron donors affect the enhanced H_2 generation activity, for instance, nature and initial concentration of electron donors, and mutual influence between donors etc.

Types of electron donor greatly influence the yield efficiency of H_2 generation. Sreethawong et al. (Sreethawong et al., 2007) found that alcohol species exhibited considerably higher photocatalytic activity than aldehyde, acid, and ketone species. They explained that this might be attributed to the ease of donating lone-pair electrons to the VB holes (Hameed et al., 2005), as compared to other kinds of sacrificial reagents. They also found that among the alcohol series, methanol was the most effective and strongest sacrificial reagent. It appears that compounds with very high polarity, such as ketones and acids, could not effectively suppress the electron/hole recombination, probably owing to their stable electronic configuration. Galinska et al. also found methanol was the most efficient sacrificial reagent for H_2 production compared with EDTA, Na_2S, and IO_3^-/I^- ions (Galinska et al., 2005). Li et al. reported the efficiency order of electron donors was $H_2C_2O_4$ > HCOOH > HCHO, which was consistent with the order of adsorption affinity of the electron donors on TiO_2 surface (Li et al., 2003). This suggested the linkage between the strength of surface interaction and the efficiency of H_2 evolution.

Initial concentration of electron donors (C) also affects photocatalytic H_2 generation rate (r), but different relationship between C and r was reported by different researchers. Some researchers found that H_2 evolution rate varied as a function of sacrificial reagent concentration in according to a Langmuir-type isotherm (Li et al., 2001; Li et al., 2006; Al-Mazroai et al., 2007; Strataki et al., 2007), resulting from active centres saturation on the limited quantity of photocatalysts. Sreethawong et al. reported that an optimum methanol concentration existed over Pt loaded mesoporous TiO_2, and excess methanol beyond its optimum concentration might block the adsorption of hydronium cations at surface active sites (Sreethawong et al., 2007). Patsoura and Kondarides demostrated that r increased linearly with increment of log C when they employed ethanol, glycerol and galactose as sacrificial reagent with concentration less than 1 M (Patsoura et al., 2007; Kondarides et al., 2008). This inconsistency requires further study.

Li et al. observed competitive inhibition kinetics when they studied photocatalytic H_2 production in a mixture system of electron donors (Li et al., 2003). However, if a donor adsorbed strongly on TiO_2 surface in a state of saturated adsorption in the mixture system, the overall rate of the H_2 evolution would be consistent with decomposition of this donor, and the mixture system could be treated as a single component system.

Unlike addition of electron donors, redox mediators are employed in a two-step water splitting system to mimic Z-scheme mechanism of photosynthesis as shown in Figure 2.11a. This reaction is probably a promising way to achieve photocatalytic water splitting under visible light since the two-step processes reduce the energy required for both oxidation and reduction processes, which can be found by comparison between Figures 2.11a and b. In the two-step system, on

the H_2 generation side, water is reduced to H_2 by photo-excited electrons, and the electron donor (D) is then oxidized by holes to become electron acceptor (A). On the O_2 evolution side, electrons reduce the A back to D, while holes oxidize water to produce O_2. Since H_2 and O_2 evolutions happen on different sites of photocatalyst, backward reaction of water formation from H_2 and O_2 can be suppressed. However, backward reactions still easily proceed over both sides of H_2 and O_2 formation, as shown in Figure 2.12. The reduction of the A to D, instead of reduction of H^+ to H_2, is a thermodynamically advantageous backward reaction, and will proceed preferentially when the concentration of A reaches a certain level. Oxidation of D to A, instead of O_2 formation, can occur as well. Therefore, to realize the two-step water splitting process, it is necessary to create the photocatalytic system with excellent selectivity for the forward reactions.

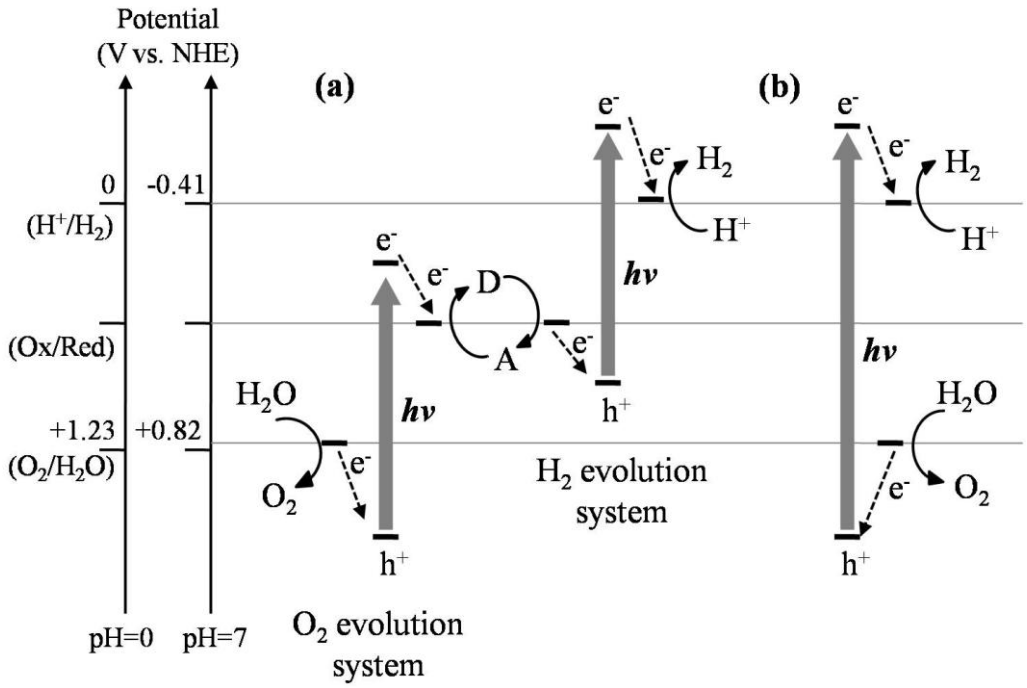

Figure 2.11 Conceptual scheme of water splitting systems: (a) two-step system and (b) one-step system (Abe et al., 2005).

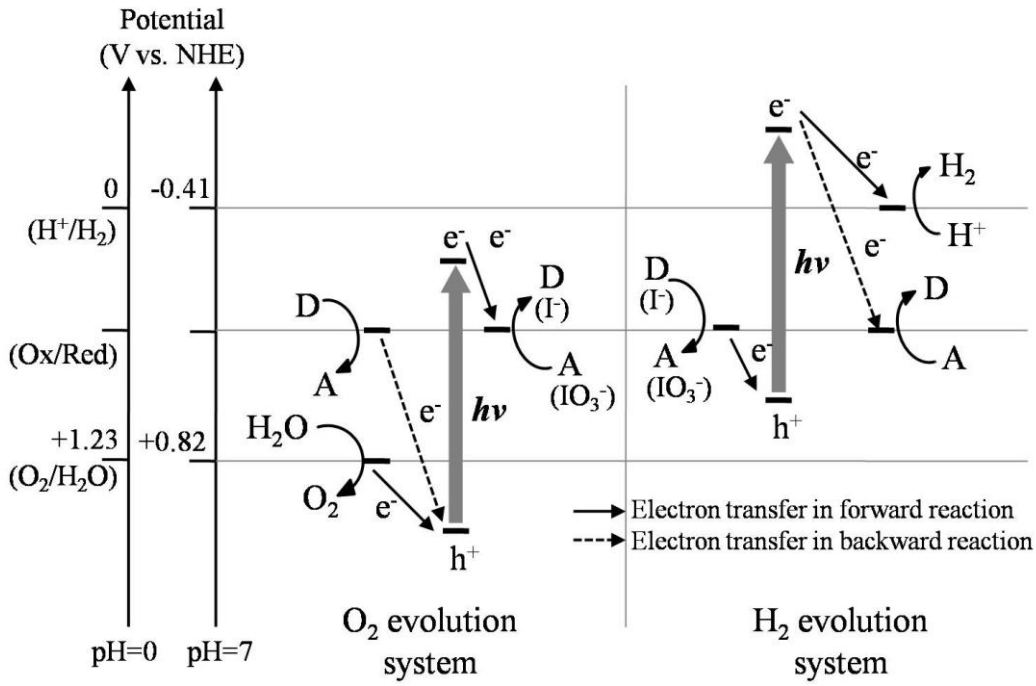

Figure 2.12 Forward and backward reactions in the two-step water-splitting system (Abe et al., 2005).

Abe et al., Fujihara et al. and Sayama et al. respectively employed IO_3^-/I^-, Fe^{3+}/Br^-, and NO_3^-/NO_2^- as redox mediators, and all obtained encouraging results (Fujihara et al., 1998; Abe et al., 2001; Sayama et al., 2001; Abe et al., 2003; Abe et al., 2005; Sayama et al., 2006). Abe et al. also found that I^- was adsorbed preferentially on Pt cocatalyst as iodine atom, and this iodine layer could effectively suppress backward reaction of water formation from H_2 and O_2. In Fujihara's study, oxidation and reduction reactions were carried out in the separate compartments which were combined via Pt electrodes and cation-exchange membranes (Figure 2.13). In this study, water was reduced to H_2 by Br^-, and oxidized to O_2 by Fe^{3+}. The reduced Fe^{2+} was then oxidized by Br_2 at the electrodes, and H^+ was transported through the membrane to maintain the electric neutrality and solution pH in the two compartments. As a result, H_2 and O_2 were continuously produced in the separated compartments, with large prevention of backward reaction of water

formation.

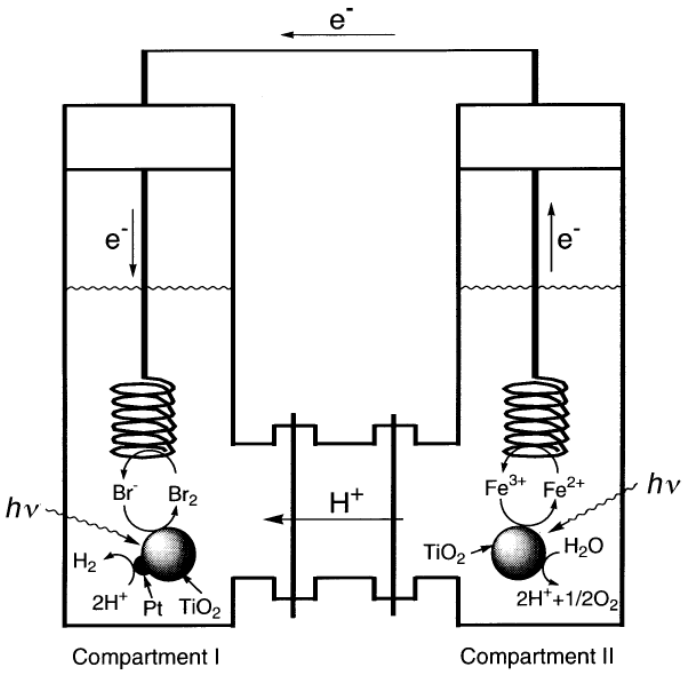

Figure 2.13 Schematics of the photocatalytic reaction cell employing Fe^{3+}/Br^- as redox mediators (Fujihara et al., 1998).

Addition of carbonate salts into reaction solution was also proved to be effective to enhance the stoichiometric water splitting efficiency of Pt-TiO_2 and Pt-ZrO_2 (H_2/O_2: 570/290 μmol h^{-1}, 610/320 μmol h^{-1}, for Pt-TiO_2 and Pt-ZrO_2, respectively) (Sayama et al., 1992, 1996, 1997; Arakawa et al., 2000). Researchers found that efficient water splitting was not directly contributed by solution pH or the presence of cations, but by a high concentration of carbonate ions. The carbonate ions affected both Pt particles and TiO_2 surface. With the presence of carbonate ions, Pt was covered by some titanium hydroxide compounds; therefore, rate of the backward reaction of water formation from H_2 and O_2 on Pt was suppressed effectively. On the other hand, the TiO_2 surface was covered by several kinds of carbonate species, which were supposed to aid desorption of O_2 from TiO_2 surface,

and minimize the formation of H_2O through the backward reaction. However, although carbonate ions enhanced H_2 generation activity to a high extent, mechanism has yet not been fully understood.

2.2.1.2 Metal loading

Metal (Pt, Au, Pd, Ni, Cu and Ag) loading, especially noble metal loading has been shown to be very effective to enhance photocatalytic activity of TiO_2 (Sato et al., 1980; Kim et al., 2002; Sakthivel et al., 2004; Wu et al., 2004). The enhancement was first observed in photo-conversion of water to H_2 and O_2 over Pt/TiO_2 system (Sato et al., 1980), which was studied more commonly later than other $metal/TiO_2$ system. Metal loading modifies the distribution of electrons within the semiconductor by forming Schottky barrier. When the two species come in contact, as the Fermi levels of metals are lower than that of TiO_2, photo-excited electrons in CB of TiO_2 are inclined to migrate to the deposited metal particles, leaving VB holes remaining in TiO_2. This greatly inhibits recombination of electron/hole pairs in TiO_2. Electron transfer from TiO_2 to metal particles (Pt) has been observed by Electron Spin Resonance (ESR) signal (Anpo et al., 2003). Anpo et al. found that Pt loading reduced the amount of Ti^{3+}, which would increase with irradiation time without contact with Pt. This result confirms the occurrence of electron transfer from TiO_2 to Pt particles. Accumulation of electrons on metal particles leads to a negative shift in Fermi level of metal (Subramanian et al., 2004), and the raised Fermi level further enhances electrons transfer to protons, and endows the deposited metal acting as an efficient proton reduction site.

Photocatalytic H_2 generation activity of metal loaded TiO_2 depends on many factors, for example, type of the metal, metal content, preparation method and calcination temperature etc.

Bamwenda et al. compared H_2 production over Pt-TiO_2 and Au-TiO_2 from ethanol solution (Bamwenda et al., 1995). They discovered that Pt-TiO_2 exhibited much better activity than Au samples. Boccuzzi et al. investigated the activity of Au, Ag, and Cu loaded TiO_2, and found that Ag sample was almost completely inactive, and Cu and Au samples showed intermediate and very high activity, respectively (Boccuzzi et al., 2001). The strong differences had been interpreted on the effect of co-adsorbed species, where catalyst possessed better adsorption ability of reagents led to higher H_2 generation activity.

Existence of optimal metal content on TiO_2 has been reported by many studies (Bamwenda et al., 1995; Sreethawong et al., 2007). Bamwenda et al. (1995) found that H_2 yield depended on metal content on TiO_2, and showed a maximum in the ranges of 0.3-1 wt% for Pt and 1-2 wt% for Au. Pichat et al. found that particle size of Pt on the TiO_2 surface showed a mean diameter of 2 nm with Pt content in range of 0.5-10 wt%; however, an optimum loading of Pt at concentration of 1.0 wt% was observed to achieve maximum photocatalytic H_2 generation rate (Pichat et al., 1982). The author deduced that neither morphological nor geometrical factor affected the photocatalytic properties of Pt-TiO_2, but an optimum Pt content determined the electrons distribution in the system. Attentions must be paid when a metal loaded photocatalyst is employed for study, and make sure that metal content in photocatalyst gives the optimum photocatalytic efficiency.

Preparation method is also very important for high photoactivity of metal loaded TiO_2. Bamwenda et al. (1995) reported that photoactivity of Au-TiO_2 strongly depended on the preparation method: photo-deposition method provided the most active sample, followed by deposition-precipitation, impregnation, and mixing TiO_2 directly with colloidal Au suspensions. Whereas, the activities of the Pt loaded samples were less sensitive to the fabrication methods. In addition, they

also reported that Au and Pt precursors calcined in open air at 573 K gave the highest photoactivity for H_2 generation, and photoactivity decreased with increasing calcination temperature.

It is worthy to note that although metal loading reduces recombination of electron/hole pairs to some extent, effective H_2 production from pure water splitting is still difficult to be achieved. On one hand, recombination of electron/hole cannot be completely eliminated; on the other hand, fast backward reaction of water formation from H_2 and O_2 is thermodynamically favorable, and significantly decreases the H_2 generation efficiency (Chen et al., 2010). Therefore, electron donors or other mediators are required.

Noble metals loading on TiO_2 are highly effective to enhance H_2 production; however, considering the high cost, inexpensive metals with acceptable enhancement activity are needed to be investigated. Wu et al. reported that the cost-effective Cu incorporated TiO_2 exhibited up to ten-fold enhancement at the optimum Cu loading of about 1.2 wt% (Wu et al., 2004). Other metals, such as Ag and Ni, were also found to be effective to enhance the photocatalytic activity. These cost-effective metals loaded TiO_2 are expected to be promising materials for practical applications.

2.2.1.3 Metal ion doping

Transitional metal ion and rare earth metal ion doped TiO_2 have been extensively studied to enhance photocatalytic activity of TiO_2 (Martin et al., 1994a; Chen et al., 2002a; Di Paola et al., 2002; Dvoranova et al., 2002; Xu et al., 2002; Nagaveni et al., 2004). It was reported that metal ions doping could influence interfacial electron transfer rates, electron/hole recombination, light response, and

significantly affected the photocatalytic activity of TiO_2. In the metal doped TiO_2, metal ion dopants acted as either electron or hole traps and altered the electron/hole recombination rate through the following processes (Moser et al., 1987; Gratzel et al., 1990):

Electron trap: $M^{n+}+e_{cb}^{-}\rightarrow M^{(n-1)+}$ (2-13)

Hole trap: $M^{n+}+h_{vb}^{+}\rightarrow M^{(n+1)+}$ (2-14)

Where the energy level for $M^{n+}/M^{(n-1)+}$ should lie below CB edge of TiO_2 and $M^{(n+1)+}/M^{n+}$ above VB edge of TiO_2. In addition, introduction of metal ion energy levels into band gap of TiO_2 could cause red shift of light absorption, which is attributed to the charge transfers between the d/f electrons and the TiO_2 conduction or valence band (Borgarello et al., 1982; Martin et al., 1994a).

Photoactivity of metal doped TiO_2 appears to be a complex function of the dopants' nature and concentration, and the preparation procedure etc.

Choi et al. presented a systematic investigation on the effects of 21 different metal ion dopants on the photocatalytic activity of quantum-size TiO_2 (Choi et al., 1994). Doping with Fe^{3+}, Mo^{5+}, Ru^{3+}, Os^{3+}, Re^{5+}, V^{4+}, and Rh^{3+} at content of 0.1-0.5 atom% significantly enhanced the photoactivity of TiO_2 for both oxidation and reduction, whereas Co^{3+} and Al^{3+} doping decreased the photoactivity. The different photoactivities were supposed to be related with the efficiencies of the dopants in charge carriers trapping and interfacial charge transfer mediation. Choi et al. summarized the effect of dopant energy levels on photoactivity: first, active dopants should act as both electron and hole traps (Choi et al., 1994). Trapping only electron or hole was ineffective because the trapped charge species would quickly recombined with its mobile counterparts. That was the reason for

substantially different photoactivity of Fe^{3+} and Cr^{3+} doped TiO_2 since Fe^{3+} could trap both electron and hole, meanwhile, Cr^{3+} only trapped hole, even though both ions have similar energy levels and ionic radii, and identical oxidation states. The second requirement for an effective dopant might relate with the possibility of charge de-trapping and migration to the surface with previously trapped charges. The low photoactivity of Mn^{3+} doped TiO_2 could be assigned to the small energy difference between Mn^{2+} and Mn^{3+}, which gave low driving force for electron to de-trap from Mn^{2+}.

Choi et al. also found that all dopants showed an optimum concentration with the highest quantum yields at 0.5 atom%. They explained that recombination of the trapped charge carriers depended on the distance separating the electron/hole pairs, and the recombination rate increased exponentially with increment of dopant concentration. But, at lower concentrations, photoactivity increased with dopant concentration increasing since more charge trapping sites appeared. Therefore, the existence of an optimal dopant concentration in TiO_2 could be explained by the balance of enough trapping sites leading to efficient trapping and enough trapped carriers for effective interfacial charge transfer. Choi et al. also reported that all the doped TiO_2 gradually lost their photoactivity as the calcination temperature increased. Since the small Q-sized particles agglomerated upon heating, metal dopants were isolated far from the surface, led to less chance for trapped charge carriers to be transferred to the interface. The dopants were more likely to act as a recombination center other than effective charge trapper for eventually interfacial charge transfer.

Xu et al. carried out a comparative study on the photocatalytic activity of rare earth metal doped TiO_2 (Gd^{3+}, Nd^{3+}, La^{3+}, Pr^{3+}, Er^{3+}, Ce^{3+}, Sm^{3+}), and found the formation of mixed RE/TiO_2 photocatalysts could enhance photocatalytic activity

of TiO_2 (Xu et al., 2002). The increase in activity was probably owing to prevention of electron/hole recombination. In RE/TiO_2, Ti atom could enter the lattice of rare earth metal since ionic radius of Ti^{4+} is much smaller; this created a charge imbalance (Ti^{4+} instead of RE^{3+}), and led to more hydroxide ions adsorbed onto photocatalyst surface. These adsorbed hydroxide ions could accept holes, thus suppressed the photo-induced charge carriers recombination. Among all investigated samples, Gd^{3+}-doped TiO_2 showed the highest activity because of the increase in the interfacial electron transfer rate. They also reported that the highest enhancement in photoactivity was obtained when dopant content was at 0.5 wt%, which might involve the most efficient charge carrier separation. Excess amounts of rare earth metal doing in TiO_2 would increase the number of recombination centers and depress the photoactivity.

2.2.1.4 Composite semiconductor

Large band gap materials, such as TiO_2, ZnO, and $SrTiO_3$, possess good photo-stability but only utilize limited solar energy, leading to low photocatalytic efficiency under sun light. Meanwhile, materials with small and medium band gaps, such as CdS, CdSe, and Cu_2O can harvest visible light, but suffer from severe photo anodic corrosion. Composite (coupling) semiconductors with two or more semiconductors of different band gaps and band positions provide an effective method to overcome these drawbacks: composite semiconductors can not only be induced by visible light, but also conquer the photo-corrosion. When a large band gap semiconductor is coupled with a small band gap semiconductor with a more negative CB level, the excited CB electrons of small band gap semiconductor can then be injected into the large one, leading to effective charge separation. Schematics of charge transfer in composite semiconductor is shown in Figure 2.14.

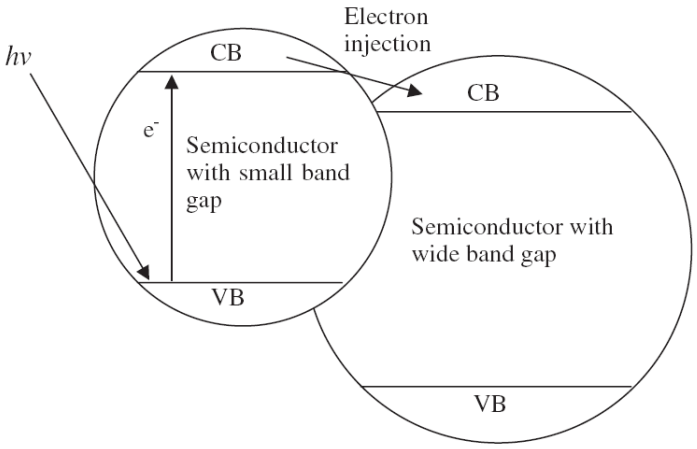

Figure 2.14 Schematics of charge separation in composite semiconductors (Ni et al., 2007).

To serve as a successful coupling semiconductor for efficient photocatalytic H_2 production under visible light irradiation, several requirements need to be met: (1) the fabricated composite semiconductor should be anti-photo-corrosion; (2) the small band gap semiconductor should be excited by visible light; (3) CB level of small band gap semiconductor should be higher than that of the large band gap semiconductor; (4) CB level of the large band gap semiconductor should be more negative than water reduction potential, and (5) electron injection should be both fast and efficient (Ni et al., 2007).

Many factors, such as, coupling ratio of semiconductors, fabrication method and nature of supporting materials etc. have been proved to affect the photoactivity of composite semiconductors.

Existence of optimum coupling ratio has been proved by many researchers. So et al. found that photocatalytic H_2 generation rates varied along with different mole ratio of CdS and TiO_2, when he conducted H_2 production test over CdS-TiO_2 composite particulate film (So et al., 2004). Optimum mole ratio of CdS/TiO_2 was 1:4, which

was in consistent with the photocurrent trend of the composite semiconductor. This suggested that effective distribution and contact between the particles was quite important. In Jang's study, the optimum molar concentration of TiO_2 in CdS (bulk)/TiO_2 composite photocatalyst was determined to be 0.67 (Jang et al., 2007).

Fabrication method determines the physical properties of photocatalyst such as crystallinity, size and morphology etc., which, therefore, significantly influence the photoactivity of composite semiconductor. Jang et al. found fabrication method of the CdS/TiO_2 composite photocatalyst was critical for their performance (Jang et al., 2006; Jang et al., 2007). CdS/TiO_2 nano-bulk composite photocatalyst comprising bulky CdS decorated with high crystallinity nanosized TiO_2 particles exhibited very high activity for H_2 production under visible light ($\lambda \geq 420$ nm). This photocatalyst was more active than other configurations of the composite, i.e., nano-CdS/bulk-TiO_2 or nano-CdS/nano-TiO_2 co-precipitates. In addition, good crystallinity of CdS was more important than that of TiO_2 in the composite configuration.

The property of supporting material also plays important roles in H_2 production over composite semiconductors. Subrahmanyam et al. investigated the effect of basic/acidic (MgO/Al_2O_3) supports on H_2 generation activity over CdS based photocatalysts from S^{2-}/SO_3^{2-} substrate (Subrahmanyam et al., 1996). They found that activity of supported CdS-based photocatalysts increased when MgO served as support. The improvement was attributed to the basic nature of the support and the excellent heterojunction that was developed. Tambwekar et al. also studied H_2 production with (CdS-ZnS)-TiO_2 composite semiconductor over different supports such as MgO, CaO, γ-Al_2O_3, SiO_2 and modified MgO and CaO (Tambwekar et al., 1999). They also found that MgO system gave the maximum H_2 production, and this photocatalyst could sustain long time reaction due to the formation of

thiosulfate cycle.

Other modification methods could also be applied to composite semiconductor to improve H_2 generation activity. Jang et al. employed noble metals loading for CdS/TiO_2 composite semiconductor, and found different metal co-catalysts exhibited a significant difference in H_2 generation activity (Pt>Rh>Pd>Ru), and an optimum amount of metal co-catalyst existed, for example, 0.75 wt % for Pt (Jang et al., 2007). Peng et al. reported that SiO_2-Pt-CdS composite photocatalyst showed high stability and photocatalytic activity for H_2 production (Peng et al., 2008). So et al. found that, for CdS/TiO_2 composite photocatalyst, surface treatment with $TiCl_4$ aqueous solution significantly enhanced the photocatalytic activity, probably due to the closer contacts between the primary particles induced by the etching effect of $TiCl_4$ (So et al., 2004). Subrahmanyam et al. reported that addition of ZnS or Ag_2S to CdS was also beneficial for H_2 evolution over MgO-supported system (Subrahmanyam et al., 1996).

It is worthy to note, CdS as photocatalyst is commonly employed in composite semiconductors, where S^{2-} and/or SO_3^{2-} are usually used as sacrificial reagents to prevent the photo-corrosion of CdS. This possesses great potential for practical applications. In Jang's study, CdS/TiO_2 composite photocatalyst could achieve simultaneous H_2 production and H_2S removal from the treatment of Claus plant tail-gas stream or vents of hydrodesulfurization plants (Jang et al., 2006). It is a quite interesting process, since it achieved energy production and pollutant removal concurrently.

2.2.1.5 Anion doping

Anion doping (N, C, S, F etc.) has been proved to be highly efficient to expand

light absorption of TiO_2 into visible region. Unlike metal ions, anions are less likely to form recombination center. Asahi et al. set following requirements for efficient anion doping for H_2 production: doping should create states in the band gap of TiO_2 to absorb visible light; CB should be negative enough to reduce H_2O; the new states in the gap should sufficiently overlap with the band states of TiO_2 to ensure efficient transfer of photo-excited charge carriers to reactive sites within their lifetime (Asahi et al., 2001). They calculated that nitrogen doping was most effective because its *p* states contributed to the band gap narrowing by mixing with O 2p states; whereas, sulfur was difficult to be incorporated into TiO_2 because of its large ionic radius; meanwhile, new states created by carbon and phosphor doping were too deep in the gap to satisfy the third condition.

In accord with the calculation results of Asahi, N has been proved to be an effective anion dopant, and can be successfully prepared by several methods. Asahi et al. (Asahi et al., 2001) first synthesized N doped TiO_2 by sputtering the TiO_2 target in an N_2/Ar or NH_3/Ar gas mixture, and dominant transitions at absorption edge of the fabricated samples were observed from N 2p to Ti 3d, instead of from O 2p as in TiO_2. They found that $TiO_{2-x}N_x$ samples showed superior photocatalytic activity than TiO_2 under visible light irradiation, although both samples yielded similar UV activity. Besides gas calcination, either direct amination of TiO_2 particles or direct heating the mixture of urea with TiO_2 successfully fabricated $TiO_{2-x}N_x$ with light absorption spectrum up to 600 nm (Burda et al., 2003; Yuan et al., 2006). Yang et al. synthesized a novel Pt-$TiO_{2-x}N_x$-WO_3 by template method, absorption edge of which was red-shifted to around 750 nm (Yang et al., 2006). With Na_2S/Na_2SO_3 as the sacrificial reagents, the composite photocatalyst showed even higher H_2 generation activity than anatase TiO_2 under UV irradiation; under visible light ($\lambda > 400$ nm), Pt-$TiO_{2-x}N_x$-WO_3 showed higher H_2 generation activity than $TiO_{2-x}N_x$, meanwhile pure anatase TiO_2 showed negligible activity. This

novel photocatalyst combined several modification methods: Pt loading, WO_3/TiO_2 composite semiconductor, and nitrogen doping. Charge transfer in the composite photocatalyst is proposed as in Figure 2.15: new energy states of N 2p above VB of TiO_2 (O 2p) and composite WO_3 both contributed to the red shift of light absorption; while Pt served as H_2 reduction site due to lower Fermi level compared to TiO_2, which has been discussed in the "Metal loading" part.

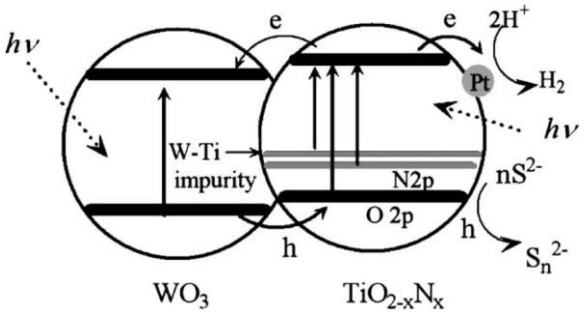

Figure 2.15 Schematic charge transfer in Pt-$TiO_{2-x}N_x$-WO_3 composite photocatalyst (Yang et al., 2006).

Besides nitrogen doping, carbon and sulfur doped TiO_2 were also found to possess exciting photocatalytic activity, which is contrary to Asahi's calculation.

Khan et al. first reported efficient photochemical water splitting by carbon doped TiO_2 (CM-n-TiO_2), maximum photo conversion efficiency of which was 8.35% when illuminated at 40 mW cm^{-2}, and the efficiency did not decrease during tests over a period of 6 months (Khan et al., 2002; Xu et al., 2007). In the CM-n-TiO_2 sample, carbon substituted some of the lattice oxygen atoms; hence a new intra-gap band was introduced into band gap of TiO_2 (shown in Figure 2.16), and extended the light utilization into visible region. In addition, they found fabrication method was quite important for efficient CM-n-TiO_2; sample prepared by controlled combustion of Ti metal in natural gas flame showed much higher

photoactivity than that prepared in electric tube furnace. Wet process was also successfully employed to synthesize active CM-n-TiO_2. During that preparation, $TiCl_4$ was first hydrolysis in the presence of glucose and NaOH, followed by extended aging and subsequent calcinations (Xu et al., 2006). The prepared CM-n-TiO_2 absorbed light well up to 800 nm, and exhibited enhanced photocatalytic activity under visible light.

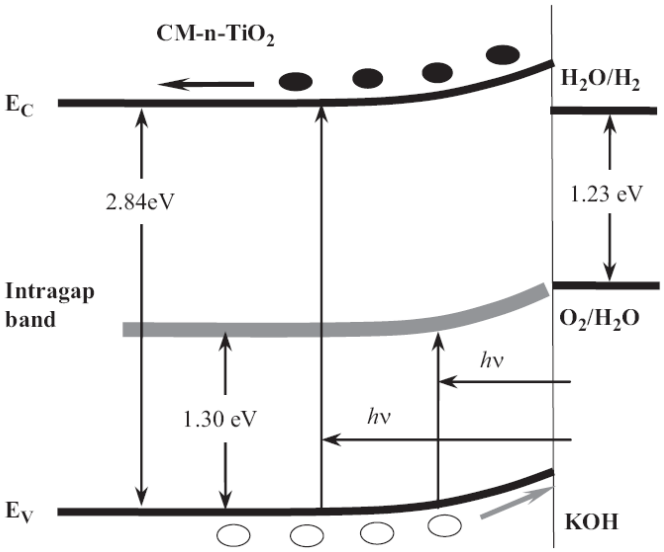

Figure 2.16 Schematic diagram of band gap structure of CM-n-TiO_2 (Xu et al., 2007).

Randeniya et al. prepared sulfur doped TiO_2 from three powders followed by heat treatment: ball milling sulfur powder with P25; ball milling thiourea with P25; sol-gel technique involving titanium butoxide and thiourea (Randeniya et al., 2008). They found light absorption of all prepared samples extended into visible region, and all samples exhibited satisfactory photocatalytic H_2 generation activity.

2.2.1.6 Dye sensitization

Dye sensitization is an important subject to explore the utilization of TiO_2 under visible light for both energy conversion and pollutant decomposition. Some dyes with redox property and visible light sensitivity can be employed to prepare the dye-sensitized TiO_2, charges transfer inside of which are illustrated in Figure 2.17. Under visible light illumination, dye molecules attached on TiO_2 surface would be excited, and subsequently inject the electrons into CB of TiO_2 to initiate the interfacial chemical reaction. The CB electrons can then be transferred to noble metal particles (Pt) loaded on the surface of TiO_2 to conduct water reduction. In order to regenerate dye, redox systems or sacrificial reagents, such as I_3^-/I^- pair (Abe et al., 2004) and EDTA (Hirano et al., 2000), can be added to the system to sustain the reaction cycle.

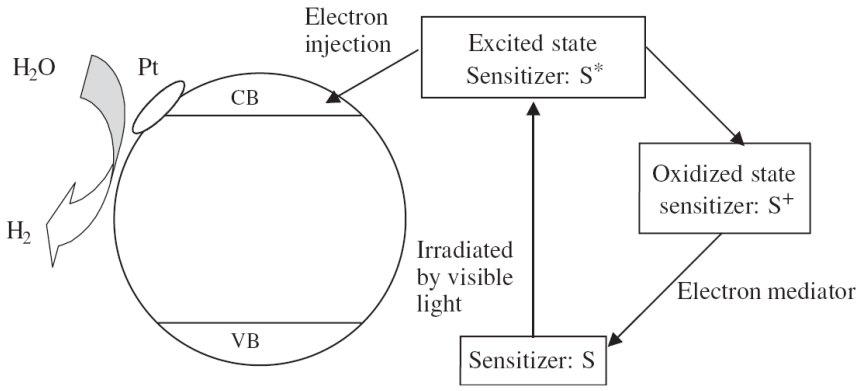

Figure 2.17 Mechanism of dye-sensitized photocatalytic H_2 generation under visible light irradiation (Ni et al., 2007).

Some of the frequently used dyes are listed in Table 2.3 with their maximum absorption wavelength.

Table 2.3 Frequently used dyes and absorption wavelength maxima λ_{max} (Jana, 2000).

Dye	Class	λ_{max} (nm)
Thionine (TH^+)	Thiazines	596
Toluidine blue (Tb^+)	Thiazines	630
Methylene blue (MB)	Thiazines	665
New methylene blue	Thiazines	650
Azure A	Thiazines	635
Azure B	Thiazines	647
Azure C	Thiazines	620
Phenosafranin (PSF)	Phenazines	520
Safranin-O (Saf-O/SO)	Phenazines	520
Safranin-T (Saf-T/ST)	Phenazines	520
Neutral red (NR)	Phenazines	534
Fluorescein	Xanthenes	490
Erythrosin	Xanthenes	530
Erythrosin B	Xanthenes	525
Rhodamine B (Rh. B)	Xanthenes	551
Rose bengal	Xanthenes	550
Pyronine Y (PY)	Xanthenes	545
Eosin	Xanthenes	514
Rhodamine 6G	Xanthenes	524
Acridine orange (AO)	Acridines	492
Proflavin (PF)	Acridines	444
Acridine yellow (AY)	Acridines	442
Fuchsin	Triphenyl methane derivatives	545
Cystal violet	Triphenyl methane derivatives	578
Malachite green	Triphenyl methane derivatives	423, 625
Methyl violet	Triphenyl methane derivatives	580

Adsorption of sensitizer on TiO_2 surface is a prerequisite for visible light adsorption and photoactivity enhancement, and both sensitizer concentration and solution pH affect the effective adsorption of sensitizer. Dhanalakshmi et al. confirmed that addition of sensitizer ($[Ru(dcbpy)_2(dpq)]^{2+}$) to Pt/TiO_2 led to efficient H_2 generation under visible light irradiation, and increment of sensitizer concentration caused H_2 generation rate increase to a maximum and then leveled off, due to limited adhering site for sensitizer on TiO_2 surface (Dhanalakshmi et al., 2001). Hirano et al. reported that high concentration of $Ru(bpym)_3^{2+}$ was required to achieve the effective photo-sensitization when they studied H_2 production with EDTA as sacrificial reagent; meanwhile, pH 7 was the optimum condition for H_2 generation, which favored the adsorption of sensitizer on TiO_2 surface (Hirano et al., 2000). Li et al. obtained similar result when they conducted H_2 production on Eosin Y-sensitized Ti-MCM41 zeolite under visible light irradiation (Li et al., 2007). They found that amount of dye molecule adhered to zeolite significantly affected the H_2 generation rate, and H_2 generation rate in the neutral or weak acidic environment was much faster than in a basic solution, due to high adsorption of dye on the catalyst surface in the former environment.

Direct mixture of dye with TiO_2 exhibited H_2 generation activity under visible light; however, H_2 evolution rate was not stable due to the unstable ester-like linkage between dye and TiO_2. In order to overcome the instability, Abe et al. attempted a strong chemical fixation of dye on TiO_2 surface by employing dehydration of carboxyl group of xanthene dye with amino group of silane-coupling reagent fixed on TiO_2 surface (Abe et al., 2000); consequently, a stable and efficient photocatalyst for H_2 production was obtained.

The property of sensitizer is another important factor that affects photoactivity of dye-sensitized photocatalyst. Nada et al. compared the effect of different

sensitizers, and found copper phthalocyanine exhibited higher efficiency than ruthenium bipyridyl and Eosin Y, in photocatalytic H_2 production with methyl viologen (MV^{2+}) as electron relay under solar irradiation (Nada et al., 2008).

Dye-sensitized TiO_2 also exhibited excellent photocatalytic activity for pollutants degradation. Bae et al. employed $Pt/TiO_2/Ru^{II}L_3$ to degrade trichloroacetate (TCA) and carbon tetrachloride (CCl_4), and observed drastic enhancement (Bae et al., 2003). In addition, although no electron donors were present in solution to regenerate the oxidized Ru-sensitizers, the photocatalytic dechlorination of perchlorinated compounds could proceed far beyond the stoichiometric limit of the initial sensitizer concentration. The researchers explained that water acted as the electron donor to regenerate the sensitizer, along with a concurrent production of O_2.

2.2.2 Cu incorporated TiO_2

As discussed earlier in Chapter 2, most of the reported high efficiency H_2 productions use Pt to modify TiO_2 photocatalyst. However, considering the high costs of noble metals, investigation of substitutional metals with high activity is urgently needed. Cu is therefore, identified as one of the excellent candidates with high availability and relatively lower cost.

Cu incorporated photocatalysts have been proved to be active and widely applied in reduction of NO to N_2 (Boccuzzi et al., 1994; Aritani et al., 1996), reduction of CO_2 to produce methanol (Yamashita et al., 1994; Bando et al., 1997), complete oxidation of CO (Larsson et al., 1998), and oxidation of organic pollutants, such as, toluene, ethanol, ethyl acetate (Larsson et al., 1998), phenol (Colon et al., 2006; Kim et al., 2007) and cyanide (Chiang et al., 2002).

Recently, some researchers tried using Cu-TiO_2 for photocatalytic H_2 production, and found this type of photocatalysts showed high photocatalytic activity enhancement similar with noble metal loaded TiO_2. Boccuzzi et al. compared photocatalytic activity of Au, Ag, and Cu incorporated TiO_2 for H_2 production by CO water gas shift reaction, and found that silver catalyst exhibited no catalytic activity; nevertheless, Cu and Au showed intermediate and very high performances, respectively (Boccuzzi et al., 1994). Sreethawong et al. carried out comparative investigation on photocatalytic H_2 evolution over Cu-, Pd-, and Au-loaded mesoporous TiO_2 photocatalysts (Sreethawong et al., 2005). H_2 evolution rates at their optimum contents for Cu, Pd, and Au loading were 360, 420, and 557 μmol h^{-1}, respectively. Although lower H_2 evolution rate was observed over Cu-TiO_2, it is of great interest if the economical viewpoint is taken into account. They also found that, compared with optimum value of Ni-loaded TiO_2, Cu-TiO_2 showed approximately two folds higher in H_2 evolution activity.

All chemical states of Cu (Cu/Cu_2O/CuO) have been studied for the enhancement of H_2 production from water reduction.

Wu et al. reported the enhanced TiO_2 photocatalysis by Cu in H_2 production from aqueous methanol solution (Wu et al., 2004). Chemical state of Cu deposited on TiO_2 in their study was metallic Cu, which was reduced by H_2 before water decomposition. During photocatalysis, Cu was oxidized. They reported that the oxidized Cu species was active for photocatalysis, and the oxidation of Cu occurred during reaction showed high activity than exterior oxidation processes, such as oxidation by prolonged exposure in air and heat treatment in air at 400 ℃. They also found that Cu doped TiO_2 with Cu dissolved into TiO_2 lattice showed a negative effect on the overall photocatalytic activity comparing to Cu deposited TiO_2.

Hara et al. revealed that Cu_2O powder was able to split water into H_2 and O_2 under visible light irradiation (Hara et al., 1998). They observed that Cu_2O was neither reduced nor oxidized during photocatalytic water decomposition. These result indicated the photocatalytic reaction on Cu_2O particle in distilled water was different from the photoelectrochemical reaction on the polarized Cu_2O electrodes in aqueous electrolyte, where Cu_2O electrode underwent photo-degradation.

Bandara et al. reported that CuO incorporated TiO_2 was active for reduction of H_2O under sacrificial conditions (Bandara et al., 2005). Both amount and crystalline structure of CuO were found to be crucial for the photocatalytic activity: the optimum CuO loading was about 5-10 wt%, and maximum H_2 generation rate was observed at sintering temperature of about 300-500 ℃. They found that accumulation of byproducts on the photocatalyst surface during photocatalysis would cause decrease in photocatalytic activity, but the original photocatalytic activity could be regained once the photocatalyst was subjected to a heat treatment regeneration, during which the accumulated byproducts were removed without altering the surface properties of photocatalyst. No copper was detected in the reaction solution even after several hours' reaction, indicating that the CuO-TiO_2 photocatalyst was highly stable. Kang's group also studied H_2 production over CuO-TiO_2 photocatalyst (Choi et al., 2007; Jeon et al., 2007). They reported that H_2 production was remarkably enhanced by CuO-TiO_2 compared to pure TiO_2. In their study, the preparation method of CuO-TiO_2 had significant effect on photocatalytic activity enhancement. Photocatalyst prepared by conventional impregnation method with most CuO deposited on the external surface of anatase TiO_2 structure gave H_2 evolution of 13500 μmol after methanol/water photo-decomposition for 10 h over the optimum 10 mol% Cu-TiO_2 photocatalyst. Cu-TiO_2 prepared by conventional sol-gel method with Cu might enter lattices of TiO_2, showed biggest H_2 evolution of 16520 μmol after 24 h reaction with rutile

TiO_2. The different activities caused by different preparation method appeared also in Wu's study (Wu et al., 2004), but the reason is still not understood thoroughly. Opposite to Bandara's stable photocatalyst, in Kang's study, CuO component was reduced to either Cu_2O or Cu, which was supported by XRD and XPS results.

Dye sensitization could further enhance the photocatalytic H_2 generation activity of Cu-TiO_2 under visible light irradiation. Jin et al. studied the combination of eosin sensitization with CuO-TiO_2 photocatalyst (Jin et al., 2007), and significant enhancement of apparent quantum yield (5.1%) and good stability were observed over the dye-sensitized 1.0 wt% CuO-TiO_2 photocatalyst. The activity of eosin sensitized CuO-TiO_2 benefited from strong adsorption of eosin, and efficient electron transfer and charge separation. On one hand, addition of CuO greatly improved the adsorption capacity of TiO_2 towards eosin dye by multidentate complexation; on the other hand, the electrons which were excited from the sensitizer molecules by the visible light could inject into CB of both TiO_2 and CuO, and the electrons in CB of TiO_2 subsequently transferred to CB of CuO, which resulted in a build-up of excess electrons, and caused a negative shift in the Fermi level of CuO. As a result, CuO served as active H_2 reduction site, resulting in efficient photocatalytic activity.

Photocatalytic performance of the Cu-TiO_2 is strongly dependent on the preparation method, preparation procedure, chemical property and Cu content etc. In the above discussions, we have mentioned the different photocatalytic activity of "loaded" and "doped" Cu-TiO_2 in both Wu and Kang's studies. Boccuzzi et al. compared characteristics of Cu-TiO_2 prepared by wet impregnation and chemisorptions-hydrolysis, and found that samples with same chemical compositions could have very different properties: different behaviors under electron beam, different peak positions and widths in temperature programmed

reduction (TRP) profiles, and different FTIR data (Boccuzzi et al., 1997). Tseng et al. reported three factors --- copper precursor type, adding time with sol, and post-treatments --- heavily affected characteristics and activity of the Cu-TiO_2 photocatalyst prepared by modified sol-gel process (Tseng et al., 2004). They revealed that Cu-TiO_2 prepared from $CuCl_2$ and added in the early stage of sol-gel process was more photoactive than that fabricated from copper acetate since $CuCl_2$ precursor increased the Cu dispersion. They also found, additional H_2 reduction of calcined photocatalysts before photocatalytic reaction decreased the yield due to change of Cu dispersion and oxidation state. In addition, for high H_2 generation activity, both Bandara and Kang reported the existence of optimum Cu content in their separate studies, as mentioned before. Bandara also recommended suitable sintering temperature to achieve high photocatalytic activity of Cu-TiO_2.

It is necessary to discuss the stability of Cu-TiO_2 in photocatalytic reactions, since good stability of photocatalyst and photocatalytic activity is a prerequisite for an excellent photocatalyst. It is a common problem that non-noble metals, for example, Cu, leach out from metal-modified TiO_2 in PEC process or other liquid media reaction, resulting in a poor stability of the metal-modified TiO_2 (Kim et al., 2001; He et al., 2005; Nguyen et al., 2008; Gombac et al., 2010). For Cu-TiO_2 in photocatalytic H_2 production, some researchers deemed that Cu-TiO_2 possessed excellent stability without leaching into the reaction medium due to an efficient inter-particle charge transfer process (Bandara et al., 2005; Jin et al., 2007); however, some other researchers observed Cu leaching and changes in the chemical states of Cu from their studies (Choi et al., 2007; Gombac et al., 2010; Lalitha et al., 2010). In order to explore the potential of Cu-TiO_2 in photocatalytic H_2 production, further investigation on stability of Cu-TiO_2 is necessary owing to the diverse observations and opinions presented in open literature.

2.2.3 Factors influencing photocatalytic H_2 production

As mentioned above, photocatalytic activity of photocatalyst for H_2 production can be affected by many factors such as preparation method (Section 2.2.1.2 - 4, Section 2.2.2), modification method (Section 2.2.1.4, Section 2.2.2), calcination temperature (Section 2.2.1.2, Section 2.2.2), nature and content of loaded metal (Section 2.2.1.2 - 3, Section 2.2.2), coupling ratio of composite semiconductors (Section 2.2.1.4), and nature of sensitizers (Section 2.2.1.6), all of which should be considered for efficient H_2 production.

In terms of electron donors, photocatalytic H_2 production could be influenced by the nature and initial concentration of sacrificial reagents, and mutual influence between the donors. This has been discussed in Section 2.2.1.1.

In addition, operational conditions, for instance, pH and temperature of solution, photocatalyst concentration, light intensity, and presence of inorganic ions in the system etc., can influence H_2 production as well.

Reaction system pH can affect semiconductor's surface charge state, energy band edge, and interaction and affinity between TiO_2 and electron donors (Sreethawong et al., 2007; Chiou et al., 2008; Wu et al., 2009). It is reported that mild and neutral pH conditions were usually favorable for photocatalytic H_2 production; whereas, strong basic or acidic pH conditions would result in lower H_2 generation activity, since such pH conditions inhibited the adsorption of sacrificial reagent (and/or H^+) onto TiO_2 surface, or induced lower stability of photocatalyst (Sreethawong et al., 2007; Wu et al., 2009).

Dosage of photocatalyst is an important parameter in suspended photocatalytic process. For photocatalytic H_2 production, it is reported that H_2 generation rate

first increased and then decreased with the increment of photocatalyst dosage (Sreethawong et al., 2007; Wu et al., 2009). Adequate dosage of photocatalyst increases the availability of active sites, but an excess dosage of photocatalyst blocks light illumination, decreases light penetration via shielding effect of the suspended particles and therefore, inhibits light absorption of TiO_2, leading to a lower H_2 generation activity (Sreethawong et al., 2007; Chiou et al., 2008; Wu et al., 2009). No universal optimum dosage was reported to date, and it should be experimentally determined for specific photocatalyst and conditions.

The optimum temperature for photocatalytic reaction is reported between 20 ℃ to 80 ℃, where lower or higher temperature would decrease the photocatalytic activity (Herrmann, 1999). Within the optimum temperature range, increase of temperature favored the reaction due to more e^-/h^+ utilization other than recombination (Reutergardh et al., 1997).

Light intensity is proven to establish a positive effect on photocatalytic reaction (Chiou et al., 2008). With increase of light intensity, photocatalytic reaction rate is proportional to the radiant flux (Φ), which confirms the photo-induced nature of the photocatalytic process. However, when radiant flux is above ca. 25 mW/cm^2, the reaction rate becomes proportional to $\Phi^{1/2}$ (Herrmann, 1999).

Effect of inorganic ions in solution on photocatalytic H_2 production was investigated by some researchers, and presence of SO_4^{2-} and $H_2PO_4^-$ were reported to reduce the H_2 generation rate to an extent of 30-70%, which can be attributed to strong adsorption of the anions on TiO_2 surface, thus hampering adsorption of sacrificial reagents (Li et al., 2001). Wiszniowski et al. also observed the inhibition effect of HCO_3^- in photocatalytic reaction, due to pH shift by introduction of HCO_3^- salt. (Wiszniowski et al., 2004).

Apart from the factors mentioned above, there may be other parameters which would influence H_2 generation activity of photocatalyst; therefore, it is significantly important to optimize fabrication and operating conditions to attain the maximum potential of H_2 generation activity from a specific photocatalyst.

2.2.4 Summary

In summary, it can be found that there are several effective modification methods for TiO_2 to enhance its H_2 generation activity, but noble metal loading with high costs appears to be indispensable in most of the modifications. Cu is reported to possess excellent activity enhancement for TiO_2, and it may play the role to substitute the noble metals. So far there is little information about H_2 production utilizing Cu-TiO_2 photocatalyst. No systematic investigations about its optimum operation conditions and effect of fabrication methods could be found. In addition, highly efficient TiO_2 nanotube has exhibited great potential in many applications; however, attempt to utilize TNT for photocatalytic H_2 production is rare, while the report of utilization of Cu-TNT is not available from literatures. In order to provide cost-effective H_2 source for the mitigation of climate changes caused by the greenhouse gases generated from the combustion of fossil fuels, there is a need to study the novel Cu-TiO_2 photocatalyst, especially Cu-TNT, for photocatalytic H_2 production with the optimal operation conditions. This requires more systematic investigations, which will pave way for the future industrial application of photocatalytic H_2 production using the novel and highly efficient Cu-TiO_2 photocatalyst.

CHAPTER 3

OPTIMAL OPERATION CONDITIONS AND ACTIVITY MAINTENANCE OF Cu-TiO_2 IN PHOTOCATALYTIC H_2 PRODUCTION

3.1 Introduction

The literature reviews presented in Chapter 2 clearly indicated that Cu-TiO_2 photocatalysts had been preliminary investigated for H_2 production. Several factors were found to influence the photocatalytic activities, for example, Cu content, chemical properties of Cu and post treatment etc. (Wu et al., 2004; Bandara et al., 2005). However, no systematic study of H_2 production over Cu-TiO_2 has been conducted. Little is known about the effect of operation conditions on H_2 generation and stability of Cu-TiO_2 under intensive photocatalytic reaction.

Hence in this chapter, Cu-TiO_2 photocatalyst was fabricated by employing wet impregnation method which is a well known and widely practiced wet chemical method. Systematic study of utilizing the fabricated Cu-TiO_2 for H_2 production was carried out to determine its efficiency, where the effects of Cu content in the photocatalyst, sacrificial reagent concentration, pH of reaction solution and photocatalyst dosage were studied. Based on the results, optimal Cu content and operation conditions were obtained for further studies. In addition, maintenance of Cu-TiO_2 photocatalyst activity in long-term reaction and changes of Cu-TiO_2 during photocatalytic reaction were also investigated via XRD, EDS, etc.

3.2 Experimental

3.2.1 Preparation of Cu-TiO_2 photocatalyst

Cu-TiO_2 photocatalyst was prepared by wet impregnation method with Degussa P25 (Germany) as support. P25 powder was added into $Cu(NO_3)_2 \cdot 3H_2O$ solution (QREC, analytical grade) with powder to solution ratio of 1g/3ml, followed by ultrasonic process and thorough mixing on a magnetic stirrer to obtain homogeneous slurry. After wet impregnation, the sample was dried at 105 ℃ overnight, and finally calcined in open air for 4 h at 350 ℃. Cu content in final photocatalyst was determined by concentration of $Cu(NO_3)_2$ solution used in impregnation, and was denoted by mole percentage of Cu in the photocatalyst: mol% = $n_{Cu}/n_{(Cu+TiO_2)}$.

3.2.2 Characterization of Cu-TiO_2 photocatalyst

Characterization of the photocatalyst was carried out before and after photocatalytic H_2 generation to investigate properties of photocatalyst, and changes during H_2 generation.

Crystal structure and composite of the fabricated Cu-TiO_2 photocatalyst were analyzed by a Bruker AXS D8 advance X-ray diffractometer (XRD) with monochromated high-intensity Cu Kα radiation (λ=1.5418 Å). The X-ray pattern was acquired from 20 °to 80 °with a step size of 0.02 °and a step time of 1.0 s, and the analysis was carried out at a voltage of 40 kV and an accelerating current of 30 mA. The obtained XRD spectrum was then matched with a Powder Diffraction File (PDF) database maintained by the International Center for Diffraction Data (ICDD).

Sample morphology was observed by a scanning electron microscope (SEM, Jeol JSM-6360) and a transmission electron microscope (TEM, Jeol JEM-2010). Prior to TEM analysis, an ethanol suspension of the samples was spread on an amorphous carbon-coated copper grid.

Element compositions of photocatalyst were detected by an Oxford energy dispersive X-ray spectrometer (EDS) attached to the SEM (Jeol JSM-6360).

Inductively coupled plasma emission spectroscopy (ICP, Perkin Elmer Optima 2000DV) was employed to confirm Cu content in the Cu-TiO_2 photocatalyst, and quantify the dissolved Cu in the solution during H_2 generation. Cu in the photocatalyst was extracted by microwave digestion first, and then the solution was subjected to the analysis for the Cu determination. The total Cu concentration in solution was evaluated using a 6-point (0, 0.1, 1, 10, 50, 100 ppm) calibration curve, and means of standard solutions had correlation coefficient higher than 0.998.

3.2.3 Photocatalytic reaction system

The setup for photocatalytic reaction utilized in this study is illustrated in Figure 3.1. The photocatalytic reaction was performed in an inner-irradiation Pyrex reactor (volume: 1.45 L) with a 400 W high pressure Hg lamp (Riko, UVL-400HA, λ_{max} of 365 nm) as the light source, where high pressure Hg lamp was chosen so that results from works of other researchers may be fairly compared (Abe et al., 2003; Sayama et al., 2006; Sreethawong et al., 2007; Kudo et al., 2009). To maintain a constant reactor temperature at 25 ℃, a quartz jacket, which was cooled with recycled water, was employed to cover the lamp. For the H_2 generation process, certain amount of powdered Cu-TiO_2 was suspended into 1.35 L methanol

water mixture. A magnetic stirrer was placed at the bottom of the reactor to ensure homogeneity of the suspension during reaction. Prior to the irradiation, the photocatalyst suspension was de-aerated thoroughly for 30 min by nitrogen gas purging.

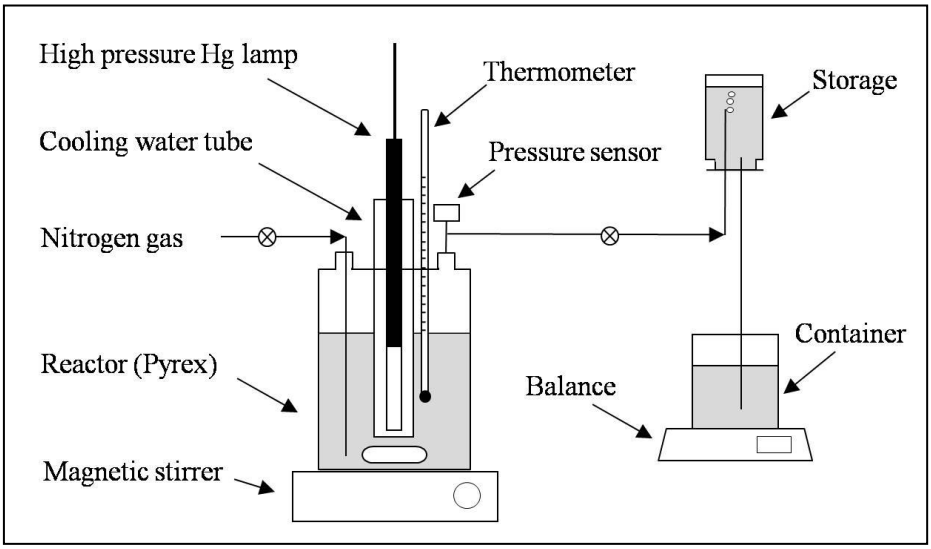

Figure 3.1 Schematic diagram of setup for photocatalytic reaction.

3.2.4 Optimization of operation conditions

To optimize H_2 generation activity of Cu-TiO_2, effect of several factors, for instance, Cu content in the photocatalyst, sacrificial reagent concentration, pH of reaction solution and photocatalyst dosage, were tested. The ranges of each factor are listed as follows: Cu content in Cu-TiO_2 photocatalyst (0, 0.1, 0.5, 1.0, 4.8, 7.0, 9.1, 11.1, 13.0, 28.6, 60.0, and 100 mol%), initial concentration of methanol solution (0, 1, 5, 10, 20, 50, 80, 100 volume%), dosage of photocatalyst (0.1, 0.25, 0.5, 1, 2 g L^{-1}), and initial pH of solution (3.0, 5.8, 7.0, 10.1, 12.0). Solution pH was adjusted by NaOH and HCl, and determined by Horiba F-53 pH/ion meter.

Unless stated otherwise, basic conditions employed in this study were: Cu-TiO_2 (Cu: 9.1 mol%, 1 g L^{-1}), methanol/water solution (10 volume%), and no adjustment of pH was performed.

3.2.5 H_2 detection

Gas produced via the photocatalytic reaction was first collected by a water displacement gas trap, from which the volume of the trapped gas can be determined. A small volume of the gas was periodically extracted by a gas tight syringe, through a silicon septum on the gas trap for gas chromatography (GC) analysis. The H_2 concentration was then evaluated using an Agilent 7890A GC with a thermal conductivity detector (TCD) and a HP-PLOT MoleSieve/5A column. Figure 3.2 presents a typical GC spectrum of the gas product.

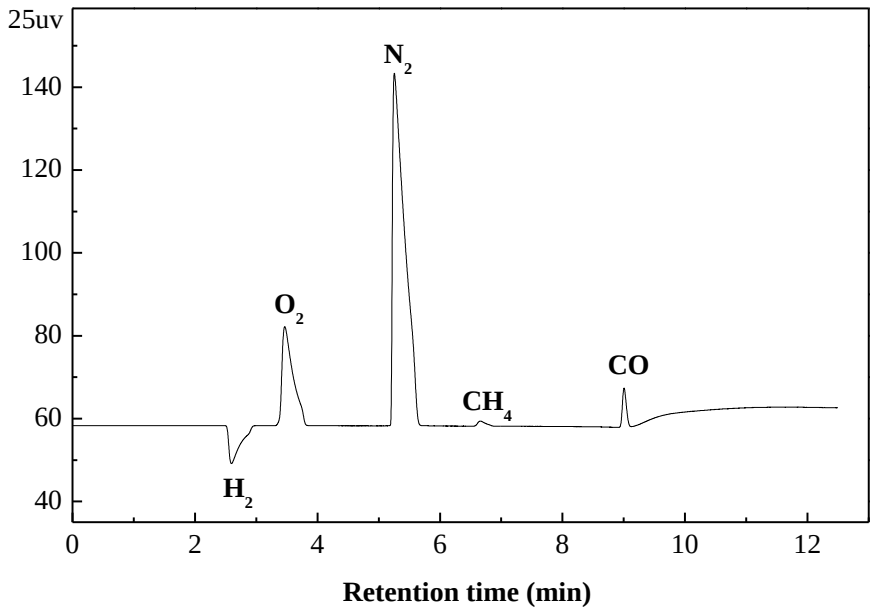

Figure 3.2 GC spectrum of gas produced from the photocatalytic reaction.

Owning to the limitation of off-line GC analysis, air trespass was inevitable,

leading to viewable peaks of O_2 and N_2. However, since the ratio of detected O_2 and N_2 corresponded exactly to that of ambient surrounding air and neither O_2 nor N_2 was supposed to be produced during the photocatalytic reaction, both gases were deemed adventitious and the concentration of H_2 was calculated without their due consideration. Note that helium (He) was used as the carrier gas; hence H_2 peak was negative and relatively small, due to the difference of their thermal conductivity (He: 0.1513, H_2: 0.1805 W m^{-1} K^{-1}). However, after calibration using the standard H_2 gas, H_2 was identified as the core component in the collected gas.

3.3 Results and Discussion

3.3.1 Characterization of as-prepared Cu-TiO_2

Figure 3.3 shows the XRD patterns of Cu-TiO_2 photocatalysts with variation of Cu content. For Cu content lower than 5 mol%, no characteristic peak of either metallic Cu or Cu oxide was detected. At higher Cu content, only characteristic peaks of CuO crystal (2θ=35.5°, 38.7°) were observed, and their intensities were enhanced with increment of Cu content. No other crystalline forms of Cu oxide (i.e. Cu_2O) were presented, indicating that Cu existed as CuO crystal after calcination at 350 ℃. This result is in agreement with previous reports (Bandara et al., 2005; Choi et al., 2007; Kim et al., 2007). Kim and Ihm (2007) found, from results of electron spin resonance (ESR), that the chemical state of Cu in the CuO_x/TiO_2 photocatalysts, synthesized by incipient wetness impregnation method, was highly dispersed Cu^{2+} cluster for Cu content lower that 5 wt%, and bulk CuO for higher Cu content.

As also clearly shown from the XRD patterns in Figure 3.3, for all photocatalysts with variation of Cu content (except 100 mol%), characteristic peaks of P25 were

observed, and there were no significant changes in peak intensities and full widths at half maximum (FWHM). It indicated that TiO_2 had scarcely undergone phase transformation and particle size change during the preparation processes.

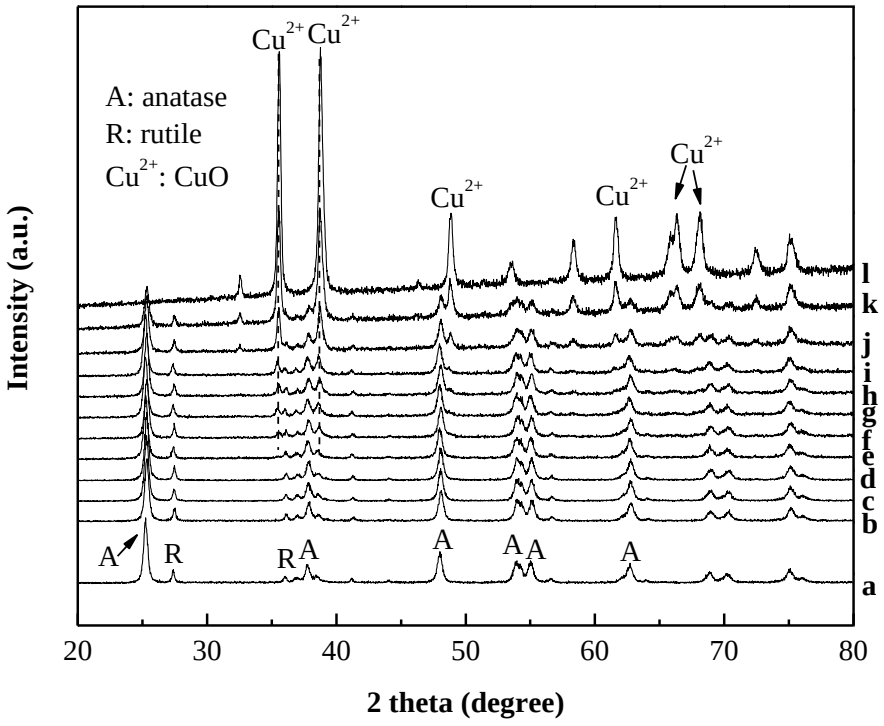

Figure 3.3 XRD patterns of Cu-TiO_2 with variation of Cu content (a-l: 0, 0.1, 0.5, 1.0, 4.8, 7.0, 9.1, 11.1, 13.0, 28.6, 60.0, and 100 mol%).

From TEM image, as shown in Figure 3.4, it can be found that particle sizes of Cu-TiO_2 (Cu content: 9.1 mol%) were in the range of 6.5-16.5 nm. Surface morphology of the Cu-TiO_2 (Cu content: 9.1 mol%) was further studied by SEM. SEM image in Figure 3.5 revealed that Cu-TiO_2 nanoparticles constituted aggregated clusters with relatively uniform sizes. EDS analysis results as shown in Figure 3.5, provided elemental distribution information of the Cu-TiO_2 photocatalyst. The existence of dots in the elemental mapping images indicated the presence of the investigated components, and all the elements were well distributed

throughout the bulk photocatalyst.

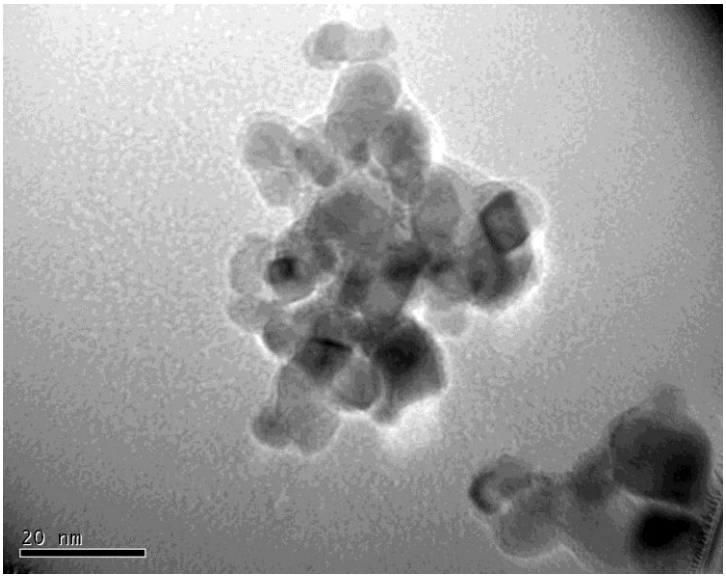

Figure 3.4 TEM image of 9.1 mol% Cu-TiO_2.

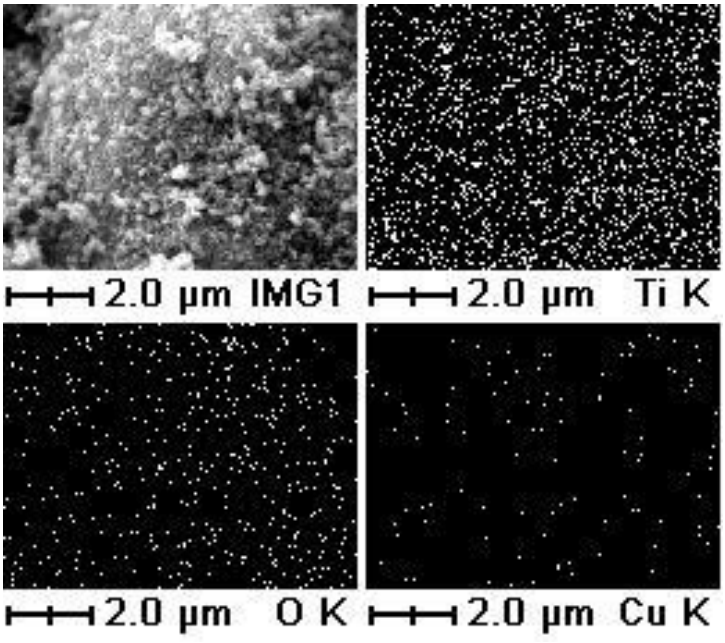

Figure 3.5 SEM image and elemental mapping of 9.1 mol% Cu-TiO_2.

3.3.2 Photocatalytic activity of as-prepared Cu-TiO_2

Figure 3.6 shows time courses of H_2 evolution over Cu-TiO_2 photocatalysts with variation of Cu content from 10 volume% methanol/water solution; the H_2 evolution rate with its dependence on Cu content is summarized in Figure 3.7. It can be found that the as-prepared Cu-TiO_2 exhibited excellent activity in photocatalytic H_2 production compared to bare TiO_2, and Cu content in the Cu-TiO_2 photocatalyst had great influence on H_2 generation activity. With the increase of Cu content, H_2 evolution rate increased dramatically from nearly zero (pure TiO_2) to a maximum of 10.2 ml min^{-1} (18500 μmol h^{-1} $g^{-1}_{catalyst}$) at an optimal Cu content of 9.1 mol% (Cu/Ti atom%=10%); above that, H_2 generation rate progressively declined to zero (pure CuO).

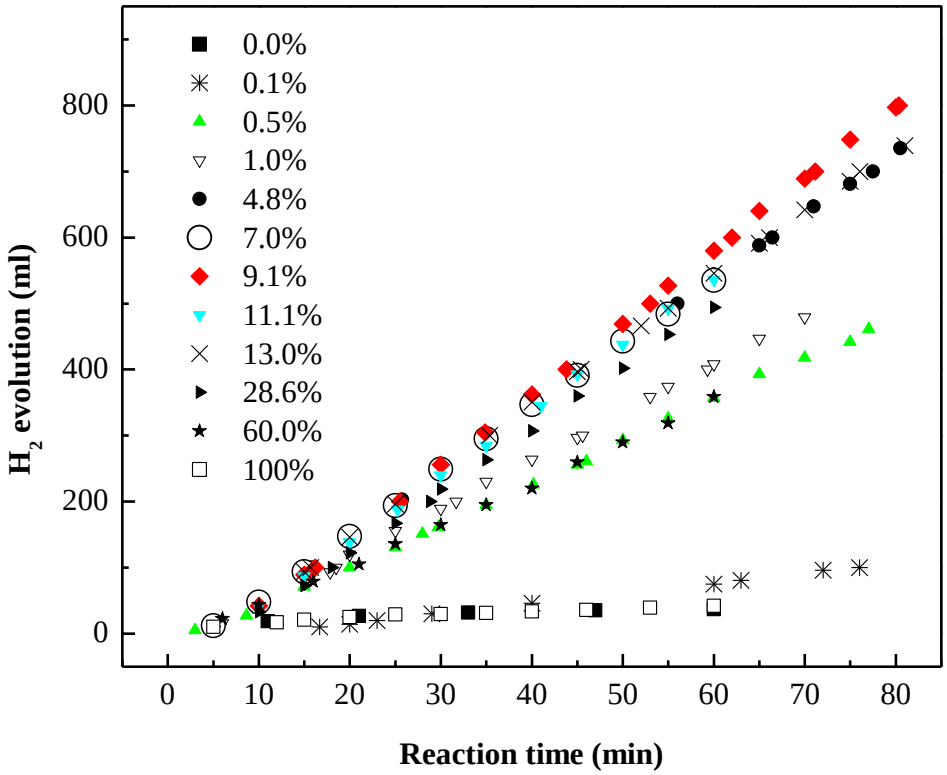

Figure 3.6 Effect of Cu content (mol%) in Cu-TiO_2 photocatalyst on H_2 generation (photocatalyst: 1 g L^{-1}; methanol: 10 volume%).

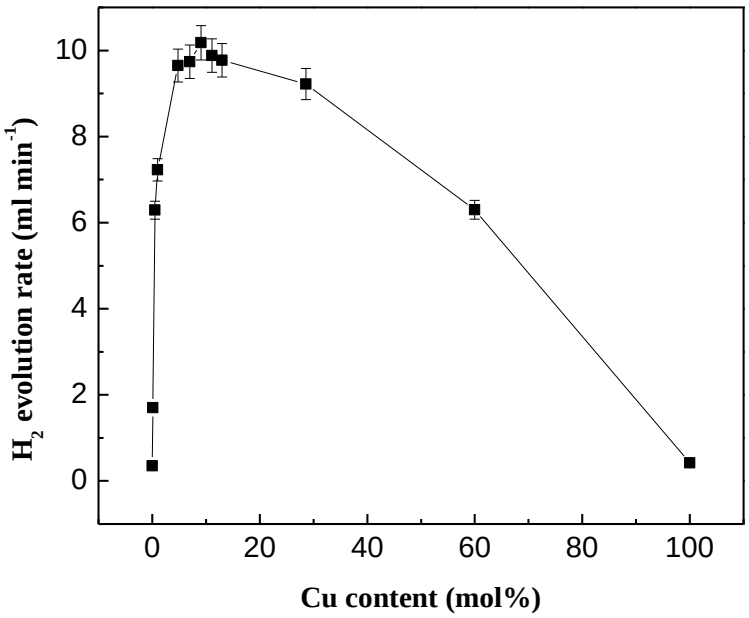

Figure 3.7 Dependence of H_2 generation rate on Cu content (photocatalyst: 1 g L^{-1}; methanol: 10 volume%).

TiO_2 or CuO alone hardly generated H_2 in 1 h reaction, which suggested that the coexistence of TiO_2 and CuO was necessary for the high photocatalytic activity. Since the conduction band of CuO is lower than that of TiO_2, the excited electrons in the CB of TiO_2 could easily transfer to CB of CuO, resulting in accumulation of excess electrons in CuO, which led to a negative shift in Fermi level of CuO (confirmed by Bandara et al., 2005). The raised Fermi level endowed CuO with the required overvoltage for efficient water reduction reaction, and made CuO act as the water reduction site. The efficient inter-particle charge transfer prevented electron/hole recombination in TiO_2, resulting in high H_2 generation activity of Cu-TiO_2 photocatalyst.

The existence of optimal "activator" concentration in the incorporated TiO_2 photocatalysts has been reported, for example, metal to TiO_2 (Martin et al., 1994a), CuO to TiO_2 (Bandara et al., 2005; Choi et al., 2007), Pd to TiO_2 (Bowker et al.,

2003). Choi et al. (1994) deemed that it was due to the balance of an increase in trapping sites leading to efficient trapping and fewer trapped carriers leading to longer lifetime for interfacial charge transfer.

From the view point of active site, we may derive another explanation for the optimal Cu content for H_2 generation over Cu-TiO_2 photocatalyst. The active site of Cu-TiO_2 photocatalyst for H_2 generation was probably located at the interface rather than on the isolated CuO or TiO_2 since no H_2 evolved over pure CuO or TiO_2, as discovered earlier in this study. From data fitting result of H_2 generation rate against Cu content ranging from zero to optimal 9.1 mol%, the rate showed dependence on Cu content to the power of 0.35. This value remarkably approached to Bowker's model (Bowker et al., 2003) for methanol reforming over Pd/TiO_2 photocatalyst. He suggested that the rate of reaction where active site was at the periphery of loaded metal particles on the support (TiO_2), should show a cubic root (to the power of 1/3) dependence on loading before optimal loading, and the optimal loading should appear only when a monolayer of metal particles completely covered the support. In terms of Cu in our study, this value should be 10 mol%, which was coincident with result obtained from our experiments: 9.1 mol%. Since both optimal Cu content and dependence of H_2 generation rate on Cu content could be predicted by Bowker's model, active site for H_2 generation was probably at the periphery of CuO on TiO_2.

According to Bowker's model, at higher loadings, there should be an inverse cosine dependence on the reciprocal of loading since the loaded metal particles merged together and the total periphery began to shrink. However, in our results, the rate drop was not as sharp as described in Bowker's model. Main reason for the unconformity was probably due to the difference in combination mode: in Bowker's case, Pd was presented on a flat TiO_2 support in the form of

hemispherical particles with diameter of around 3-5 nm, while in our experiments, CuO was coexistent with TiO_2 with diameters in the same order of magnitude, where the shrink in total perimeter was not so pronounced with the increment of Cu content. Apart from the periphery shrink, another reason for the drop of activity at higher content of Cu can be deduced that the light sensitization of TiO_2 was blocked by surrounding CuO, which led to a lower density of excited electron accumulation in CB of CuO, and thus weakened the photocatalytic H_2 generation.

Compared with limited studies on Cu-TiO_2 for H_2 production as shown in Table 3.1, the 9.1 mol% Cu-TiO_2 prepared in this study showed extremely high H_2 generation activity, even higher than some Pt and Pd loaded TiO_2 photocatalyst.

Table 3.1 Comparison of H_2 production over various Metal-TiO_2.

No.	Photocatalyst	Preparation method	Sacrificial reagent (v/v)	H_2 generation rate		Reference
				μmol h^{-1} $g^{-1}_{catalyst}$	μmol h^{-1} $ml^{-1}_{solution}$	
1	10 mol% CuO-TiO_2 TiO_2: anatase nanoparticle	Wet impregnation	1:1 methanol/water	675	0.7	(Choi et al., 2007)
2	1.2 wt% Cu-TiO_2 TiO_2: anatase nanoparticle	Incipient-wetness	1:1.4 methanol/water	2400	3	(Wu et al., 2004)
3	2.5 wt% Cu/Cu_2O/CuO-TiO_2 TiO_2: anatase	Water-in-oil micro-emulsion	1:1 ethanol/water	1400	2.9	(Gombac et al., 2010)
4	1.5 wt% CuO-TiO_2 1 wt% PdO-TiO_2 2 wt% Au-TiO_2 TiO_2: mesoporous nanoparticle	Single step sol-gel	1:10 methanol/water	1800 2100 2800	1.6 1.9 2.5	(Sreethawong et al., 2005)
5	0.6 wt% Pt-TiO_2 TiO_2: mesoporous nanoparticle	Single step sol-gel	1:10 methanol/water	6900	6.3	(Sreethawong et al., 2007)
6	1.0 wt% Pt-TiO_2 TiO_2: mesoporous nanoparticle	Photo-deposition	1:10 methanol/water	6000	1.1	(Yi et al., 2008)
7	7 mol% NiO-TiO_2	In-situ hydrothermal	3:7 methanol/water	900	0.9	(Jang et al.,

	TiO_2: titanate nanotube	method				2009)
8	0.5 wt% Pt-TiO_2	In-situ	1:9 methanol/water	4300	4.9	(Jeon et al.,
	TiO_2: anatase nanowire	photo-deposition				2007)
9	Eosin-1.0 wt% CuO-TiO_2	Wet impregnation	1:5.7 diethanolamine	540	0.2	(Jin et al., 2007)
	TiO_2: P25		/H_2O			
10	7 wt% CuO-TiO_2	Wet impregnation	1:19 methanol/water	4300	--	(Bandara et al.,
	TiO_2: P25					2005)
11	1 wt% Cu_2O/CuO-TiO_2	Ion impregnation	1:4 ethanol/water	2705	0.8	(Wu et al., 2009)
	TiO_2: P25					
12	0.3 wt% Pt-TiO_2	Dry impregnation	1:40 methanol/water	25560	19.2	(Galinska et al.,
	TiO_2: P25					2005)
13	0.5 wt% Pt-TiO_2	Wet impregnation	1:30 ethanol solution	27750	37	(Patsoura et al.,
	TiO_2: P25					2007)
14	9.1 mol% CuO-TiO_2	Wet impregnation	1:9 methanol/water	18500	18.5	In this study
	TiO_2: P25					

(CuO-/Cu_2O-/ Cu-/ PdO-/ Au-/ Pt-/NiO- represent chemical state of metals before hydrogen generation)

This excellent activity of Cu-TiO_2 prepared in this study could firstly be attributed to the stable P25 support, which consists of both anatase and rutile (70:30) phases, and possesses a high surface area of 50 m^2 g^{-1} and an average particle diameter of 30 nm. Comparing SEM images with other researchers (Sreethawong et al., 2005; Choi et al., 2007), it can be easily observed that photocatalyst with P25 as support remained highly dispersed after fabrication. High dispersion degree of P25 support promised excellent combination between CuO and TiO_2; moreover, homogeneous dispersion of final Cu-TiO_2 photocatalyst in solution ensured uniform contact of photocatalyst with reagents and light.

Another important factor for high H_2 generation activity could be the way that CuO and TiO_2 combined. In Wu's study (Wu et al., 2004), H_2 generation activity of photocatalyst with Cu dissolved within TiO_2 lattice was lower than that achieved when Cu was deposited as individual particles on TiO_2 surface with the same loading. Tseng et al. (2004) found that photocatalytic activity of Cu-TiO_2 synthesized via sol-gel process was affected heavily by Cu precursor's adding time due to changes of Cu distribution in the final product (Tseng et al., 2004). Widely practiced impregnation method used in this study is employed frequently in most of the Cu-TiO_2 photocatalyst applications. It not only ensured high dispersion of CuO on TiO_2 support, but also maintained the individual characteristics of CuO and TiO_2 without lattice trespass.

In order to investigate the effect of combination mode of CuO and TiO_2, direct mixture of CuO/TiO_2 and $Cu(NO_3)_2$/TiO_2 were tested as photocatalysts for H_2 production. The results are shown in Figure 3.8. Compared to impregnation method, direct mixing of CuO with TiO_2 which provided few contact between Cu component and TiO_2 showed inferior activity. However, it was interesting to find that mixture of $Cu(NO_3)_2$ and TiO_2 showed much higher activity than CuO and

TiO_2 direct mixture. This was further investigated in detail and would be reported in Chapter 6.

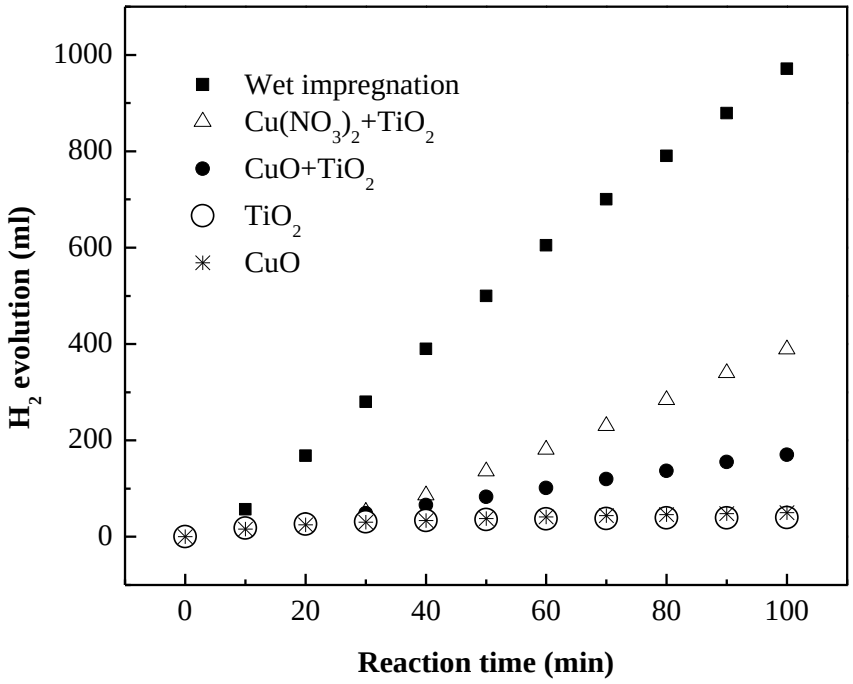

Figure 3.8 Effect of combination mode between Cu component and TiO_2 on H_2 generation (photocatalyst: 1 g L^{-1}; methanol: 10 volume%).

In all experiments, H_2 started to evolve steadily from about 5 min after lamp was turned on. This delay was probably due to the stabilization of light source and saturation of generated gas in the solution.

Blank experiments (data not shown) were also conducted without light or photocatalyst. No gas was evolved without light irradiation even with the most active 9.1 mol% Cu-TiO_2; under irradiation, without photocatalyst, a negligible gas evolution (0.3 ml min^{-1}) was observed. Blank experiments indicated that light irradiation was a prerequisite, and Cu-TiO_2 photocatalyst greatly enhanced H_2 generation from the methanol/water solution.

Since 9.1 mol% Cu-TiO_2 showed the highest H_2 generation activity, it was used as the main photocatalyst for further experiments.

All the experiments presented here were carried out for 3-4 times, and the repeatability of these results was good within ±5% variation.

3.3.3 Optimization of operation conditions for Cu-TiO_2

3.3.3.1 Concentration of sacrificial reagent

From mechanistic and practical points of view, it is essential to study the dependence of H_2 generation rate on initial concentration of sacrificial reagent. In this study, methanol was chosen as a representative. Figure 3.9 shows time courses of H_2 evolution over 9.1 mol% Cu-TiO_2 from aqueous solutions containing various volume percentage of methanol, and the dependence of H_2 evolution rate on methanol concentration is summarized in Figure 3.10.

It can be seen that, increasing methanol concentration from 1 to 80 volume% resulted in a monotonous increase of H_2 evolution rate from 0.4 to 28.1 ml min^{-1}, where in 100 volume% pure methanol, H_2 was still generated at a substantial rate of 9.8 ml min^{-1}. Compared with pure water, addition of a small quantity of methanol could induce a substantial H_2 evolution rate, which resulted from methanol acting as a sacrificial electron donor and preventing electron/hole recombination.

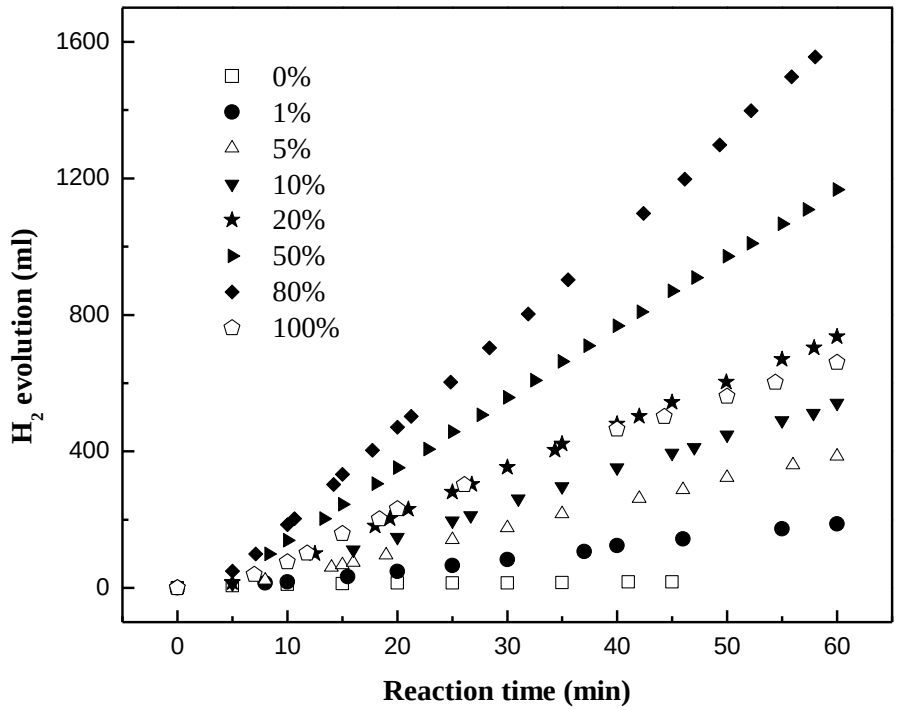

Figure 3.9 Effect of initial methanol concentration (volume%) on H_2 generation (photocatalyst: 9.1 mol% Cu-TiO_2, 1 g/L).

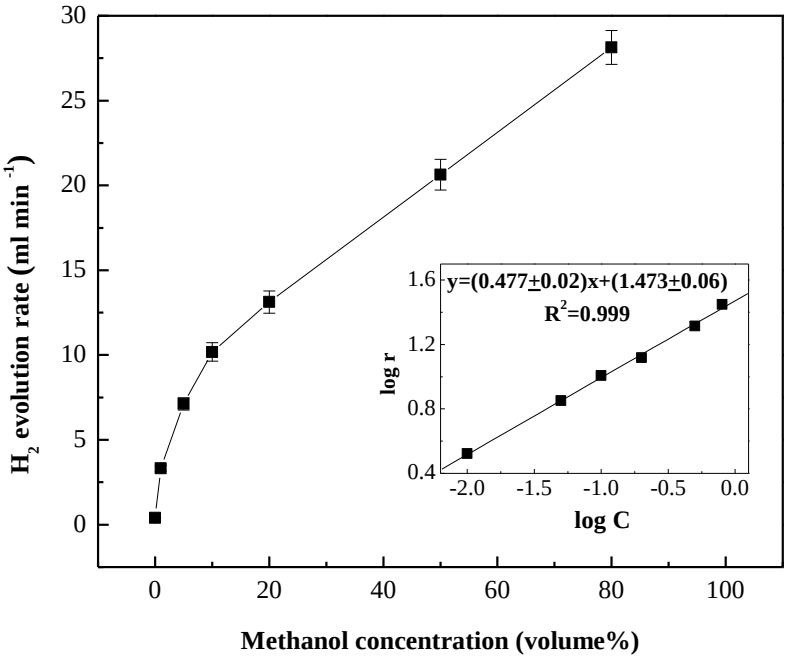

Figure 3.10 Dependence of H_2 generation rate on initial methanol concentration (photocatalyst: 9.1 mol% Cu-TiO_2, 1 g L^{-1}). Inset: log r~log C, r: rate, C: concentration.

Effect of sacrificial reagent concentration on H_2 evolution rate has been studied extensively. Some researchers found that H_2 evolution rate varied as a function of sacrificial reagent concentration in according to a Langmuir-type isotherm (Li et al., 2001; Li et al., 2006; Al-Mazroai et al., 2007; Strataki et al., 2007), resulting from active centres saturation on the limited quantity of photocatalysts. Some other researchers found that an optimum methanol concentration existed (Sreethawong et al., 2007); excess methanol beyond its optimum concentration might block the adsorption of hydronium cations at surface active sites. However, neither of the relationships above could exactly fit the situation in the current study. If the results gathered from this study were plotted in logarithm form, a linear relationship between log r (rate) and log C (concentration) could be obtained as shown in inset of Figure 3.10. This was a typical kind of Freundlich adsorption behaviour, and presented relationship between H_2 generation rate and methanol concentration as $r=29.7\ C^{0.477}$. This indicated adsorption of methanol on photocatalyst was a crucial part of the reaction mechanism; moreover, the adsorption was not a uniform monolayer adsorption, and might favour the active interface of CuO and TiO_2. More adsorption sites appeared on the photocatalyst after CuO incorporation, resulting in an evident increase of H_2 generation rate with increment of methanol concentration.

In this photocatalytic H_2 generation process, besides methanol, water also functioned as a sacrificial reagent, and produced proton when scavenging surface trapped holes (Bamwenda et al., 1995). Then, reduction of protons by excited electrons led to H_2 generation. This may be the reason for the shrinkage of H_2 generation rate when no water was present in the solution.

From pollutant removal point of view, excellent H_2 generation rate under various methanol concentration promises the applications of the prepared Cu-TiO_2

photocatalyst for water and wastewater treatment. For further study, 10 volume% methanol/water mixture was chosen as reaction solution.

3.3.3.2 pH of reaction solution

Solution pH is an important parameter affecting the photocatalytic reactions, since it influences the band gap positions and surface chemistry of photocatalyst, which has been discussed in Chapter 2. In addition, the physicochemical characteristic of methanol that related to the proton concentration and the electron donating ability are affected by the solution pH as well. The role of initial solution pH on photocatalytic H_2 generation activity of Cu-TiO_2 was studied over a pH range of 3-12, and results are shown in Figure 3.11. Note initial pH of the original solution (10 volume% methanol solution) was 5.8.

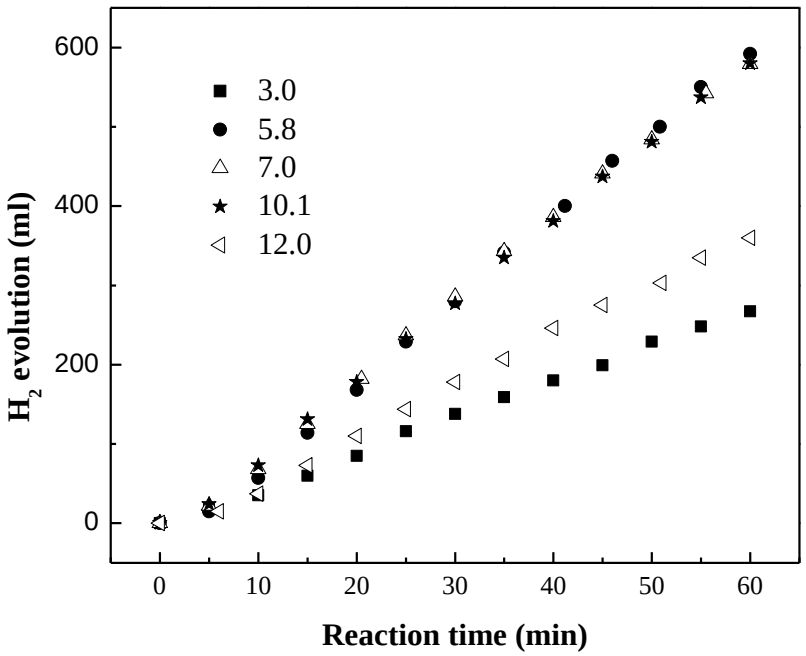

Figure 3.11 Effect of solution pH on H_2 generation (photocatalyst: 9.1 mol% Cu-TiO_2, 1 g L^{-1}; methanol: 10 volume%).

From results of Figure 3.11, it can be seen that middle-range pH conditions favored H_2 generation, activity of Cu-TiO_2 was not affected over pH range of 5.8-10, but ultra acidic (pH=3) or basic (pH=12) conditions significantly depressed H_2 generation activity.

CuO dissolved into solution under acidic conditions was expected to affect the photocatalyst H_2 generation activity. Figure 3.12 shows Cu leaching of 9.1 mol% Cu-TiO_2 photocatalyst over pH range of 1-13. It can be found that pH had pronounced influence on Cu leaching. Under acidic condition with pH<5, serious Cu leaching occurred: 83.8% of Cu from the Cu-TiO_2 would be released into the solution after 1 h soak when pH=1; 54.0% when pH=3. Nevertheless, when pH>5, almost no Cu^{2+} could be found in solution even after 5 h soak. Low H_2 generation activity in ultra acidic condition (pH=3 in this study) was deduced mainly caused by the serious Cu leaching, where Cu^{2+} could not serve as excellent electron reservoir as CuO, which has been proved by results shown in Figure 3.8.

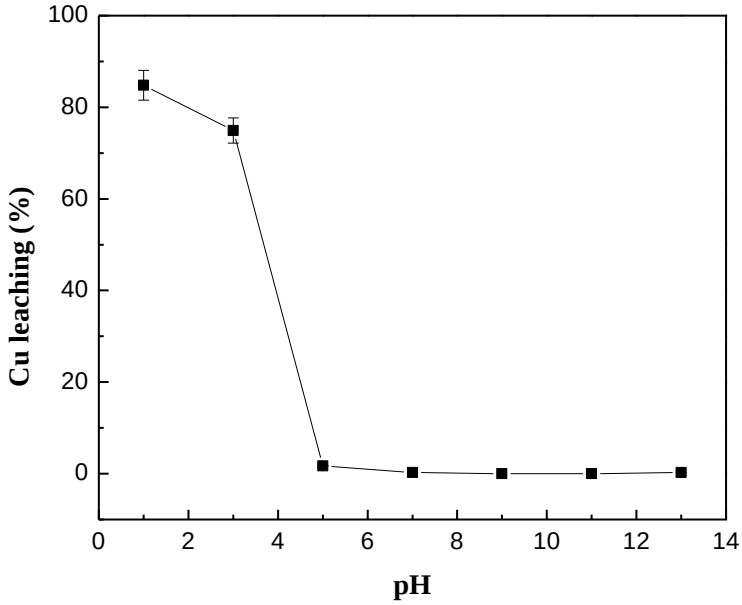

Figure 3.12 Cu leaching (%) over pH range of 1-13 in 5 h soak (photocatalyst: 9.1 mol% Cu-TiO_2, 1 g L^{-1}).

At basic pHs ($pH>pH_{zpc}$), surface of TiO_2 is negatively charged. The electrostatic repulsion between the negatively charged photocatalyst and molecules of sacrificial reagent (methanol: long pair electron donor) inhibited adsorption of sacrificial reagent to scavenge the VB holes for preventing electron/hole recombination (Sreethawong et al., 2007). In addition, photo-induced electrons could not easily transfer to photocatalyst surface due to the negative charge repulsion, leading to high chances of recombination of electron/hole pairs. Both of these factors depressed H_2 generation rate at basic conditions. To achieve high photocatalytic reaction activity, photocatalysts shall carry zero charge for the sacrificial reagents to reach photocatalyst surface easily.

Cu-TiO_2 photocatalyst possessed big potential for practical applications since it exhibited high photocatalytic H_2 generation activity over a pH range of 5.8-10, where no serious Cu leaching and electrostatic repulsion occurred.

3.3.3.3 Dosage of photocatalyst

Dosage of photocatalyst should be optimized in order to avoid unnecessary excess photocatalyst and undesirable depression of photocatalytic activity. Figure 3.13 illustrates time courses of photocatalytic H_2 generation as a function of Cu-TiO_2 photocatalyst dosage in the range of 0.1-2.0 g L^{-1}, and the dependence is summarized in Figure 3.14. The H_2 generation rate first increased and then decreased along with the increment of photocatalyst dosage, and an optimum concentration of 1 g L^{-1} was found.

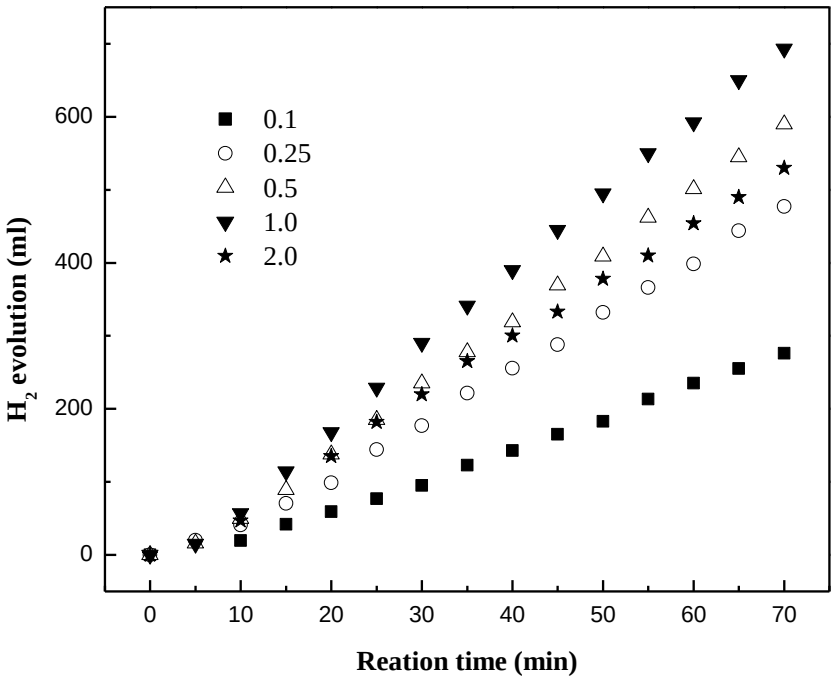

Figure 3.13 Effect of photocatalyst dosage (g L^{-1}) on H_2 generation (photocatalyst: 9.1 mol% Cu-TiO_2; methanol: 10 volume%).

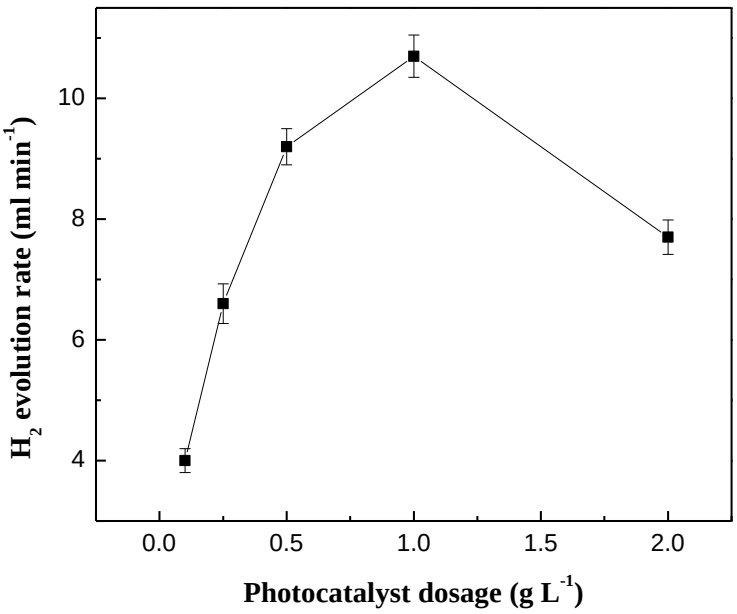

Figure 3.14 Dependence of H_2 evolution rate on photocatalyst dosage (photocatalyst: 9.1 mol% Cu-TiO_2; methanol: 10 volume%).

Optimum photocatalyst concentration balanced availability of active sites on photocatalyst surface and the penetration of photo-activating light into the suspension. With increase of photocatalyst concentration, the available active sites increased, but the light penetration shrank, inducing block of illuminating light. Although the light absorption on the outer photocatalyst increased, activity of H_2 generation from inner photocatalyst decreased due to blockage of light. In addition, deactivation of activated photocatalyst molecules by collision with ground-state molecules might be another reason for decrease of photocatalytic activity at high photocatalyst dosage. As a result, optimum photocatalyst dosage existed, and overall H_2 generation decreased under high photocatalyst concentration.

Based on the results above, basic conditions employed for further study were as follows: Cu-TiO_2 (Cu: 9.1 mol%, 1 g L^{-1}), methanol/water solution (10 volume%), and no adjustment of pH (pH=5.8) was performed.

Duplicate/triplicate tests were carried out in Section 3.3.3, and variation of the results was calculated within ±5%, which indicated good repeatability of the results.

3.3.4 Maintenance of H_2 generation activity of Cu-TiO_2

To study stability of H_2 generation over the prepared Cu-TiO_2 photocatalyst, an extended reaction was conducted for 10 h over 9.1 mol% Cu-TiO_2 from 10 volume% methanol solution. From the results of Figure 3.15, H_2 evolution rate decreased progressively with time, 41% (4.2 ml min^{-1}) remained after 10 h continuous irradiation. In order to recover H_2 generation activity, many attempts had been carried out, and the results are shown in Figure 3.16.

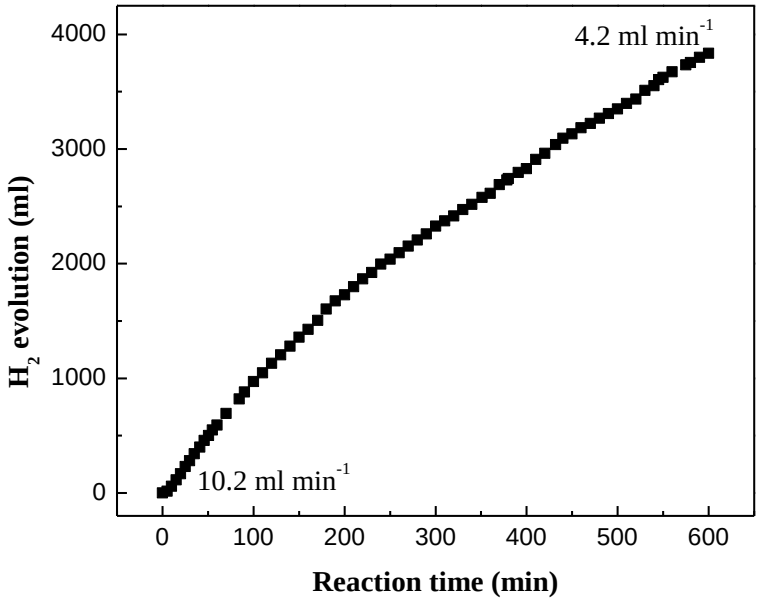

Figure 3.15 Time course of H_2 evolution under 10 h irradiation.

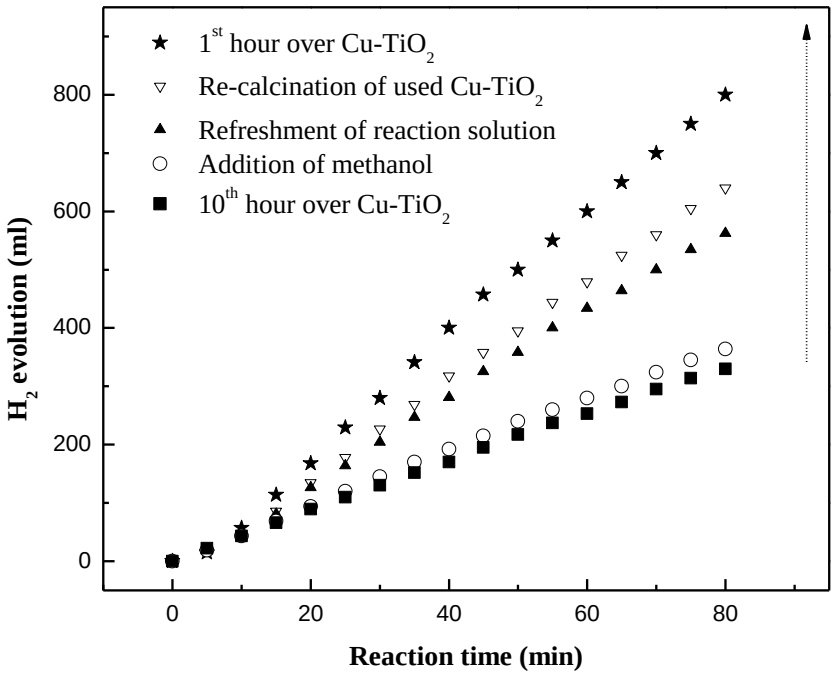

Figure 3.16 Recovery of H_2 generation activity.

Addition of methanol with amount converted from generated H_2 (1 methanol → 3 H_2) showed no evident effect since the consumption of methanol was low and H_2

evolution rate was not strongly affected by reactant concentration changes during the experiment, proved by nearly linear H_2 evolution during the first hour's reaction in all tests.

H_2 evolution rate could be recovered from 41% up to 77% (7.9 ml min^{-1}) with refreshment of reaction solution, indicating that accumulation of by-products might be a main cause for the decline of H_2 evolution rate. But the by-products did not poison the photocatalyst severely since biggish deactivation could be recovered without treatment to the photocatalyst.

If the photocatalyst was subjected to heat regeneration (350 ℃ for 4 h) further, H_2 evolution rate could be regained up to 85% (8.7 ml min^{-1}). This suggested that chemical state change of CuO to Cu_2O/Cu (proved by the following XRD results) could also be a reason for the deactivation. Since Cu_2O still possesses good photocatalytic activity to decompose water into H_2 and O_2 (Hara et al., 1998), it indicates that metallic Cu as compared to Cu oxides, may limit electron transfer from TiO_2, hence leading to a lower H_2 generation activity.

Another reason for the decline of H_2 generation rate could be Cu leaching from the photocatalyst since pH value of solution dropped due to accumulation of by-products (CO_2 and HCOOH). After 10 h reaction, pH dropped from 5.8 to 4.8, and Cu content in the photocatalyst reduced to 8.1 mol%. Jin et al. also found that H_2 evolution over dye-sensitized Cu-TiO_2 decreased to a minimum when pH value dropped to 1 (Jin et al., 2007), but they failed to mention the effect of Cu leaching. According to Figure 3.12, when solution pH was 1, 83.8% of Cu in Cu-TiO_2 photocatalyst would be released into the solution after soaking for 1 h (54.0%, 2.2% for pH=3 and 5, respectively). Cu^{2+} in solution weakened the ability to accept excited electrons from TiO_2, causing deactivation of H_2 generation.

Degree of causes for decrease of H_2 generation rate can be ranked as follows, accumulation of by-products (61.7%), reduction of CuO (13.3%), and Cu leaching (6.7%). There are still some unidentified factors, which hold 18.3% of total deactivation. Efforts should be made to discover all the relevant factors, and prevent deactivation of the efficient Cu-TiO_2 photocatalyst.

All the experiments presented in this section were repeated 2-3 times, and the results were highly reproducible with ±5% variation.

3.3.5 Characterization of Cu-TiO_2 after H_2 generation

To investigate the crystal phase and morphology changes during H_2 generation, representative characterizations of Cu-TiO_2 were carried out after photocatalytic reaction from methanol/water solution.

From the XRD patterns (Figure 3.17), no obvious transformation of TiO_2 was observed; however, characteristic peaks of CuO disappeared in all used photocatalysts, replaced by Cu_2O (2θ=36.4°, 42.3°) and even metallic Cu (2θ=43.3°, 50.4°). Metallic Cu could be observed in photocatalyst with higher Cu content. The transformation of Cu chemical states after reaction justified the mechanism expatiated before: excited electrons transferred from CB of TiO_2 to CuO, resulting in efficient electron/hole separation, excellent photocatalytic H_2 generation, and reduction of CuO.

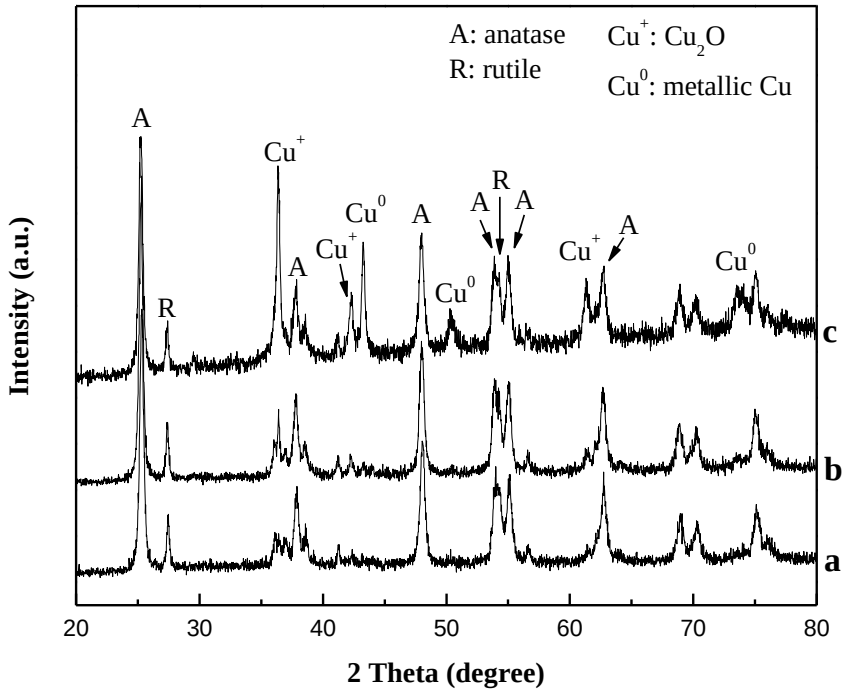

Figure 3.17 XRD patterns of Cu-TiO_2 after H_2 generation (a: 9.1 mol% for 1 h; b: 9.1 mol% for 10 h; c: 28.6 mol% for 1 h).

Comparing the three representative patterns in Figure 3.17, it can be found that high Cu content and extension of reaction time enhanced the reduction of CuO. Cu components in samples with higher Cu content should be larger than that with lower Cu content. The larger Cu components then extended the electrons' retention time inside, due to the longer transfer distance from TiO_2 to protons, and enhanced the reduction of CuO in the as-prepared Cu-TiO_2 along with the photocatalytic reaction. Extension of reaction time further provided long time for contact of Cu components with electrons, and induced deeper reduction of CuO.

Reduction of CuO and Cu leaching during the reaction can also be identified by EDS analysis as shown in Figure 3.18. Comparing to the elemental mapping images of as-prepared photocatalyst as shown in Figure 3.5, dots density of O and Cu in the used photocatalyst diminished. This is a visual evidence for the chemical

transformation of the photocatalyst. From the EDS results, elemental distribution after reaction was still homogeneous which was advantageous for efficient photocatalytic reaction.

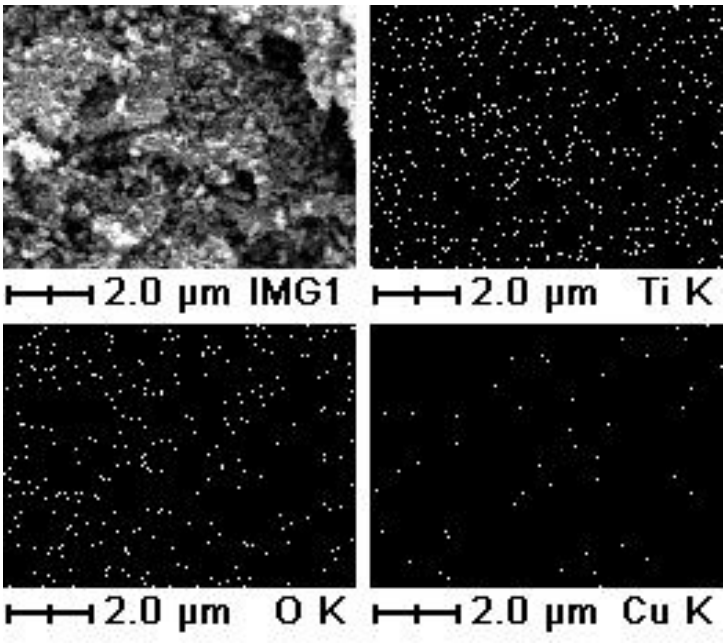

Figure 3.18 SEM image and elemental mapping of 9.1 mol% Cu-TiO_2 after H_2 generation for 1 h.

Particle sizes and morphology of photocatalyst after H_2 generation reaction showed no significant changes from the TEM image, as illustrated in Figure 3.19. No serious merging or aggregation occurred during the reaction, which meets the requirement for a stable photocatalyst.

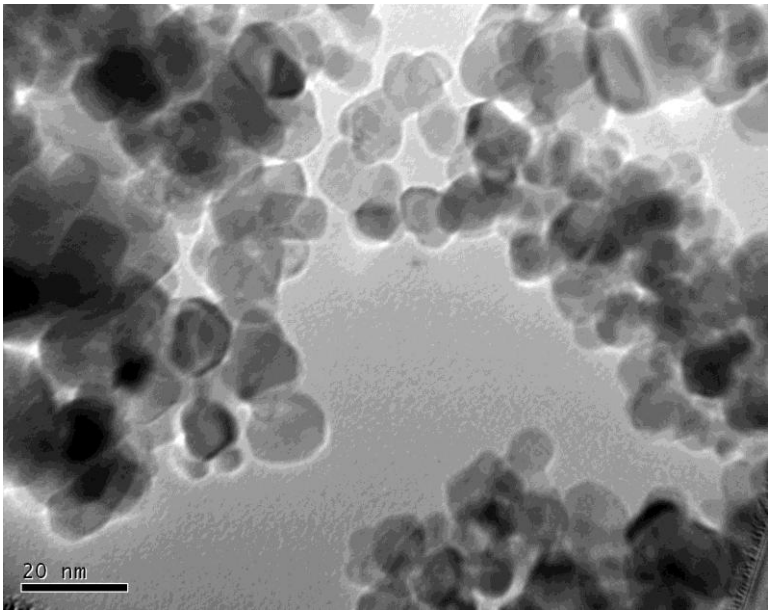

Figure 3.19 TEM image of 9.1 mol% Cu-TiO_2 after H_2 generation for 1 h.

Reduction of CuO suppressed H_2 generation activity, but the impact was not significant since Cu_2O also possesses ability to reduce water, and CuO could be regenerated by a simple calcination process, resulting in recovery of photocatalytic H_2 generation activity.

3.4 Conclusion

Enhanced Cu-TiO_2 prepared by impregnation method, with P25 as support, was found to be a remarkable and efficient photocatalyst for H_2 production under sacrificial conditions. H_2 evolution rate of 10.2 ml min^{-1} (18500μmol h^{-1} $g^{-1}_{catalyst}$) was obtained over 9.1 mol% Cu-TiO_2 photocatalyst (Cu/Ti atom%=10%) from 10 volume% methanol/water solution. This rate was much higher than ever reported Cu-TiO_2, even in comparison with some Pt and Pd loaded TiO_2.

From XRD results, Cu existed in the form of CuO, which enhanced the separation

of photo-induced electrons and holes, leading to significant improvement of H_2 generation activity comparing to bare TiO_2. Cu content in the photocatalyst was crucial for photocatalytic activity, and a high H_2 evolution rate of 10.2 ml min^{-1} was obtained at an optimum Cu content of 9.1 mol%, resulting from maximum active sites and limited blockage of light to reach TiO_2. H_2 generation rate could be enhanced further by increasing the methanol concentration in accordance to Freundlich adsorption isotherm, indicating that photocatalytic H_2 generation was based on adsorption of methanol on photocatalyst, and the fabricated Cu-TiO_2 photocatalyst provided plentiful adsorption sites. In pH range of 5.8-10, H_2 generation over Cu-TiO_2 was not affected by pH changes, but ultra acidic or basic conditions did depress the H_2 generation activity. In addition, optimum dosage of photocatalyst was found to be 1 g L^{-1}. However, H_2 generation rate dropped to a certain degree under long irradiation time, mainly due to the accumulation of by-products, reduction of CuO and Cu leaching.

High H_2 generation activity, low cost (comparing with noble metal loading) and simple synthesis procedure, affirm the potential of Cu-TiO_2 in photocatalytic H_2 production.

CHAPTER 4

EFFECT OF FABRICATION METHOD OF Cu-TiO_2 ON PHOTOCATALYTIC H_2 PRODUCTION

4.1 Introduction

Chapter 3 investigated the effect of operation conditions on H_2 generation over Cu-TiO_2 photocatalyst. With an optimum Cu content of 9.1 mol% (Cu/Ti=10 atom%), the fabricated Cu-TiO_2 exhibited excellent H_2 generation activity, even higher than some noble metal loaded TiO_2 photocatalyst. This affirms the potential of Cu-TiO_2 in photocatalytic H_2 production.

In Chapter 3, CuO was deposited on P25 TiO_2 via widely employed wet impregnation method. As discussed in literature reviews presented in Chapter 2, there are several other methods to load metal(s) on TiO_2, and different fabrication methods also were found to influence the H_2 generation activity of the final photocatalysts to a large extent (Wu et al., 2004). For instance, Au-TiO_2 photocatalyst as fabricated by photo-deposition showed greater activity in H_2 generation than samples prepared by deposition-precipitation and wet impregnation methods (Bamwenda et al., 1995). Likewise for Cu-TiO_2 photocatalysts, fabrication methods also affected its photocatalytic activity, as well as characteristics of the end-products. Boccuzzi et al. compared properties and activity of Cu-TiO_2 prepared by wet impregnation and chemisorption-hydrolysis methods, and found that samples with the same chemical composition exhibited a remarkable difference of up to 100 times in the hydrogenation of 1,3-cyclooctadiene (Khan et al., 2008; Jang et al., 2009). Wu et al. reported that Cu

doping within the TiO_2 lattice had a negative effect on photocatalytic H_2 generation as opposed to Cu deposition (Wu et al., 2004). Different H_2 generation activity of Cu-TiO_2 prepared via varying preparation methods had also been mentioned by Kang's group (Choi et al., 2007; Jeon et al., 2007). However, to date, majority of the reported Cu-TiO_2 photocatalysts employed for H_2 production were fabricated by the wet impregnation method like that employed in Chapter 3 (Bandara et al., 2005; Choi et al., 2007; Jin et al., 2007; Xu et al., 2009). No systematic study about the effect of Cu-TiO_2 preparation methods on H_2 production has been reported. In this chapter, effect of fabrication method of Cu-TiO_2 on H_2 production was systematically investigated. This may pave way for fabrication of highly productive Cu-TiO_2 photocatalysts for H_2 production.

This chapter highlights four different methods that are widely used in the fabrication of metal-TiO_2, namely, in-situ sol-gel (SG), wet impregnation (WI), chemical reduction of Cu salt by $NaBH_4$ (NR) (Khan et al., 2009), and in-situ photo-deposition (PD) (Rosseler et al., 2010). These four methods were employed to fabricate Cu-TiO_2 photocatalysts, and their H_2 generation activities were subsequently compared. It was discovered that the fabrication methods determined the chemical state of Cu, distribution ratio of Cu within the photocatalyst, BET surface area of the product, and crystal structure of the TiO_2 support. Influences of these factors on H_2 generation activity were also discussed in this chapter.

4.2 Experimental

4.2.1 Preparation of Cu-TiO_2 photocatalysts

With reference to Chapter 3, Cu content in all samples was controlled at 8 atom% Cu/Ti, with $Cu(NO_3)_2$ $3H_2O$ (Merck, GR) as the Cu precursor.

In the sol-gel process, $Ti(OBu)_4$ (Merck) was employed as the titanium precursor, and TiO_2 was synthesized in a 1:20:6:0.8 molar ratio of $Ti(OBu)_4$:C_2H_5OH (Merck, GR):H_2O (Milli-Q, ultrapure):HNO_3 (Merck, AR) (Zhou et al., 2006). 17 ml $Ti(OBu)_4$ was dissolved in 38 ml absolute ethanol with stirring for 10 min; 2.5 ml HNO_3 was then dripped into the above solution and vigorously stirred for 30 min. Another solution containing 20 ml absolute alcohol, 4.3 ml H_2O, and required amount of $Cu(NO_3)_2$ was slowly added into the above solution, to produce transparent sol under rigorous stirring. After 7 days of aging, the obtained gel was evaporated at 105 ℃, and calcined at 450 ℃ for 4 h to obtain the final product. SG-TiO_2 was produced via identical procedures, with the exception of omitting Cu salt addition.

Degussa P25 was employed as the TiO_2 precursor in the following three processes.

For WI sample, the detailed fabrication procedures were given in Chapter 3.

For NR sample, solid $NaBH_4$ (Merck, GR) was added into a vigorously stirred, homogeneous suspension containing $Cu(NO_3)_2$ and P25 in an ice water bath. The amount of $NaBH_4$ and $Cu(NO_3)_2$ were decided by complete reduction of required amount of Cu on TiO_2. During the reduction process, the originally white TiO_2 was turned into a chocolate-brown coloured precipitate. After continuous mixing for 2 h, the colour turned blackish green. Final product was recovered and washed thoroughly with ultrapure water, and dried at 105 ℃ overnight.

In-situ photo-deposition was employed to prepare PD sample. P25 suspension was first mixed and sonicated to break up loosely attached aggregates. Required amounts of $Cu(NO_3)_2$ and methanol (Fisher, HPLC) were then added, and made up to the final volume in view of photocatalytic H_2 generation.

4.2.2 Characterization of Cu-TiO_2 photocatalysts

X-ray photoelectron spectroscopy (XPS) analyses were carried out in an ultrahigh vacuum chamber with a base pressure below 2.66×10^{-7} Pa at room temperature. Photoemission spectra were recorded by a Kratos Axis Ultra spectrometer equipped with a standard monochromatic Al Kα excitation source (hν=1486.71 eV). The pass energy and step size of low-resolution XPS scan were performed at 160 and 1 eV, respectively. For the high-resolution XPS scan, the parameters above were adjusted to 40 and 0.1 eV. Curve fitting was performed using a non-linear least square Gaussian-Lorenzian function after subtraction of Shirley background. All binding energies (BE) were referenced to C 1s at 284.8 eV.

SEM used in this chapter was Zeiss Evo 50. Prior to the SEM analysis, the powder specimen was first mounted on SEM stub using carbon tape, and then sputter-coated with gold for the examination with SEM.

The specific surface area and pore size distribution of the photocatalyst were analyzed by N_2 adsorption and desorption at 77 K using a Micromeritics ASAP 2010 system. Before the measurement, the samples were out-gassed under vacuum for 10 h at 150 ℃. The specific surface area was obtained by Brunauer, Emmett and Teller (BET) model which employs low-temperature gas adsorption to determine the specific surface area of the sample. Pore volume of the nanostructured materials was determined by Barrett, Joyner and Halenda's (BJH) mathematical model.

UV-vis diffuse reflectance spectra of Cu-TiO_2 photocatalysts were recorded by Thermo Scientific Evolution 300 UV-visible spectrophotometer equipped with an integrating sphere assembly and a xenon lamp source. $BaSO_4$ was used as the reflectance standard.

XRD, TEM, EDS and ICP analyses were also carried out for this study, and detailed information are given in Chapter 3.

4.2.3 Photocatalytic reaction

Detailed experimental procedures for H_2 generation were given in Chapter 3. Basic conditions for H_2 generation in this study was as follows: Cu-TiO_2 (1 g L^{-1}), methanol/water solution (10 volume%), and no adjustment of pH was performed.

4.3 Results and Discussion

4.3.1 Characterization of Cu-TiO_2

Figure 4.1 shows the XRD patterns of the as-prepared Cu-TiO_2 photocatalysts, with P25 as comparison. In the XRD patterns of WI and NR samples, signals of Cu components were clearly observed. In the case of WI sample, diffraction peaks at 2θ= 35.5° and 38.7° were ascribed to the respective (1 1 $\overline{1}$) and (1 1 1) planes of CuO (JCPDS 48-1548); while, for NR sample, diffraction peaks at 2θ= 36.4° and 42.3 ° were respectively identified as (1 1 1) and (2 0 0) planes of Cu_2O (JCPDS 05-0667). However, no obvious phases of Cu components were detected in SG and PD samples. As results of EDS and ICP confirmed the existence of Cu in all photocatalysts, it is believed that the dimensions of Cu components in SG and PD samples were below detection limit of the XRD, thus evidencing high Cu dispersion in the samples (Xu et al., 1998). Taking into account the fabrication process, Cu component in PD sample might be in ground metal state, since in-situ photocatalytic reduction of Cu salt favored formation of metallic Cu (Gombac et al., 2010). The chemical state of Cu in SG sample was identified by XPS analysis.

With regard to TiO_2, the XRD pattern of SG sample exhibited characteristic features of anatase phase (JCPDS 21-1272), with an average crystal size of 8.5 nm, as calculated by Scherrer's equation from the full width at half maximum of anatase (1 0 1), after correction for instrumental broadening.

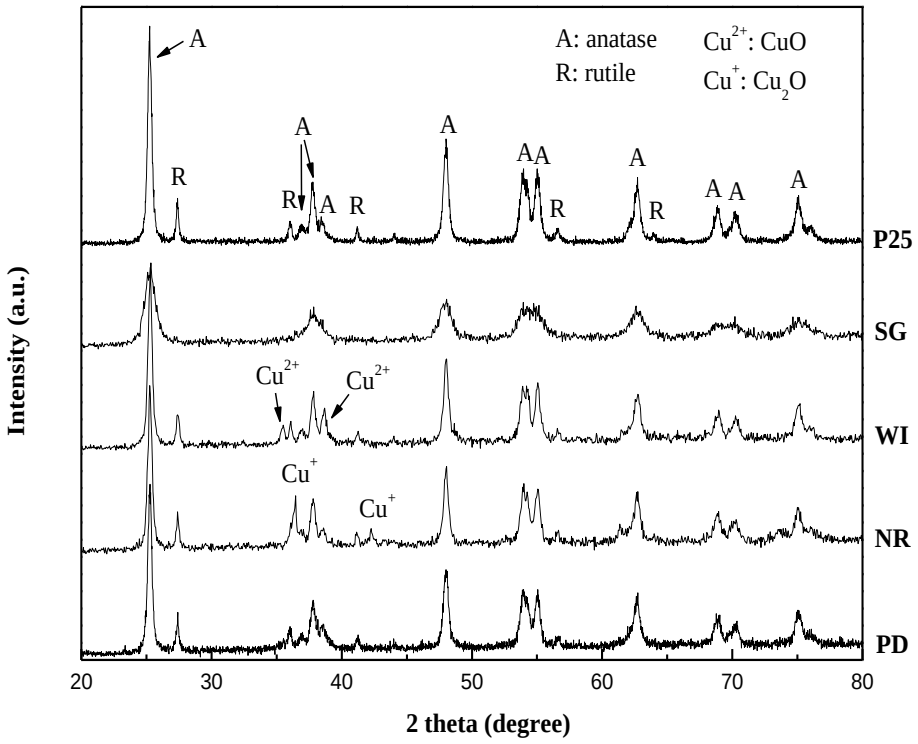

Figure 4.1 XRD patterns of as-prepared Cu-TiO_2 photocatalysts. (Pattern of PD sample was obtained after reaction due to the limitation of in-situ fabrication.)

For P25-based photocatalysts (WI, NR, PD), no significant changes of P25 diffraction patterns were observed, indicating that the TiO_2 support had scarcely undergone changes in particle size and phase transformations during the synthesis processes.

Quantitative XPS analysis of SG sample was performed, and the survey spectrum and high-resolution scans are shown in Figure 4.2.

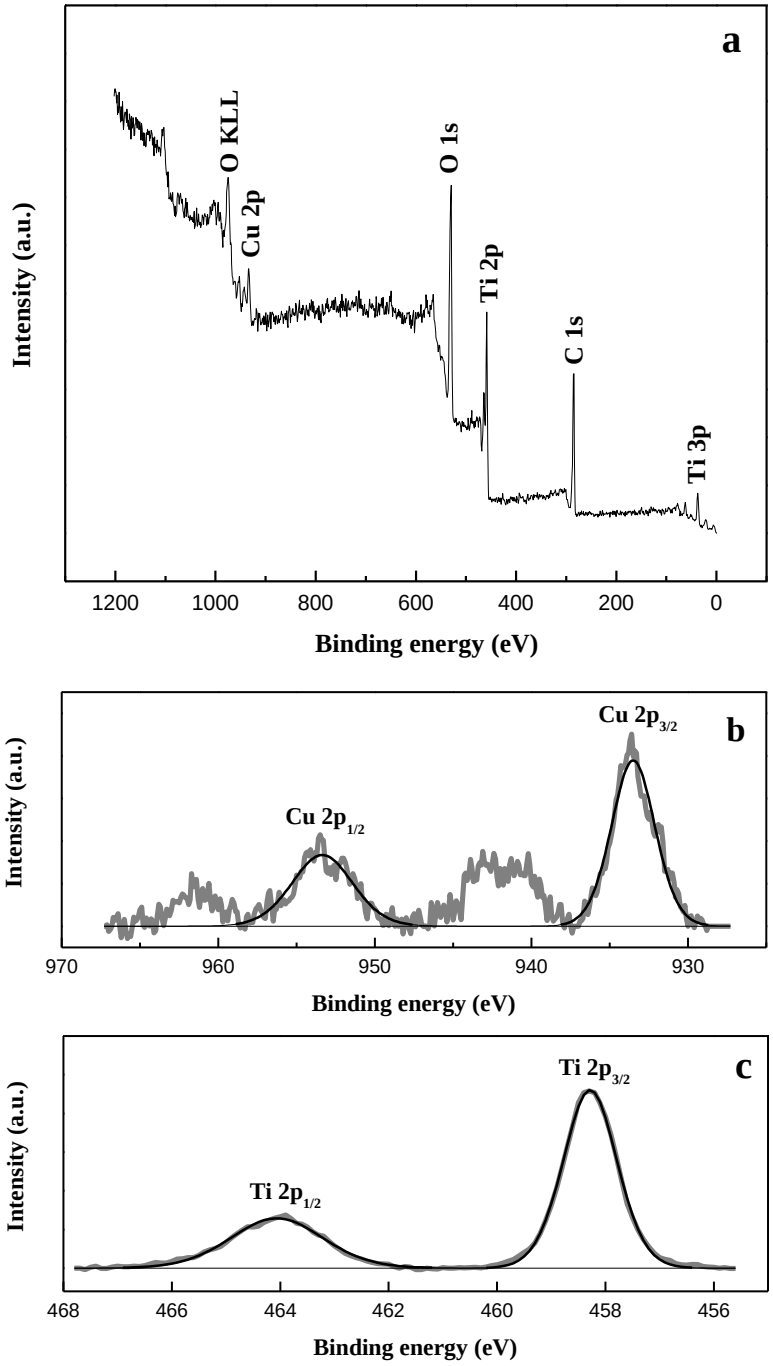

Figure 4.2 (a) XPS survey spectrum of SG photocatalyst; (b) High-resolution Cu 2p spectrum; (c) High-resolution Ti 2p spectrum.

In the XPS spectra, Cu, Ti and O photoelectron lines from SG sample were clearly

detected along with C peaks. The XPS observations were consistent with EDS results that apart from Cu, Ti and O, no other elements were detected from the samples. In Figure 4.2b, Cu $2p_{3/2}$ and Cu $2p_{1/2}$ spin orbital splitting photoelectrons were located at binding energies of 933.5 and 953.4 eV respectively. These were assigned to the CuO compound (Tseng et al., 2004). The respective binding energies of Ti $2p_{3/2}$ and Ti $2p_{1/2}$ were found to be 458.3 and 464.0 eV. These bands were assigned to typical Ti^{4+} (Choi et al., 2007), which was consonant with the XRD analysis. The XPS spectra confirmed the chemical composition of SG sample to be CuO and TiO_2.

Morphologies of the synthesized Cu-TiO_2 were observed by TEM, and the representative images of WI and SG are shown in Figure 4.3. From the TEM image shown in Figure 4.3a, it is apparent that the WI sample consisted of two types of particles coalesced together, with diameters of ca. 10 nm and 25 nm. With reference to the XRD patterns, particles of 10 nm were most likely CuO component, and the larger particles of 25 nm were postulated as TiO_2 support. The agglomeration of small Cu component particles around TiO_2 endorsed efficient charge transfer and high photocatalytic activity. A similar result was obtained for the NR sample (image not shown). It is noteworthy that for both SG and PD samples, only particles assigned to the TiO_2 support could be distinguished from the TEM images. According to the XRD analysis, Cu components within SG and PD samples were highly dispersed, and this resulted in poor identification from the TEM images.

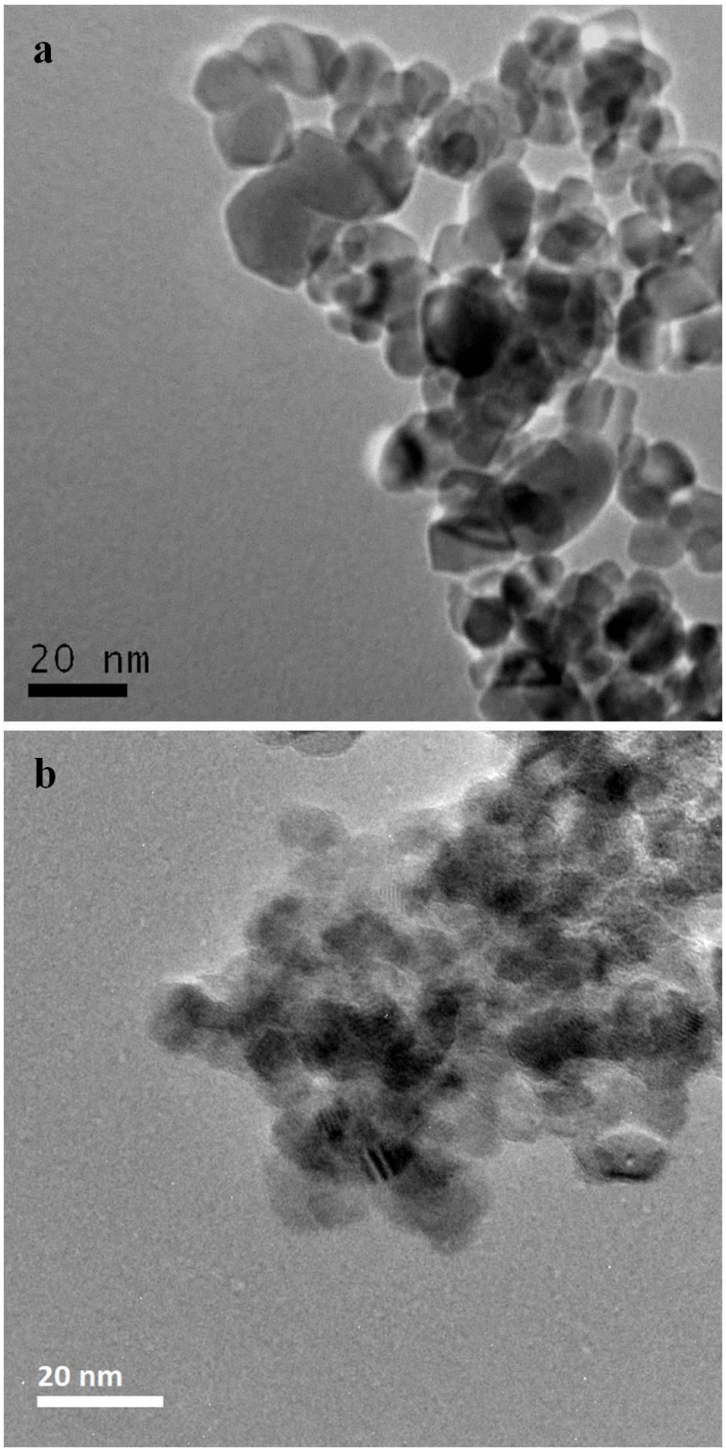

Figure 4.3 TEM images of Cu-TiO_2 photocatalysts (a: WI; b: SG).

Table 4.1 summarizes surface atomic composition, Cu content, and BET specific surface area of the as-prepared photocatalysts. All prepared Cu-TiO_2 possessed

similar Cu content and the ratios of Cu/Ti in all bulk samples were about 8 atom%. Nevertheless, from the EDS results, Cu content on the surface were relatively higher, especially for P25-based photocatalysts (WI, NR and PD). Difference of Cu/Ti ratio in the surface and bulk phases, gives a good indication of whether the Cu component was deposited on the surface of TiO_2 or dissolved into the crystal lattices of TiO_2. During the preparation process of WI, NR and PD samples, interactions between Cu and TiO_2 support were confined to the TiO_2 surface, and the existing TiO_2 crystal structure limited dissolution of Cu into its lattice, leading to relatively greater accumulation of Cu component on the surface. Contrary to the P25-based samples, Cu in the SG sample was allowed to homogenize with TiO_2 in the molecular scale during the sol-gel process (Wu et al., 2004). This resulted in a relatively uniform dispersion of Cu component on both the surface and bulk of the sample.

Table 4.1 Summary of surface elemental composition, Cu content and BET specific surface area of as-prepared Cu-TiO_2 photocatalyst.

Catalyst	Surface elemental composition (atom %)			Cu/Ti (surface, %)	Cu/Ti (bulk, %)	BET surface area (m^2 g^{-1})
	Cu	Ti	O			
SG	4.1±0.2	43.0±1.7	53.0±2.2	9.4±0.4	8.1±0.4	87.3±3.6
WI	3.5±0.1	30.7±1.4	65.9±2.7	11.3±0.5	8.5±0.4	36.1±1.5
NR	4.2±0.2	34.7±1.4	61.1±2.5	12.2±0.5	8.6±0.4	44.8±1.8
PD	4.3±0.2	30.8±1.3	64.9±2.6	13.8±0.6	8.2±0.4	46.8±1.9

From Table 4.1, it can be noted that all Cu-TiO_2 photocatalysts possessed a moderate BET surface area, thus facilitating adsorption of reactants on the photocatalyst surface. Among all the samples, SG possessed the largest surface

area, mainly due to composition of 8.5 nm TiO_2 crystals; while, particles in P25-based samples (WI, NR, PD) were ca. 25 nm. Moreover, P25-based photocatalysts tended to agglomerate into larger secondary particles during the synthesis processes, which led to lower surface areas. SEM images (Figure 4.4) and pore size distribution results (Figure 4.5) further manifested the formation of secondary particles.

In the SEM image of the SG sample, dense cakes instead of particulates were observed, owing to coagulated particles of small dimensions. Under the same conditions, nanoscale particles of P25 and uniformly large agglomerates in P25-based samples (pointed in squares) were apparent in the SEM images.

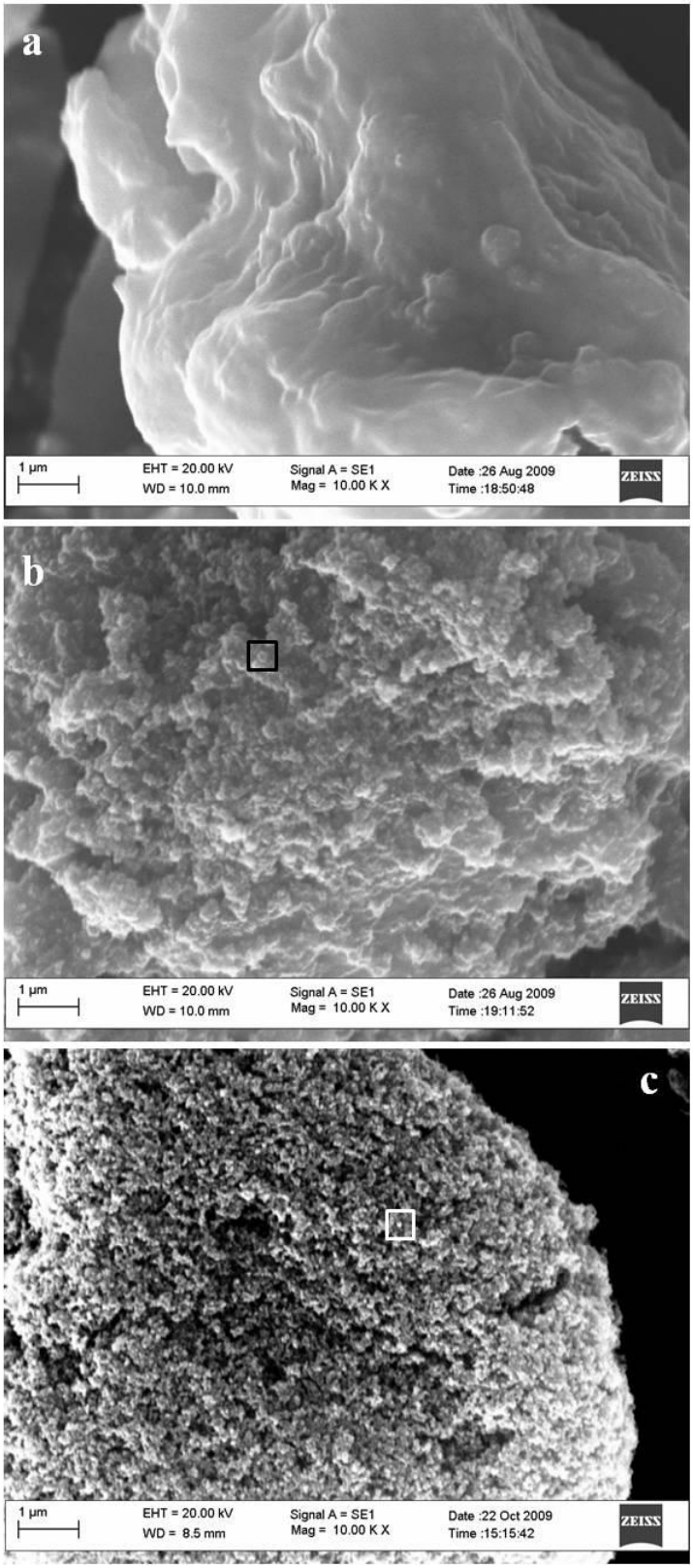

Figure 4.4 SEM images of Cu-TiO_2 photocatalysts (a: SG; b: NR; c: P25).

The pore size distribution of Cu-TiO_2 photocatalysts in Figure 4.5 supported the existence of larger secondary particles formed in all P25-based samples.

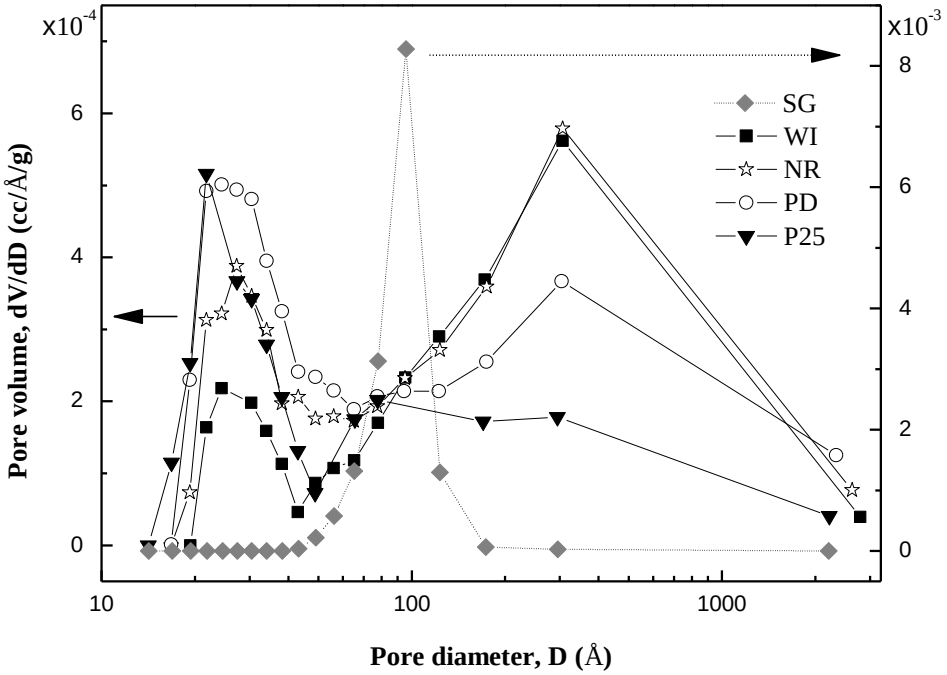

Figure 4.5 Pore size distribution of Cu-TiO_2 photocatalysts.

It is clear that the curves of P25-based samples had at least two components with peak values of 2-3 nm and 30 nm. When compared against P25, intensity of the first component decreased in the order of PD, NR, WI; whereas, intensity of the second component exhibited the reverse sequence. Incorporated with the BET data and SEM images, it is reasonable to hypothesize that the first component corresponded to the pore volume distribution of primary nanoparticles (ca. 25 nm); the second component correlated to pores formed within the larger secondary particles (Bavykin et al., 2004), and intensity of the second peak corresponded to the amount of secondary particles present in the sample. In accordance to this hypothesis, the dominant composite of P25 was primary nanoparticles; whereas secondary particles were prevalent gradually in P25-based samples, in the sequence of PD, NR, and WI. This sequence was associated with the preparation

processes, where the in-situ PD method allowed preservation of P25 structure to a big extent, and the calcination procedure used to prepare WI sample further promoted formation of secondary particles. For the SG sample, there was only one pore size distribution peak that was centered at 10 nm, and apparently, the low position of this peak corresponded to large surface area of the photocatalyst.

Figure 4.6 shows the UV-visible absorption spectra of Cu-TiO_2 photocatalysts. In addition to the strong absorption bands at around 350 nm which were associated with excitation of O 2p electron to the Ti 3d level, large absorption bands between 400-800 nm were distinct, which was attributed to the presence of Cu species. These visible light absorption bands might be due to metallic Cu absorption (225-590 nm) (Praliaud et al., 1998), 3-D Cu^{1+} clusters (400-500 nm) (Colon et al., 2006), excitation of CuO electron from the valance band to the exciton level (<730 nm), and d-d transition of Cu^{2+} (600-800 nm) (Praliaud et al., 1998). Improvement of visible light absorption of Cu-TiO_2 photocatalysts led to a reduction of its inherent band gap. For example, band gap of SG sample decreased from 3.1 eV of bare SG-TiO_2 to 2.4 eV, as calculated with application of the Kubelka-Munk function. Cu species (CuO/Cu_2O/metallic Cu) with smaller band gap and higher work function than bare TiO_2 facilitated light harvest and charge carrier separation in Cu-TiO_2 samples, and were highly regarded to improve photocatalytic reaction efficiencies.

In addition, the differential reflectance spectra of WI, NR and PD samples showed two maxima: one was in the UV region, and the other was under the visible light range. It indicated that there were two-phase materials or two different types of electron transitions in those samples (Michalow et al., 2009), which could be respectively attributed to TiO_2 and Cu species. For the SG sample, only one peak in the visible light region was observed, which suggested relatively high dispersion

of Cu component in the sample, and good contact between the Cu component and TiO_2 (Bokhimi et al., 1997).

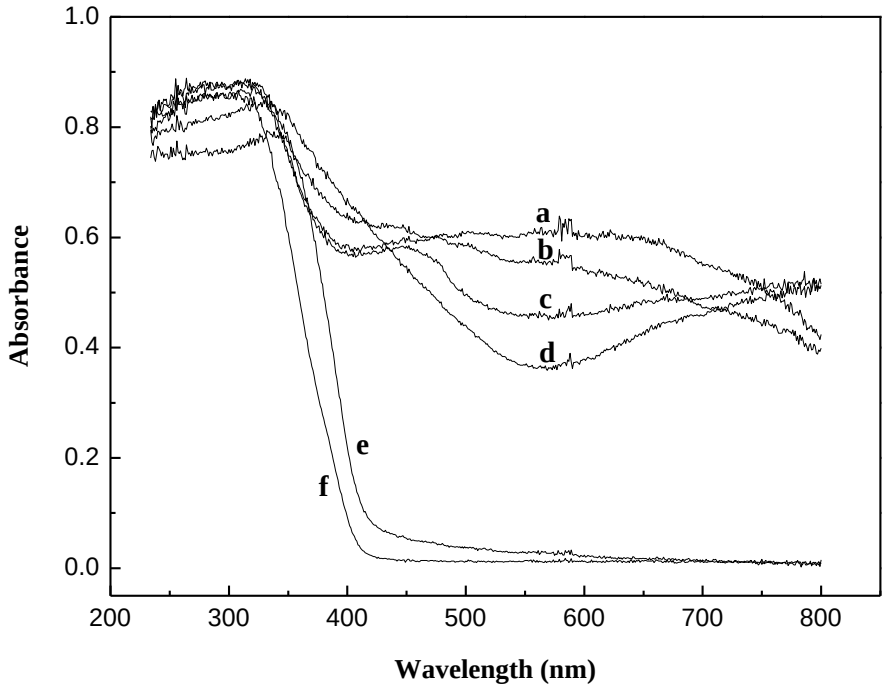

Figure 4.6 UV-visible absorption spectra of Cu-TiO_2 photocatalysts (a: WI; b: PD; c: NR; d: SG; e: SG-TiO_2; f: P25).

4.3.2 Photocatalytic H_2 production over Cu-TiO_2

Figure 4.7 shows time courses of H_2 evolution over fabricated Cu-TiO_2 photocatalysts, with bare TiO_2 supports (P25, SG-TiO_2) as comparison. Changes of H_2 generation rates as calculated on basis of time courses are summarized in Figure 4.8.

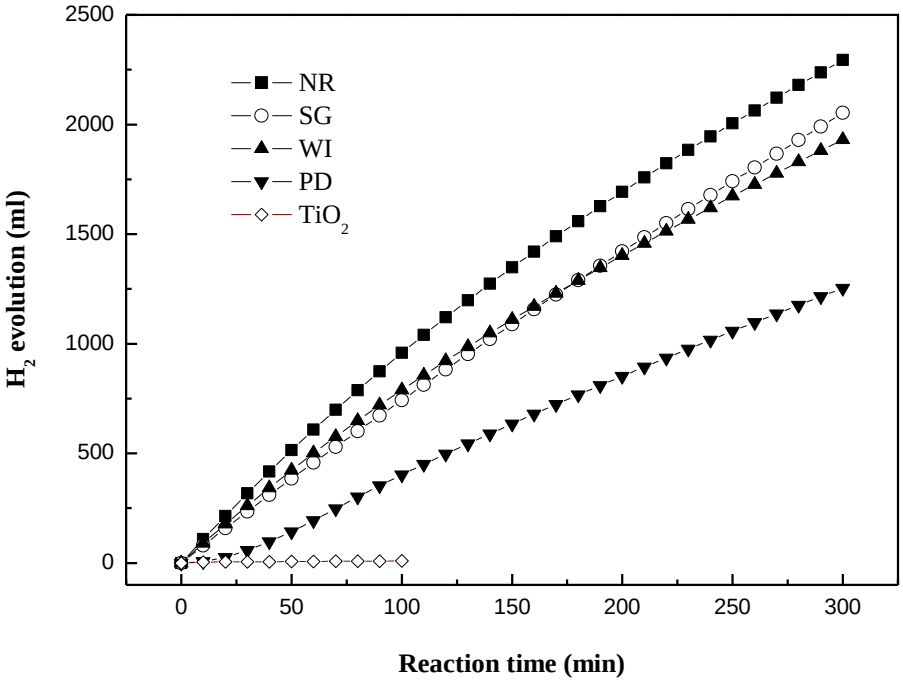

Figure 4.7 Time courses of H_2 evolution over Cu-TiO_2.

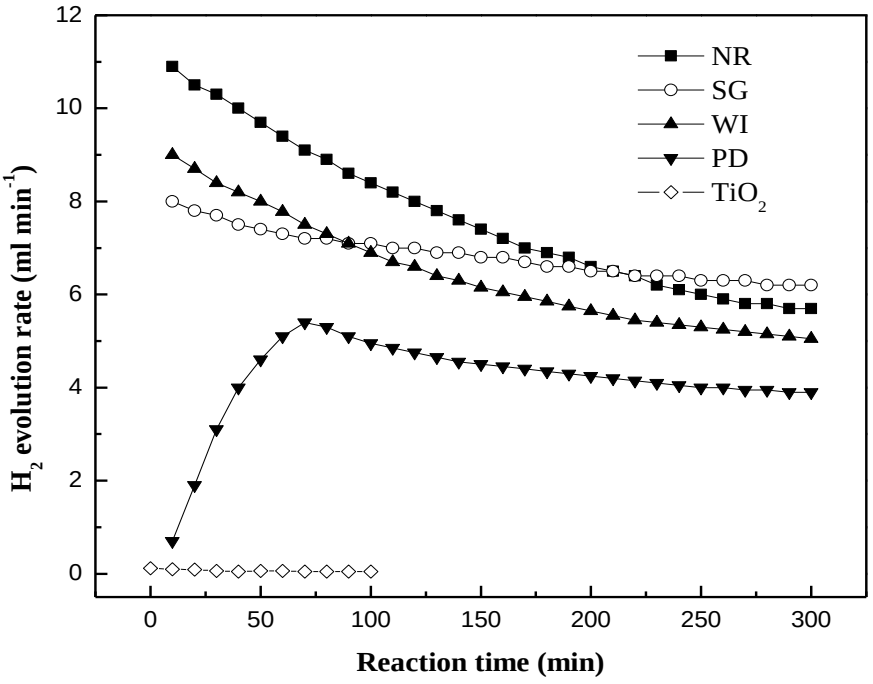

Figure 4.8 Changes of H_2 evolution rates over Cu-TiO_2.

It can be seen that the addition of Cu components significantly promoted H_2 generation activity over bare TiO_2. For pure TiO_2, H_2 evolution rate was a mere 0.05 ml min^{-1} (about 90 μmol h^{-1} $g^{-1}_{catalyst}$), and this poor H_2 generation efficacy had been reported before (Choi et al., 2007; Puangpetch et al., 2009), under similar reaction conditions. A much higher H_2 generation rate was achieved in the range of 5-11 ml min^{-1} (9-20 mmol h^{-1} $g^{-1}_{catalyst}$) over Cu-TiO_2 photocatalysts, as dependant on the preparation process.

The great improvement rooted primarily from efficient separation of photo-induced electrons and holes in TiO_2. In SG, WI and NR samples, conduction band of Cu_xO (CuO/Cu_2O) is lower than TiO_2 (Jin et al., 2007), hence excited electrons in TiO_2 were inclined to transfer to Cu_xO, instead of staying in TiO_2 to recombine with holes. In PD sample, electron migrated from the semiconductor to Cu metal owing to the higher work function that Cu possesses (Linsebigler et al., 1995). Formation of Schottky barrier at the metal-semiconductor interface served as an efficient electron trap in preventing electron/hole recombination. Accumulation of electrons enabled the Cu component to act as water reduction sites in enhancing production of H_2. In addition, all fabrication methods employed in this study, equipped Cu-TiO_2 photocatalysts with good dispersion of Cu components, moderate BET surface area, and excellent light absorption ability. These characteristics are advantageous for efficient photocatalytic H_2 production. Thus, under similar reaction conditions, H_2 generation rates of the as-synthesized Cu-TiO_2 photocatalysts were even higher than some noble metal (Pt/Au) loaded TiO_2 (Sreethawong et al., 2005; Sreethawong et al., 2007).

From Figure 4.7, it can be found that the chemical state of Cu component and Cu content in the photocatalyst, were two major factors that would affect H_2 generation of Cu-TiO_2.

Effect of Cu chemical state on H_2 generation activity can be elucidated by comparing initial H_2 generation rates of all samples. NR with Cu_2O showed the highest activity, followed by WI and SG samples with CuO, while PD with metallic Cu was the most inferior out of the four samples. The diverse performances of Cu components were due to different competencies of Cu species (CuO/Cu_2O/ metallic Cu) in the capture of electrons. As compared to metallic Cu, Cu oxides were more inclined to receive electrons from TiO_2; while under the same conditions, the redox potential of Cu^+/Cu is higher than Cu^{2+}/Cu, inferring that electrons would preferentially attack Cu_2O than CuO. The increase in efficiency of electron/hole separation resulted in a higher H_2 generation rate.

In this study, it was found that high Cu content in photocatalyst, within the range of Cu<8 atom% Cu/Ti, significantly enhanced H_2 generation activity. Take PD for example, during Cu^{2+} reduction and concurrent in-situ formation of the sample (first 30 min reaction), Cu was gradually deposited on TiO_2, thereby increasing Cu content of the sample. An increase in the subsequent H_2 generation rate was correspondingly recorded. During H_2 generation over mature PD sample (after 70 min), a slight reduction in Cu content was observed, since pH of reaction solution declined gradually due to formation of CO_2 and HCOOH byproducts, leading to Cu dissolution into the liquid phase (Figure 4.9). As a result, efficiency of H_2 generation was observed to abate slightly with time. Decline of H_2 generation rate corresponding with decreased Cu content in the photocatalyst was also observed for SG, WI and NR samples during H_2 generation.

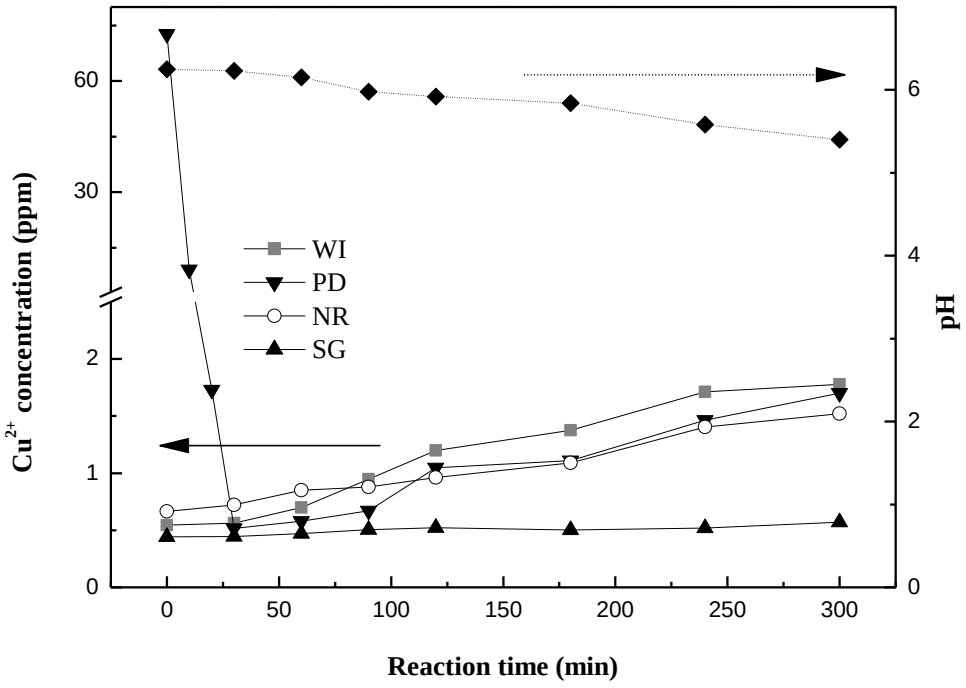

Figure 4.9 Cu leaching from Cu-TiO_2 into the aqueous phase corresponding to pH decline across the 5 h reaction. (For PD sample, Cu^{2+} reduction occurred in the first 30 min of reaction.)

It gives a strong indication that higher Cu content in photocatalyst would yield higher H_2 generation efficiency. In Chapter 3, optimum Cu content in maximizing active surface sites and UV penetration to TiO_2 was 10 atom% Cu/Ti (Cu content: 9.1 mol%) for WI sample. In this study, Cu content in all four photocatalysts (SG, WI, NR, and PD) were less than 10 atom% Cu/Ti; moreover, a positive effect of Cu content on H_2 generation activity was observed. Therefore it is predicted that the optimum Cu content for all four preparation methods should be higher than 8 atom% Cu/Ti. Optimum Cu content may be primarily determined by nature of Cu and TiO_2, and less affected by the preparation methods. Further investigation is still required to clarify the relationship between optimum Cu content and fabrication methods.

Considering the initial difference of H_2 generation rates between SG and WI samples, distribution of Cu component in the photocatalyst might also affect photocatalytic activities, since Cu content and chemical states for both samples were similar. In the WI sample, more Cu was accumulated on the TiO_2 surface than the SG sample. This improved H_2 generation due to an increased probability for protons in the aqueous phase to come into contact with reduction sites. More Cu loaded on the surface of photocatalysts would assist in electron transfer and consumption.

It is noted that the SG method produced sample with the highest stability. In SG synthesis, the Cu component was allowed to dissolve into the lattice of TiO_2, which restricted Cu component from leaching into the liquid phase during photocatalytic reactions, hence resulting in stable and consistent H_2 generation throughout the 5 h reaction. After 220 min of reaction, H_2 generation rate of the SG sample was highest among all four Cu-TiO_2 samples. Excellent stability endowed SG sample to be a potential candidate in performing intensive photocatalytic reactions.

During H_2 generation, Cu components underwent physicochemical and kinetic transformations. As the reaction progressed, the discrepancy in photocatalytic activities due to different chemical states of Cu became less apparent. This indicates that chemical state of Cu in the photocatalysts tended to transform and homologize during photocatalytic reactions. In addition, according to the results of EDS and ICP, there was no significant changes in Cu content present in the spent photocatalysts. However, after the process of H_2 generation, no XRD diffraction peaks of Cu species in all Cu-TiO_2 photocatalysts could be found as shown in Figure 4.10. Disappearance of diffraction peaks implied that all Cu components were well dispersed after the photocatalytic reactions. This is a direct evidence for

Cu component transformation during the photocatalytic reaction.

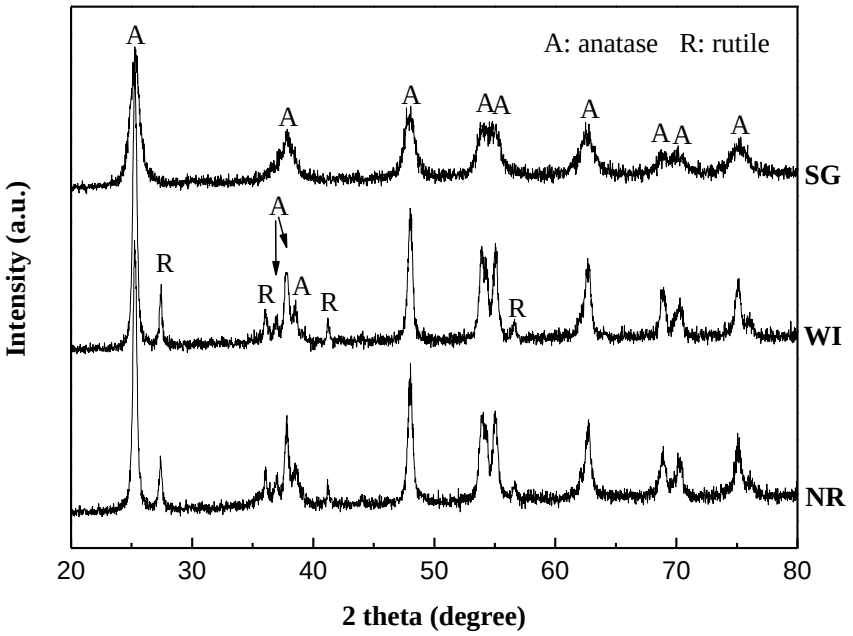

Figure 4.10 XRD patterns of Cu-TiO_2 photocatalysts after 5 h reaction. (Pattern of PD sample was given in Figure 4.1.)

We postulate that the kinetic transformations were redox in nature, and were related to the dissolution and deposition of Cu components in aqueous solution and TiO_2 support. Cu oxides were first dissolved in acid solutions to form Cu^{2+}, and the Cu^{2+} ions then captured excited electrons to form metallic Cu, which was in-situ photo-deposited on TiO_2. This process produced highly dispersed metallic Cu with small dimension on the photocatalyst. Finally, metallic Cu on TiO_2 was oxidized back to Cu oxide by photo-generated holes, and closed the Cu transformation cycle.

Characteristics of the TiO_2 support were found to be non-critical in influencing H_2 generation. Pure anatase phase in SG samples showed similar trends as anatase/rutile mixture in the WI sample. Difference in BET surface area of the

TiO_2 supports also had insignificant influence on H_2 generation activity. Therefore, it can be concluded that an active crystal phase with a moderate BET surface area were the main requirements for TiO_2 support in Cu-TiO_2 photocatalysts.

All the experiments presented in this chapter were carried out for 2-3 times, and the results were highly reproducible with ±5% variation.

4.4 Conclusion

This chapter highlighted four fabrication methods of Cu-TiO_2 photocatalyst, namely, SG, WI, NR and PD, and investigated the effect of individual synthesis method on the photocatalytic H_2 generation activity. Cu-TiO_2 photocatalysts fabricated via the four methods were equipped with good dispersion of Cu component and excellent light absorption ability. Depending on preparation process, H_2 generation rates over the as-prepared Cu-TiO_2 photocatalysts were recorded in the range of 9-20 mmol h^{-1} $g^{-1}_{catalyst}$, which was even superior to some noble metal (Pt/Au) loaded TiO_2.

The various fabrication methods led to different Cu chemical states, as well as different Cu distribution ratios in the surface and bulk phases of photocatalysts. Both factors were proven to influence photocatalytic activities. Cu_2O in the NR sample, exhibited the greatest enhancement in terms of initial H_2 generation, followed by CuO in WI and SG samples, while effect of metallic Cu in PD sample was relatively inferior among the four samples. It was also postulated that Cu components distributed on the surface of TiO_2 facilitated charge transfer more efficiently than that dissolved in TiO_2 lattice, thus leading to a higher H_2 generation rate.

Among the four photocatalysts, the SG sample demonstrated greatest potential in engineering applications. It achieved the highest rate of H_2 generation over an extended period of time owning to excellent stability, and this stability was largely attributed to the restriction of Cu leaching by its crystal configuration.

In addition, it can be concluded that within the range of Cu<8 atom% Cu/Ti, higher Cu content in photocatalysts would generally induce better photocatalytic performance; meanwhile, Cu component in all samples underwent kinetic transformation during the reaction, giving rise to unitive chemical states and higher distribution in TiO_2.

CHAPTER 5

STUDY OF HIGHLY EFFICIENT TiO_2 NANOTUBE BASED Cu-TiO_2 PHOTOCATALYST FOR H_2 PRODUCTION

5.1 Introduction

Chapters 3 & 4 investigated and enhanced the H_2 generation activity of Cu-TiO_2 via optimizing its fabrication methods and operation conditions. In both chapters, P25 with high photocatalytic activity was used as TiO_2 support, which is usually used as the benchmark for developing new TiO_2 based photocatalysts. It was found that good TiO_2 supports in developing Cu-TiO_2 photocatalysts is significantly important for high H_2 generation activity, which has been discussed in Chapter 3. However, currently, most of the reported highly efficient Cu-TiO_2 is utilizing P25 as the support. So far there is no any report discussing highly efficient TiO_2 nanotube based Cu-TiO_2 photocatalysts for H_2 production.

1-D TNT has attracted considerable research interest and exhibited immense potential in a wide variety of applications, ranging from environmental purification (Zhang et al., 2009; Li et al., 2010), energy storage (Armstrong et al., 2005) and gas sensing (Sennik et al., 2010), but little is known about its performance in photocatalytic H_2 production. In the limited studies about TNT for H_2 production, TNT with Pt (Lin et al., 2004; Khan et al., 2008; Rosseler et al., 2010), Ir and Co nanoparticles (Khan et al., 2009), or hydrated Ni complex (Jang et al., 2009) was reported to be active for H_2 production. However, no performance about Cu incorporated TNT (Cu-TNT) has been investigated yet.

Cu-TNT is supposed to possess excellent H_2 generation activity, due to efficient charge separation and fast electron transfer, which mitigate electron/hole recombination in the photocatalyst. Charge transfer and separation in Cu-TNT is presumptively illustrated in Figure 5.1. Since the conduction band of TiO_2 is more negative than that of CuO, excited electrons in TNT would easily transfer to CuO, resulting in accumulation of excess electrons in CuO, and negative shift in Fermi level of CuO (Bandara et al., 2005). This endows CuO with required overvoltage for proton reduction, and serving as H_2 formation site. In addition, unique nanotubular structure of TNT facilitates fast electron transfer in the photocatalyst (Khan et al., 2009), which would also give rise to high activity of H_2 generation.

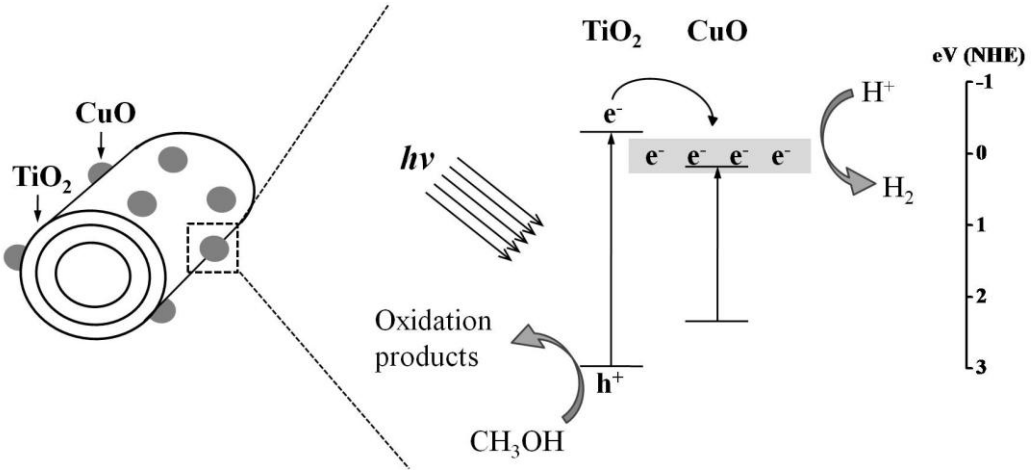

Figure 5.1 Schematic diagram of charge transfer in Cu-TNT photocatalyst under irradiation.

To verify the potential of Cu-TNT in photocatalytic H_2 production, in this chapter, TNT based Cu-TiO_2 was synthesized and tested in photocatalytic reaction. It was found that Cu-TNT possessed excellent H_2 generation activity, which was much higher than P25 based Cu-TiO_2, even superior to some Pt/Ni incorporated TNT. This study may pave way for the practical application of highly efficient Cu-TNT

photocatalyst in H_2 production.

In this chapter, 1-D TNT was fabricated via hydrothermal route, and then incorporated with Cu by adsorption-calcination (A-C) or wet impregnation (WI) method. A-C method was chosen and designed specially for TNT since its large surface area provided possibility of achieving a high loading via adsorption with a uniform distribution and high dispersion. After structure and component characterizations, the fabricated Cu-TNT was evaluated in photocatalytic H_2 production.

5.2 Experimental

5.2.1 Preparation of TNT and Cu-TNT

TNT was fabricated by a typical hydrothermal method followed by calcination process. P25 powder was added to 10 M NaOH (Merck, AR) aqueous solution, followed by an ultrasonic process and thorough mixing. The homogeneous suspension was then hydrothermally treated in a Teflon-lined autoclave at 150 ℃ for 48 h. The obtained precipitate was washed thoroughly with de-ionized (DI) water, and then dispersed into 0.1 M HCl (Merck, AR) under continuous stirring for 24 h. The acid treatment was repeated for 3 times, and the product was washed thoroughly with DI water until the resulting pH was neutral. After drying in a freeze dryer, the product was then calcined at 400 ℃ to obtain the final TNT photocatalyst.

Cu component was introduced into TNT by A-C or WI method, with $Cu(NO_3)_2$ $3H_2O$ (Merck, GR) as the precursor. With reference to Chapter 3, during fabrication, Cu/Ti ratio was controlled at 10 atom% by adjusting $Cu(NO_3)_2$

concentration.

Adsorption of Cu^{2+} on TNT in A-C method was carried out in $Cu(NO_3)_2$ solution with aqueous ammonia, since high pH promoted cation adsorption on TNT, and Cu^{2+} could be stabilized by complexation with ammonia. During preparation, aqueous ammonia solution was added into $Cu(NO_3)_2$ solution dropwise to form a clear solution. TNT was then dispersed into the respective solution and stirred for 20 h to ensure homogeneous dispersion and diffusion. After carefully washing with DI water to remove excess Cu^{2+}, the product was dried at 60 ℃ overnight and calcined in open air at 400 ℃ for 2 h. The obtained sample was denoted as TNT-A-C.

In WI method, TNT was added into $Cu(NO_3)_2$ solution at a ratio of 1g/3ml, followed by ultrasonication and thorough mixing to obtain a homogeneous slurry. After wet impregnation, the sample underwent same dry and calcination processes as TNT-A-C, to yield TNT-WI photocatalyst.

As comparison, P25 based Cu-TiO_2 photocatalysts (Cu-P25) were also fabricated by A-C and WI methods, and were denoted as P25-A-C, and P25-WI, respectively.

5.2.2 Characterization of TNT and Cu-TNT

XRD, EDS, TEM, BET, XPS, and UV-visible diffuse reflectance spectra analyses were performed in this study, and detailed information of these analyses were given in Chapters 3 & 4. Morphology of TNT was also studied using a field-emission scanning electron microscope (FESEM, Jeol JSM-6340F).

5.2.3 Photocatalytic reaction

Smaller Pyrex reactor with solution volume of 270 ml was utilized in this chapter instead of the 1.45 L reactor used in Chapters 3 & 4. Apart from this, detailed experimental procedures for H_2 generation were identical to that described in Chapter 3, and basic conditions could refer to Chapter 4.

5.3 Results and Discussion

5.3.1 Characterization of photocatalysts

Figure 5.2 shows the XRD patterns of the as-prepared TNT and Cu-TNT photocatalysts, with P25 based photocatalysts as comparison.

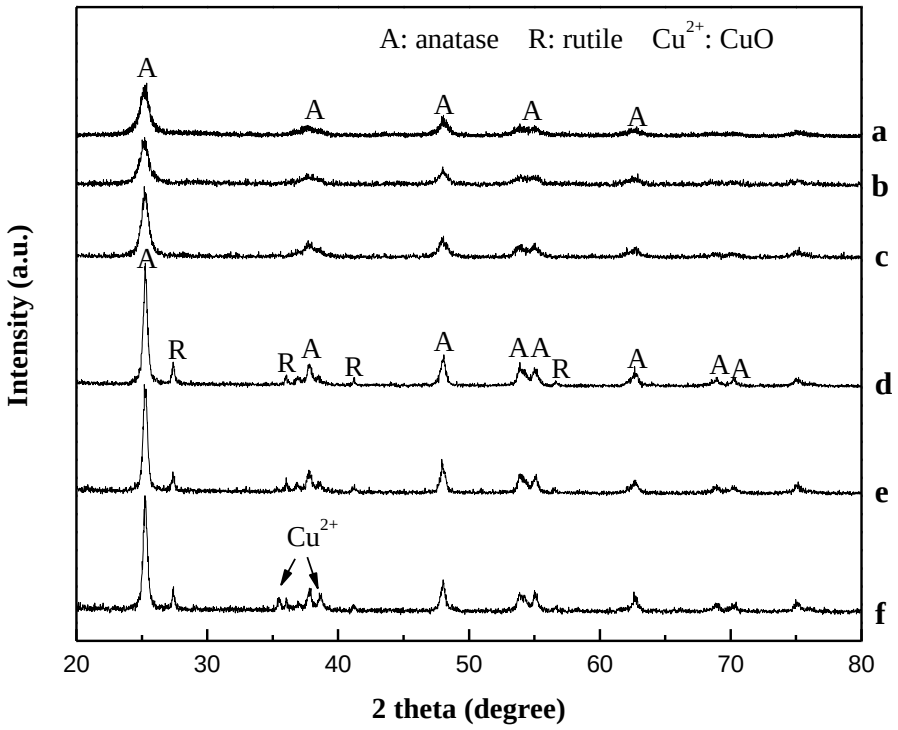

Figure 5.2 XRD patterns of photocatalysts (a: TNT; b: TNT-A-C; c: TNT-WI; d: P25; e: P25-A-C; f: P25-WI).

It can be seen that the fabricated TNT and Cu-TNT exhibited characteristic features of anatase TiO_2 (JCPDS 21-1272), but no obvious Cu components were detected in Cu-TNT samples, although EDS analysis of Cu-TNT confirmed the existence of Cu. Xu et al. reported the instances where diffraction peaks of Cu species disappeared when Cu component was highly dispersed in TiO_2 (Xu et al., 1998). Therefore, it is believed that the Cu components in Cu-TNT were highly dispersed in the samples, with small dimensions below XRD detection limit. Different from Cu-TNT samples, in XRD pattern of P25-WI, diffraction peaks of tenorite CuO (JCPDS 48-1548) were clearly observed, evidencing relatively poorer dispersion of Cu components in P25 based samples.

In addition, diffraction pattern of pure TNT indicated that crystallinity of TiO_2 in TNT was poorer than P25. The calcination process carried out during Cu incorporation improved crystallinity and enhanced the intensity of TiO_2 peaks in TNT-WI sample; whereas TNT-A-C possessed better thermal stability, and maintained similar diffraction pattern as TNT. This was related to the exchange of Cu^{2+} into TNT lattice, and would be discussed in the XPS analysis later.

EDS was employed to detect elemental compositions of photocatalysts, with spectra showed in Figure 5.3 and data summarized in Table 5.1.

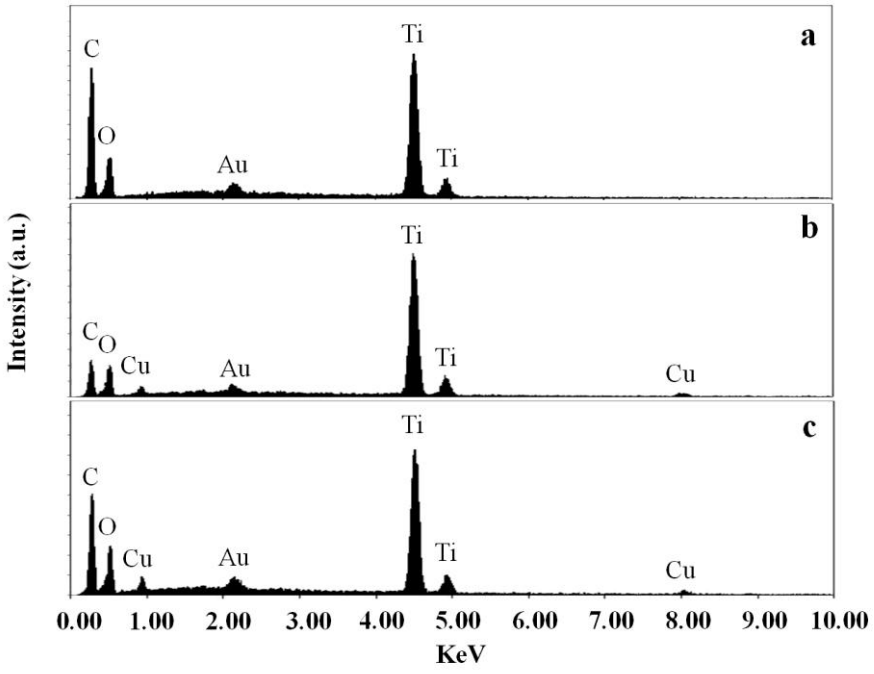

Figure 5.3 EDS spectra of photocatalysts (a: TNT; b: TNT-A-C; c: TNT-WI).

Table 5.1 Summary of elemental compositions detected by EDS and BET surface area of photocatalysts.

Catalyst	Elemental composition (atom %)			Cu/Ti (%)	BET surface area (m^2 g^{-1})
	O	Ti	Cu		
TNT	58.2±2.4	41.8±1.8	0.0	0.0	279.9±12.2
TNT-A-C	49.0±2.0	46.8±1.9	4.2±0.2	9.0±0.4	152.4±6.1
TNT-WI	54.5±2.3	41.6±1.7	4.0±0.2	9.6±0.4	96.3±3.9
P25-A-C	45.5±1.9	51.4±2.0	3.1±0.1	6.0±0.3	41.0±1.8
P25-WI	65.9±2.8	30.7±1.4	3.5±0.1	11.3±0.5	36.1±1.5

In EDS spectrum of TNT, peaks of C, O, Au, Ti were clearly observed, where C and Au were attributed to the carbon tape and gold coating required by the EDS test. Therefore, the as-prepared TNT sample was supposed to contain only O and

Ti elements. Na was expected to be introduced into the fabricated TNT during the alkaline hydrothermal process (Thorne et al., 2005). However, it was not detected in EDS analysis. This indicated that Na concentration in the sample was reduced by repeated washing in dilute HCl solution, and less than the lower detection limit of EDS. In the spectra of Cu-TNT samples, Cu peaks were clearly observed, along with elements presented in TNT.

Comparing Cu/Ti ratio in all TNT and P25 based Cu-TiO_2 samples (Table 5.1), it is interesting to find that TNT-A-C contained nearly same amount of Cu with TNT-WI, whereas Cu content in P25-A-C was much lower than P25-WI. Considering the preparation procedure, it indicated that, TNT possessed great Cu^{2+} adsorption ability, which was much higher than P25.

Microstructure of the fabricated TNT was studied by FESEM and TEM (Figure 5.4). It revealed that the as-prepared TNT possessed a multilayered nanotubular structure, and the majority of nanotubes were open at both ends. The inner and outer diameters of the nanotubes were c.a. 5-7 nm and 10-12 nm, respectively, and each tube characterized a constant diameter along its length. The TiO_2 nanotube could be long, up to hundreds of nanometers.

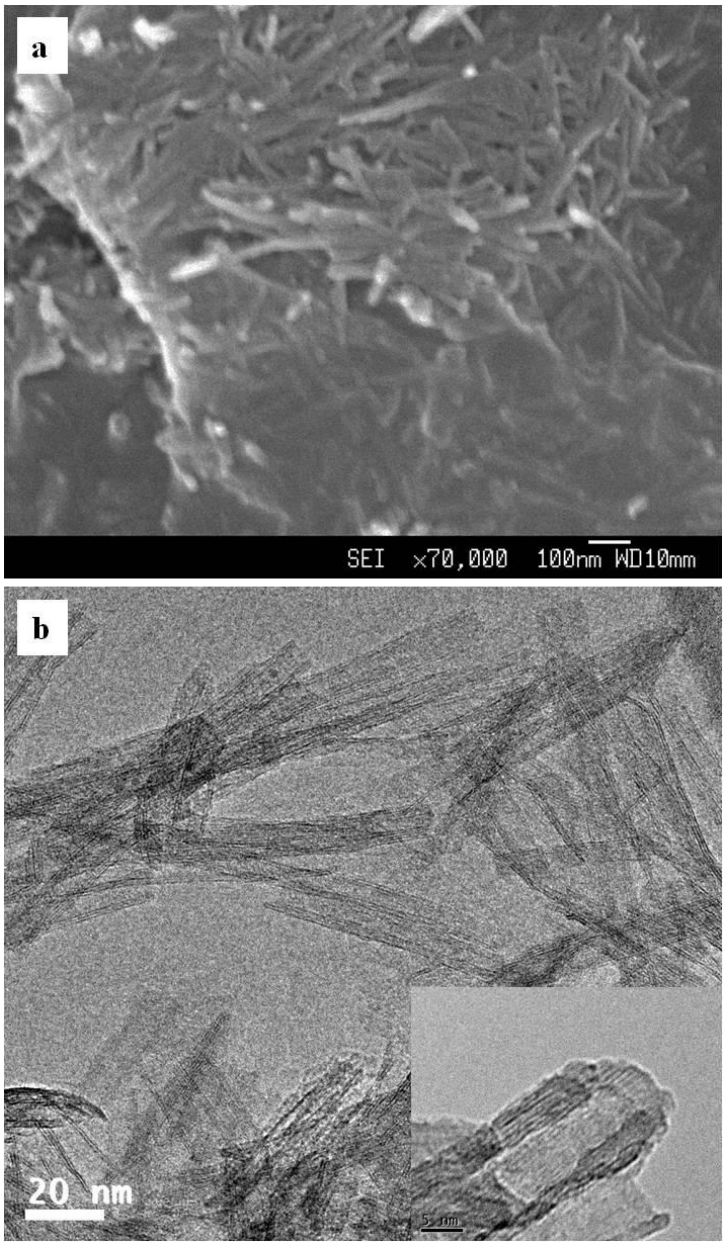

Figure 5.4 (a) FESEM and (b) TEM images of TNT.

Morphologies of Cu-TNT were also observed by TEM in this study, and the images are shown in Figure 5.5.

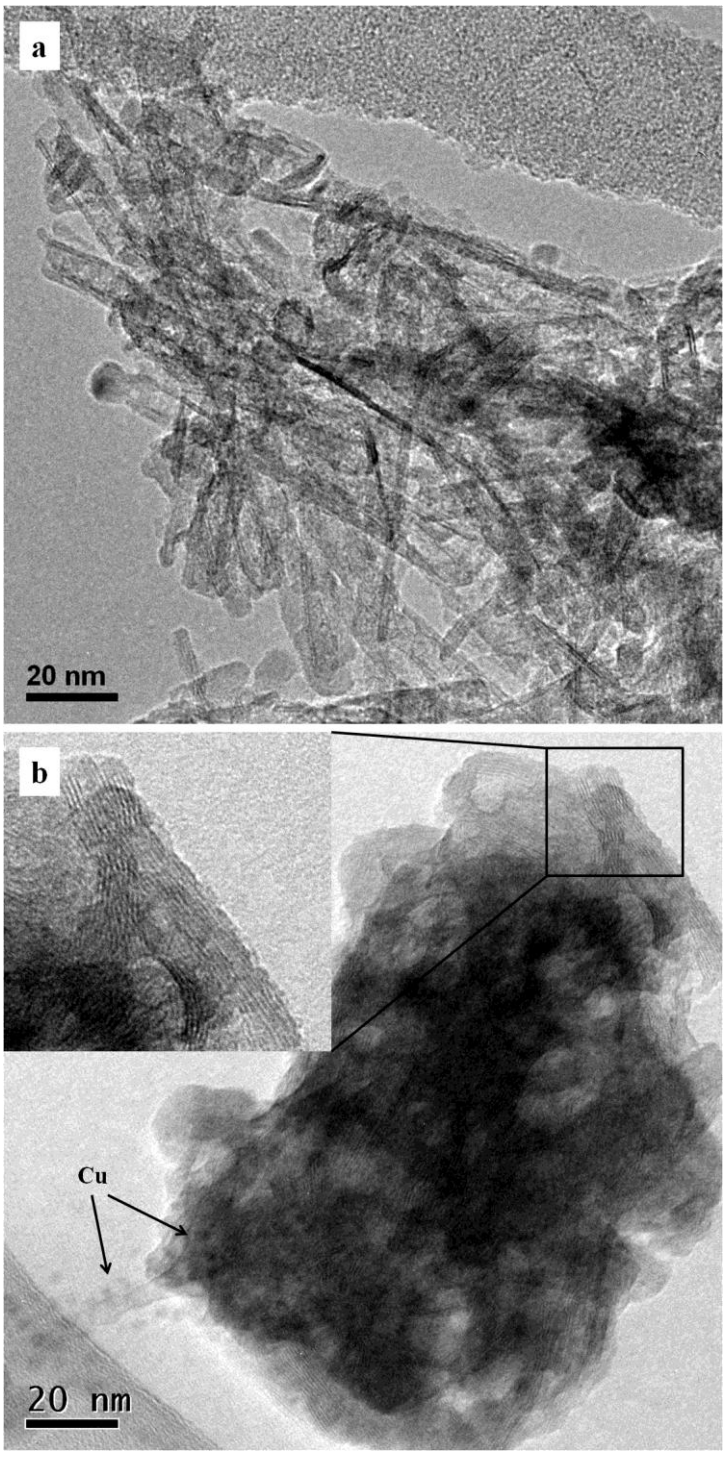

Figure 5.5 TEM images of (a) TNT-A-C and (b) TNT-WI.

It can be found that, with Cu incorporation, TNT-A-C sample still maintained

similar tubular structure with TNT, while some aggregation of nanotubes occurred. Surprisingly, no obvious Cu component could be identified from TEM image of TNT-A-C. On the contrary, in TNT-WI sample, shown in Figure 5.5b, particles of Cu component with diameter of c.a. 3 nm were clearly observed. Larger cluster of Cu component in TNT-WI than TNT-A-C might be due to characteristics of WI method: continuously variation of liquid phase composition during drying, and less adsorption of Cu^{2+} on TNT surface. In addition, for TNT-WI sample, 1-D structure of TNT was still maintained; nevertheless, the inner tubes became much narrower, even disappeared, and relatively serious aggregation of nanotubes occurred.

BET surface area of photocatalyst was determined by N_2 adsorption/desorption, with data summarized in Table 5.1. N_2 adsorption/desorption isotherm of the as-prepared TNT, depicted in Figure 5.6, exhibited a typical type IV curve with a hysteresis loop, indicating mesoporosity of the photocatalyst (Gregg et al., 1982). In addition, the relatively broad hysteresis loop of the isotherm suggested a wide distribution of pore sizes, which was clearly shown in Figure 5.7. Mesoporous nanotubular structure endowed the fabricated TNT with large BET surface area of 279.9 m^2 g^{-1}, which could account for the superior Cu^{2+} adsorption ability of TNT compare to P25. However, Cu incorporation depressed BET surface area of TNT to a certain extent; surface areas of TNT-A-C and TNT-WI reduced to 152.4 and 96.3 m^2 g^{-1}, respectively. Nevertheless, compared to Cu-P25, TNT based photocatalysts still possessed relatively large surface area, which is attractive and critically important for enhancing photocatalytic activity.

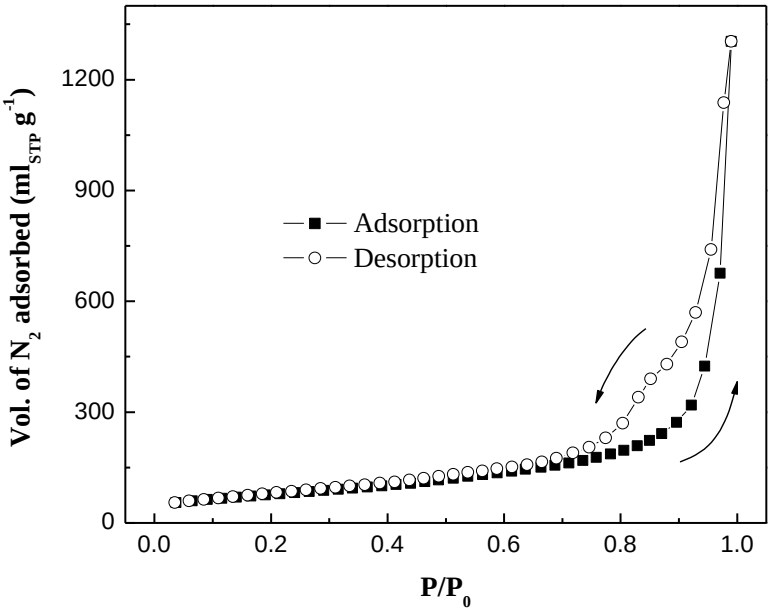

Figure 5.6 Isotherm of N_2 adsorption/desorption on the surface of TNT.

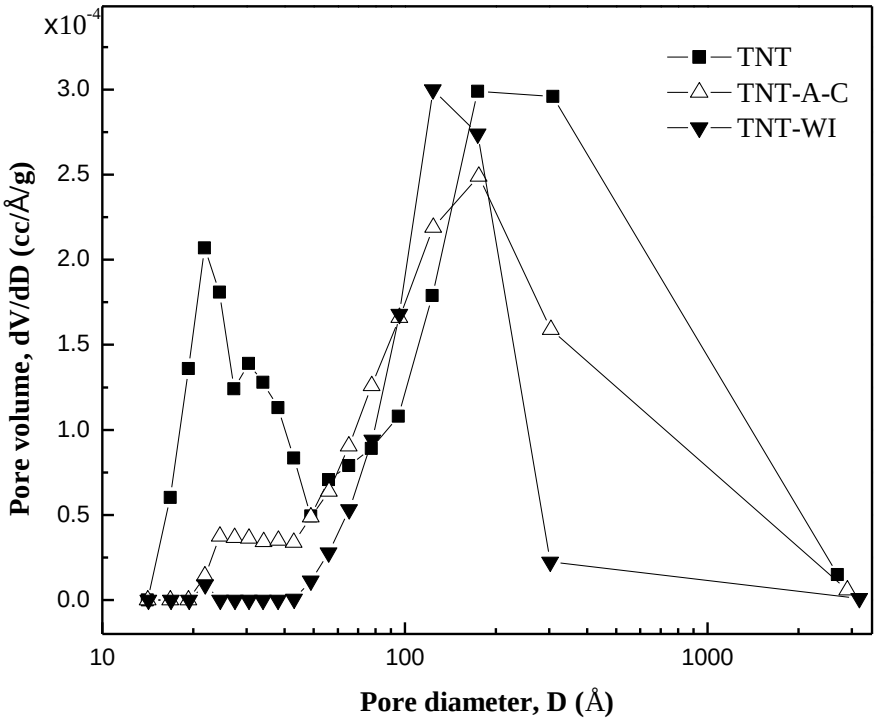

Figure 5.7 Pore size distributions of photocatalysts.

Pore size distribution curves of the photocatalysts as shown in Figure 5.7 supported the observations of TEM images and BET surface area changes. The nanotubular TNT exhibited distinct pore size distribution curve, which comprised two portions with peak values of c.a. 2-3 nm and 20-30 nm, respectively. Taking into account the morphology of TNT, the smaller pores could be attributed to the inner wall of the nanotubes, with its size similar to the inner diameter of the nanotubes; while, the larger pores should refer to the pores between the nanotubes (Bavykin et al., 2004).

With incorporation of Cu, TNT-A-C sample maintained similar pore size distribution as TNT, but pore volumes of both portions were observed to decrease. It seems that both inner and outer surfaces of TNT were occupied by Cu species. Considering pore size distribution curve with EDS and TEM results, it is believed that the Cu component in TNT-A-C sample was attached and highly dispersed on both inner and outer surfaces of TNT, without forming any visible clusters in the TEM image. For TNT-WI sample, small pores corresponding to pores inside of TNT almost disappeared; meanwhile, larger pores, associated with pores between the nanotubes, shrank to smaller size, with diameters of 10-20 nm. This is consistent with the observation of TEM image: narrowing of inner tube pores and aggregation of nanotubes. Both phenomena attributed to the large particles of Cu component prepared via WI method, where plugged Cu species particles narrowed even blocked the inner channels of TNT, while agglomerated Cu component particles on the exterior promoted aggregation of nanotubes. These resulted in the decline of BET surface area of TNT-WI compared to its TNT precursor. It is noteworthy that TNT-A-C experienced a decline in surface area from these factors as well, but to a much lesser extent than TNT-WI sample.

Quantitative XPS analyses of TNT and Cu-TNT photocatalysts were preformed,

with survey spectra and high-resolution scans shown in Figures 5.8 and 5.9, respectively.

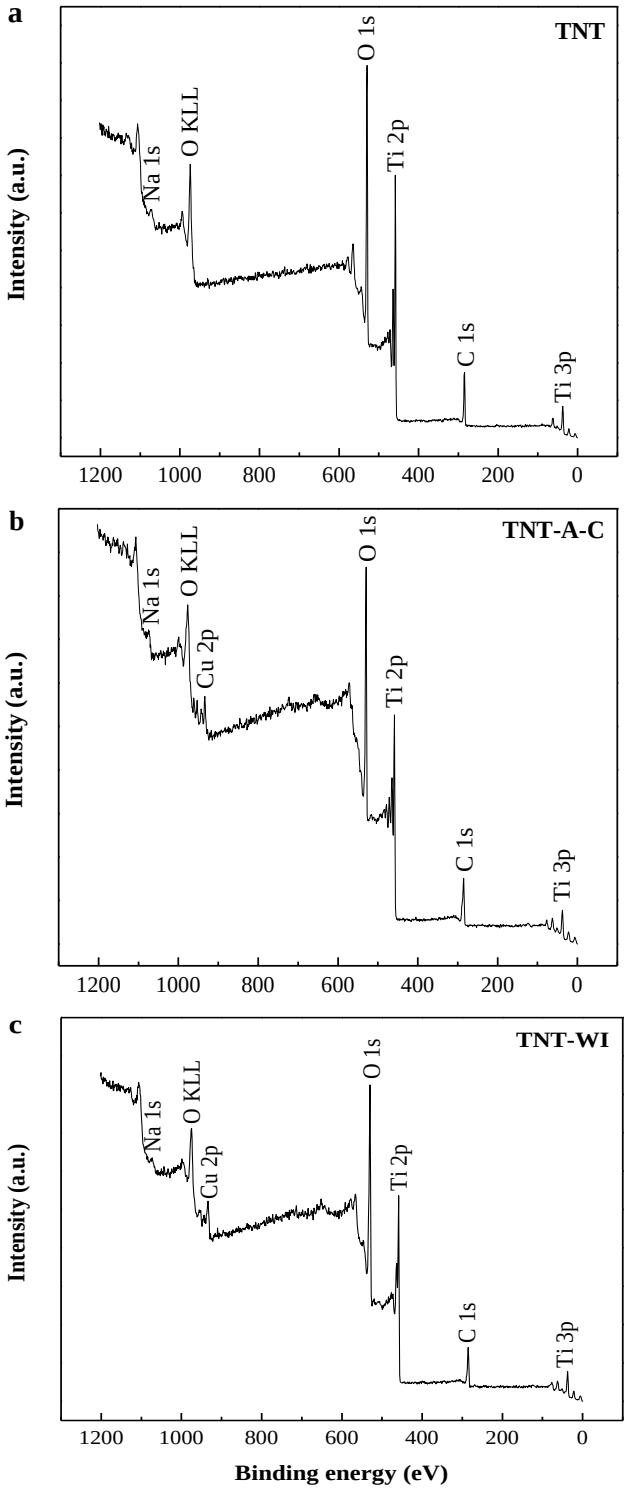

Figure 5.8 XPS survey spectra of photocatalysts (a: TNT; b: TNT-A-C; c: TNT-WI).

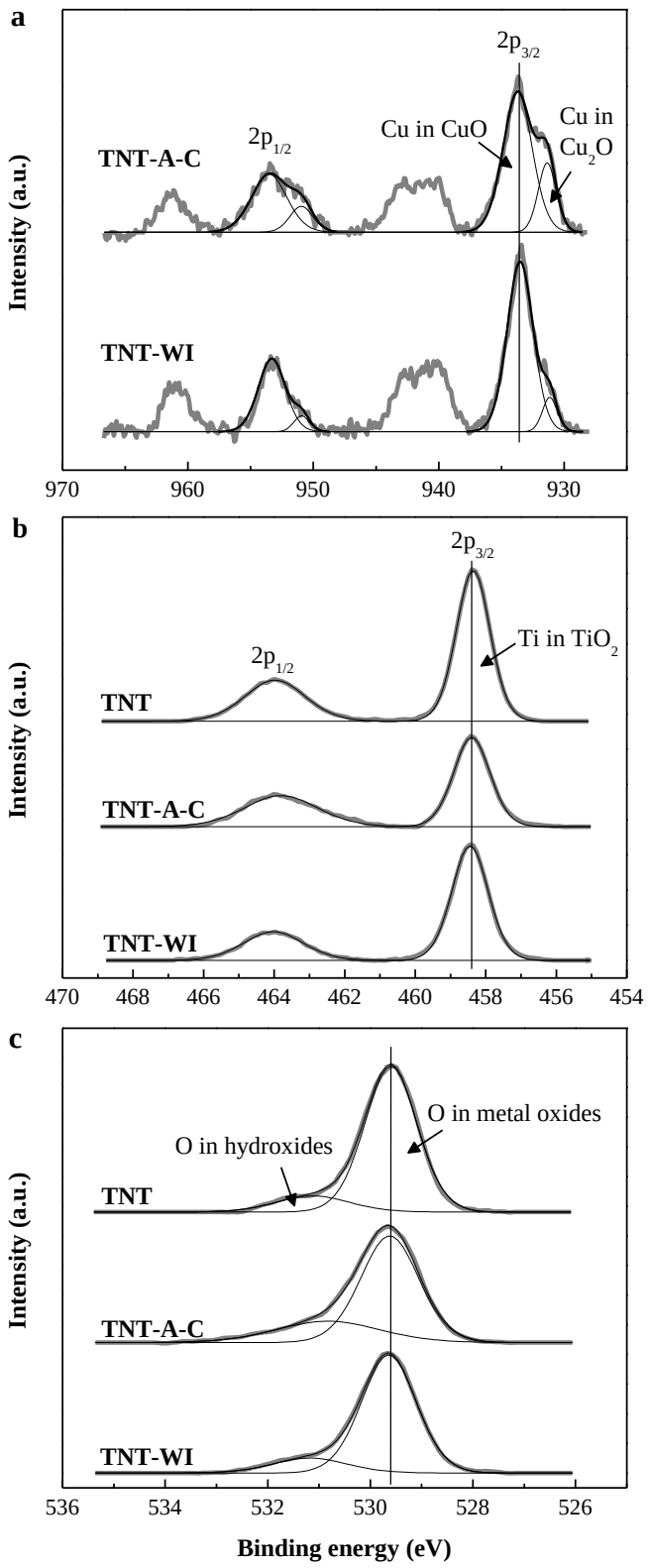

Figure 5.9 High-resolution XPS spectra of (a) Cu 2p, (b) Ti 2p and (c) O 1s.

In the survey spectra, along with peaks of C, O, Ti and Cu, small Na peaks were also observed, confirming Na residue remained in TNT after HCl washing reached the XPS detection limit.

Surface elemental compositions of TNT and Cu-TNT detected by XPS are summarized in Table 5.2.

Table 5.2 Summary of surface elemental compositions of photocatalysts detected by XPS.

Catalyst	Surface elemental composition (atom %)				Cu/Ti (%)	Na/Ti (%)
	O	Na	Ti	Cu		
TNT	71.0±2.9	2.7±0.1	26.3±1.1	0.0	0.0	10.2±0.5
TNT-A-C	72.2±3.0	1.2±0.1	25.1±1.0	1.5±0.1	6.1±0.3	4.7±0.2
TNT-WI	73.4±3.0	1.6±0.1	23.6±1.0	1.3±0.1	5.7±0.2	6.8±0.3

Surface Cu/Ti ratios of both Cu-TNT samples were smaller than values detected by EDS analysis (Table 5.1). This might be due to the depth limitation of XPS detection, where X-ray beam could not reach inner surface of TiO_2 nanotubes, resulting in detection of Cu only attached on outer surface of tubes, rather than overall Cu component. Surface Cu/Ti ratio of TNT-A-C was higher than that of TNT-WI, as separated particles of Cu component in TNT-WI sample was not evenly distributed on TiO_2 surfaces like that in TNT-A-C.

Na content in TNT decreased after Cu incorporation, indicating that Na^+ underwent ion-exchange during preparation of Cu-TNT photocatalysts. H^+ was available when TNT was dispersed in aqueous solution, and ion-exchange between Na^+ and H^+ might occur (Xing et al., 2009). According to Zhang's report that

ion-exchange between Na^+ and H^+ was pH sensitive (Zhang et al., 2000), less Na^+ should be exchanged during preparation of TNT-A-C, due to higher solution pH (TNT-A-C, pH=9-10 vs. TNT-WI, pH=3-4). However, less Na remained in final TNT-A-C than TNT-WI sample. It is supposed that Cu^{2+} complemented the ion-exchange with Na^+, and more occurred during TNT-A-C preparation. XRD results supported this inference, since Cu^{2+} exchanged into lattice of TiO_2 would benefit thermal stability of photocatalyst (Sun et al., 2003), while TNT-A-C did exhibit better thermal stability compared to TNT-WI. More exchange with Na^+ was beneficial for Cu component to be highly dispersed in TNT-A-C sample.

High-resolution scans of photocatalyst show detailed chemical environment of elements. In Cu 2p spectra of TNT-A-C and TNT-WI (Figure 5.9a), obvious shake-up satellite peaks were observed, which is typical characteristic of CuO (Poulston et al., 1996). Existence of CuO was also confirmed by the binding energies of Cu $2p_{3/2}$ and Cu $2p_{1/2}$ located at 933.5 and 953.5 eV, respectively. However, to give a good fit to the experimental total peaks, besides the predominant CuO peaks, a minor species of Cu was found, with binding energies of Cu $2p_{3/2}$ and Cu $2p_{1/2}$ located at 932.2 and 952.2 eV, respectively. This is assigned to reduced Cu species (Cu_2O or metallic Cu). According to Chusuei's study (Chusuei et al., 1999), CuO would be reduced to Cu_2O during XPS analysis, and smaller CuO particle was more susceptible to the reduction. Since calcination process employed in preparation of Cu-TNT favored formation of CuO (Poulston et al., 1996), and amount of reduced Cu species in XPS spectra was minuscule, it seems reasonable to assume the reduced Cu species to be Cu_2O, and it was reduced from CuO by X-ray. In addition, content of Cu_2O in TNT-A-C was larger than TNT-WI, indicating that CuO was smaller in size and more highly dispersed in TNT-A-C sample (Chusuei et al., 1999).

Ti 2p spectra of TNT and Cu-TNT as shown in Figure 5.9b were similar; binding energies of Ti $2p_{3/2}$ and Ti $2p_{1/2}$ were found at 458.4 and 464.0 eV, respectively, which was assigned to typical Ti^{4+} in TiO_2 (Choi et al., 2007).

In O 1s spectra of TNT and Cu-TNT (Figure 5.9c), prominent O 1s peak at about 529.6 eV was associated with oxygen in TiO_2 and CuO. In addition, a broad shoulder at a higher binding energy region was evident in all the samples, indicating the presence of surface hydroxides (Poulston et al., 1996). TNT-A-C possessed more surface hydroxides, which is advantageous for high H_2 generation activity (Jang et al., 2009).

UV-visible absorption spectra of TNT and Cu-TNT are shown in Figure 5.10, with P25 based Cu-TiO_2 as comparison. All photocatalysts exhibited strong absorption band at around 350 nm, which is associated with excitation of O 2p electron to Ti 3d level. Compared to P25, absorption onset of TNT shifted slightly towards the shorter wavelength range, giving rise to a small increase in band gap to 3.25 eV (P25: 3.15 eV), as calculated by Kubelka-Munk function.

All Cu incorporated photocatalysts showed extra large absorption band between 400-800 nm, which were attributed to the presence of Cu compounds. However, profiles of the absorption spectra were different, indicating different combination modes of Cu components with TiO_2. For P25 based Cu-TiO_2 photocatalysts, the obvious two-phase absorption in UV and visible region signified two-phase materials presented in the samples, referring to TiO_2 and Cu compounds. Nevertheless, for both Cu-TNT samples, only one absorption peak in UV region was recorded, suggesting relatively high dispersion of Cu components, and good contact between Cu compounds and TiO_2 in Cu-TNT samples (Bokhimi et al., 1997).

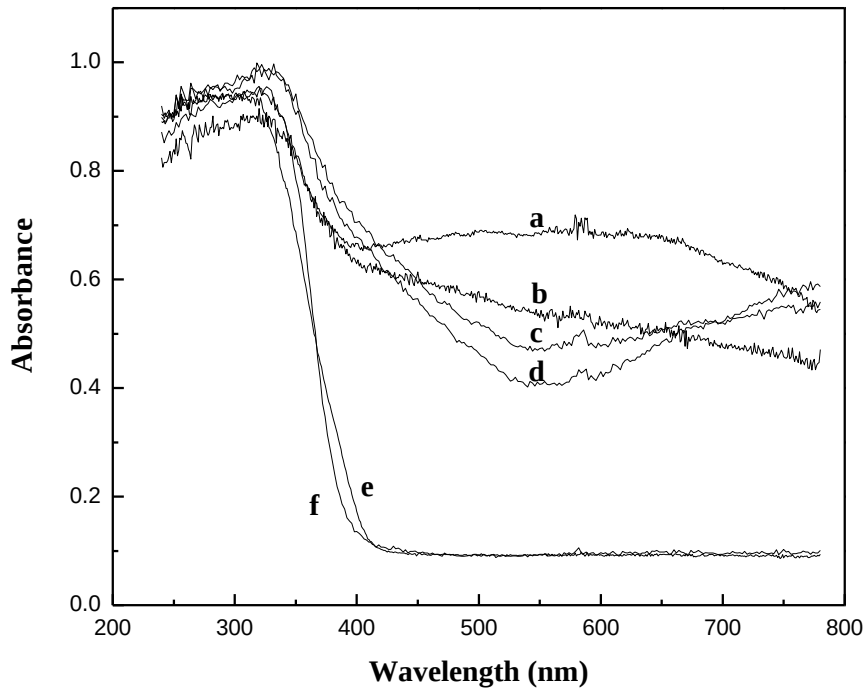

Figure 5.10 UV-visible absorption spectra of photocatalysts (a: P25-WI; b: P25-A-C; c: TNT-WI; d: TNT-A-C; e: P25; f: TNT).

Characterization of photocatalysts revealed that Cu-TNT samples maintained 1-D tubular structure, and possessed larger surface area and higher Cu components dispersion than P25 based Cu-TiO_2. In addition, Cu component, present in the form of CuO, was smaller in size and more highly dispersed in TNT-A-C sample, than TNT-WI sample.

5.3.2 Photocatalytic H_2 production

Figure 5.11 shows time courses of H_2 evolution over Cu-TNT photocatalysts, with Cu-P25 as comparison; average H_2 generation rates over 5 h reactions are summarized in Figure 5.12.

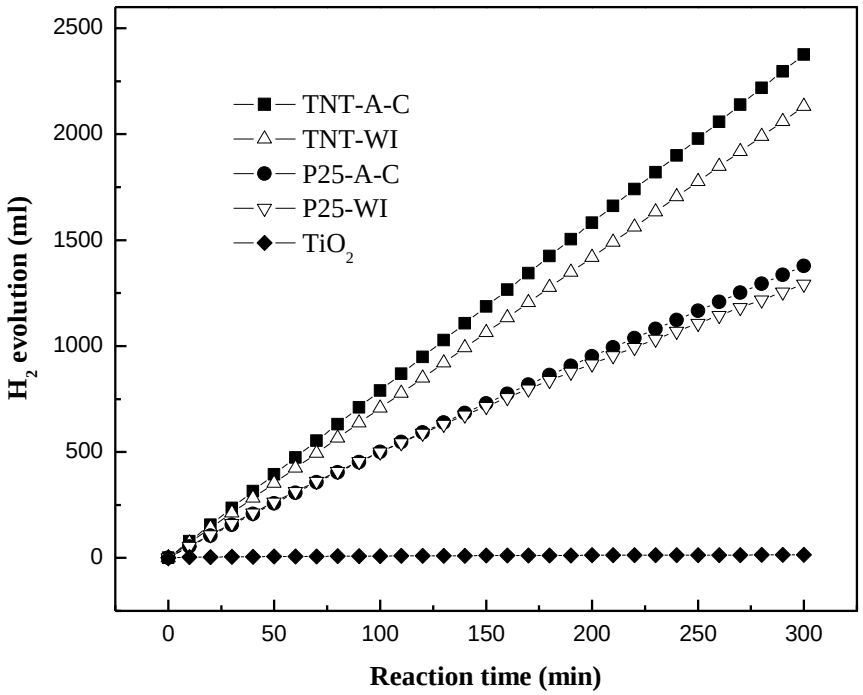

Figure 5.11 Time courses of H_2 evolution over photocatalysts under irradiation.

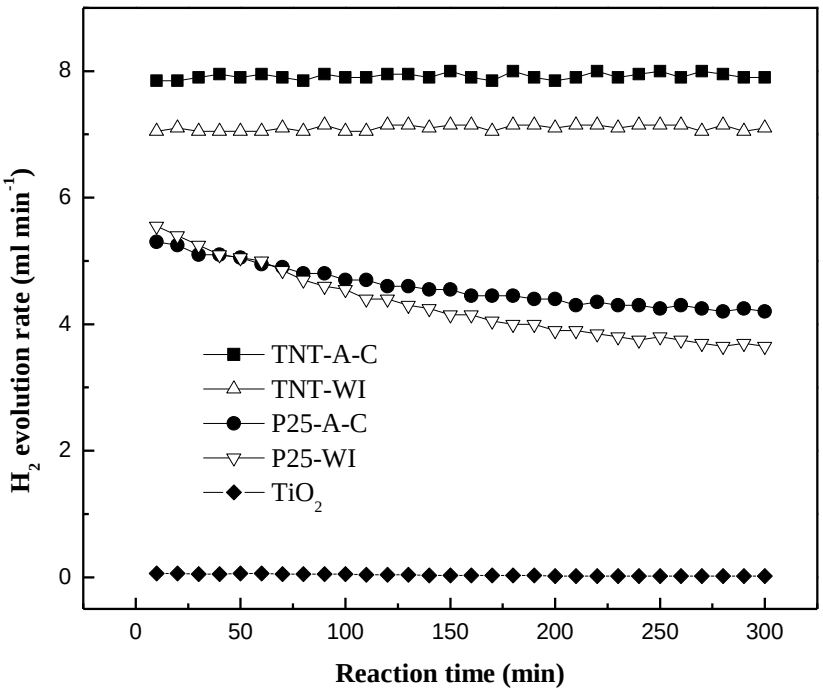

Figure 5.12 Changes of H_2 evolution rates over photocatalysts in 5 h reactions.

It was observed that negligible H_2 was evolved over bare TiO_2. As compared to bare TiO_2, presence of CuO significantly promoted H_2 generation activity. This can be credited to effective charge separation in Cu-TiO_2 photocatalysts, which is crucial for efficient H_2 generation.

From Figure 5.11, it also can be found that TNT based Cu-TiO_2 photocatalysts exhibited excellent H_2 generation activity; H_2 evolution rate over TNT-A-C was 7.9 ml min^{-1} (71.6 mmol h^{-1} $g^{-1}_{catalyst}$), which was c.a. 70% higher than P25 based Cu-TiO_2, and even superior to some Pt/Ni incorporated TNT (Lin et al., 2004; Jang et al., 2009). Nevertheless, compared to TNT-A-C, TNT-WI with relatively larger CuO particles showed inferior activity, with H_2 evolution rate recorded at 7.1 ml min^{-1} (64.2 mmol h^{-1} $g^{-1}_{catalyst}$).

Different activity of Cu-TiO_2 photocatalysts implied that, in addition to efficient charge separation, there were still several factors that influenced the activity of Cu-TiO_2. Combining H_2 generation activity with photocatalyst characterization, it suggested that 1-D tubular structure, large surface area, and high Cu component dispersion were advantageous for Cu-TiO_2 for high H_2 generation activity.

Compared with Cu-P25 photocatalysts, Cu-TNT exhibited greater H_2 generation activity. This was primarily attributed to the unique 1-D nanotubular structure, rather than pure anatase crystal structure, since pure anatase granular TiO_2 was proved to possess similar H_2 generation activity with anatase/rutile mixture of P25 in Chapter 4. 1-D tubular structure facilitated fast electrons transfer due to reduced grain boundary, and was expected to improve charge separation in photocatalytic reactions (Khan et al., 2009). In addition, large surface area inherent with nanotubular structure provided more active sites in Cu-TNT photocatalysts, which increased probability for protons in the aqueous phase to contact the reduction sites,

and hence accelerated H_2 formation further.

Comparing activity of TNT-A-C and TNT-WI, it can be induced that higher CuO dispersion in Cu-TiO_2 was beneficial for high H_2 generation activity. Both TNT-A-C and TNT-WI samples possessed similar tubular structure, Cu content, and Cu chemical state; but CuO in TNT-A-C was more highly dispersed than that in TNT-WI. Therefore, it is reasonable to attribute superior H_2 generation activity of TNT-A-C to higher Cu component dispersion. High CuO dispersion improved cohesion between Cu component with TiO_2, facilitated charge transfer from TiO_2 to Cu compound, and then enhanced proton reduction; whereas, relatively larger CuO clusters in TNT-WI might act as the recombination centers, and depressed H_2 generation activity (Khan et al., 2009). Advantage of high CuO dispersion was also manifested within Cu-P25 photocatalysts, where P25-A-C with higher Cu component dispersion but inferior Cu content, exhibited relatively higher H_2 generation activity, in comparison with P25-WI. In addition, Cu-TNT possessed higher CuO dispersion than Cu-P25, which should partly contribute to higher activity that Cu-TNT exhibited.

It is worthy to note that H_2 evolution rate over Cu-TNT photocatalysts kept vigorous during 5 h reactions, with no deactivation occurred (Figure 5.12); whereas, rate of Cu-P25 decreased with time, owing to decline of Cu content in the photocatalyst caused by Cu dissolution into liquid phase (discussed in Chapter 4). For Cu-TNT samples, large surface area and high dispersion of Cu components might accelerate the re-deposition of Cu^{2+} back to TiO_2 support, and maintained the Cu content in the photocatalysts. In addition, the expeditious dissolution and deposition processes of Cu species might promote a more uniform distribution of Cu components, resulting in robust H_2 generation activity. Excellent activity and stability ensured Cu-TNT as a potential candidate for intensive photocatalytic H_2

production.

Experimental data presented in this chapter showed good repeatability in 2-3 times reduplicate tests, and the variation was calculated within ±5%.

5.4 Conclusion

1-D mesoporous TNT was successfully fabricated by alkaline hydrothermal treatment, followed by a calcination process. The product was confirmed to be pure anatase nanotube, with a large recorded BET surface area of 279.9 m^2 g^{-1}. The fabricated TNT was then employed as TiO_2 support to conduct photocatalytic H_2 production, and exhibited superior activity compared to P25.

With Cu incorporation via adsorption-calcination (A-C) or wet impregnation (WI) method, the fabricated Cu-TNT exhibited excellent photocatalytic H_2 generation activity. H_2 evolution rates over both Cu-TNT during 5 h reaction were recorded at 7.9 and 7.1 ml min^{-1} respectively, which was much higher than P25 based Cu-TiO_2, even superior to some Pt/Ni incorporated TNT. During 5 h reaction, H_2 generation rate over Cu-TNT remained vigorous, and no deactivation occurred. Both Cu-TNT photocatalysts maintained the 1-D tubular structure, and possessed large specific surface area and high Cu component dispersion, all of which were proved to be advantageous for high H_2 generation activity. Cu-TiO_2 fabricated by adsorption-calcination process showed superior activity to that prepared by wet impregnation, due to better CuO dispersion.

High efficiency and excellent stability highlight the potential of Cu-TNT for practical applications in photocatalytic H_2 production.

CHAPTER 6

SIMULTANEOUS Cu^{2+} REMOVAL AND H_2 PRODUCTION OVER TiO_2 NANOTUBE FROM WATER

6.1 Introduction

In Chapters 3, 4 and 5, Cu-TiO_2 exhibited great potential in photocatalytic H_2 production, and H_2 generation rate over Cu-TiO_2 could be further enhanced by optimizing the TiO_2 supports, fabrication methods and operation conditions. Results of former studies affirm the potential of Cu-TiO_2 in photocatalytic H_2 production. Apart from the searching for highly efficient Cu-TiO_2 for H_2 production, TiO_2 photocatalyst was also studied for the removal of metals from water. It would be interesting and valuable if water treatment and H_2 production could be achieved simultaneously.

Cu is widely used in electrical industries, transportation, industrial machinery and military supplies, leading to fast depletion of limited Cu reserves and severe contamination of industrial wastewaters (Khan et al., 2009). Thus, waste metal recovery from water can contribute towards resource conservation and mitigation of metal pollution in water bodies. Common methods employed for Cu removal and recovery include chemical or electrolytic precipitation, activated carbon adsorption, ion exchange and membrane separation, but they are either too costly or inefficient at low concentration levels (Troupis et al., 2002). Recently, photocatalytic reduction of Cu^{2+} over TiO_2 has been investigated (Yamazaki et al., 2001; Barakat et al., 2004; Canterino et al., 2008), and shows lower cost with higher efficiency. Moreover, this method is also applicable in fabrication of Cu

deposited TiO_2 photocatalyst, which could potentially be an active photocatalyst for H_2 production. However to date, major reports about Cu^{2+} reduction over TiO_2 have merely focused on Cu^{2+} removal, and no study about simultaneous H_2 production with Cu^{2+} removal has been reported.

TNT has been proved to be more active than benchmark P25 in Chapter 5; however, no report about the utilization of TNT in metal ions removal could be found. Theoretically, effective Cu^{2+} removal and H_2 production could be simultaneously achieved over TNT, and the photocatalytic reactions are supposed to occur as illustrated in Figure 6.1.

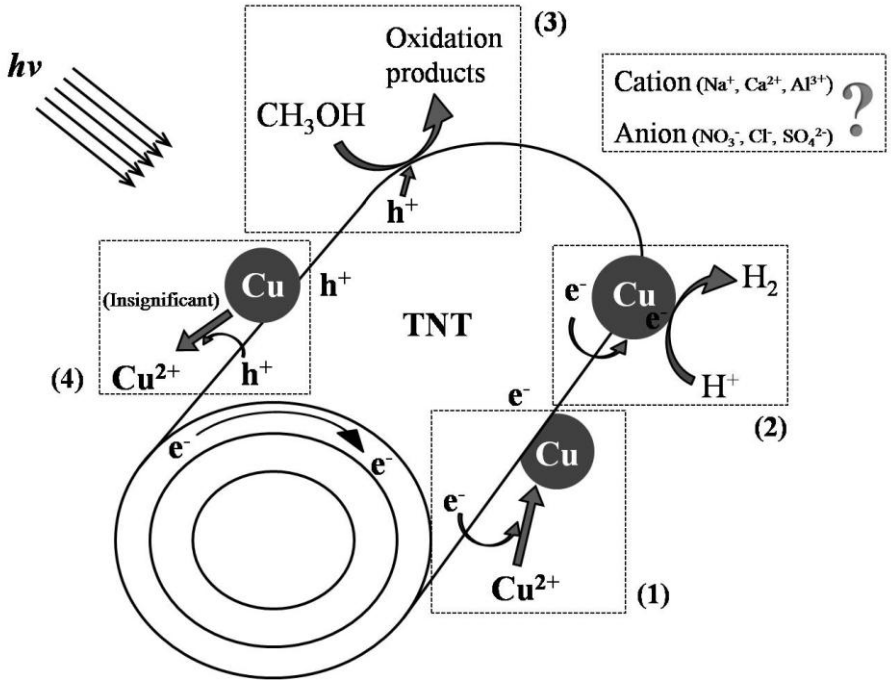

Figure 6.1 Schematic diagram of simultaneous Cu^{2+} removal and H_2 production over TNT under irradiation.

Under UV irradiation, electrons in the filled valence band of TNT are excited and promoted to the vacant conduction band, leaving behind holes in the VB. Cu^{2+} in

solution could easily be reduced to metallic Cu by electrons before depositing on TNT surface (reaction 1). The deposited Cu then serves as active sites for H_2 formation (reaction 2), since electrons in CB of TiO_2 are inclined to transfer to Cu due to its lower Fermi level. Nevertheless, Cu^{2+} reduction competes with and prior to proton reduction due to its more positive redox potential ($E^{Ø}_{Cu^{2+}/Cu}$=0.34 V), and this may suppress H_2 evolution rate at high Cu^{2+} concentrations. In addition, an optimum content of Cu over TNT is critical for efficient H_2 production, since Cu not only provides active sites for H_2 formation, but undesirably intercepts UV light from reaching the base TNT as well.

With respect to electrons consumption, holes in VB of TNT are mainly scavenged by methanol in solution functioning as electron donors (reaction 3) (Chen et al., 1999). Deposited Cu may also be oxidized back to Cu^{2+} by holes (reaction 4), although the re-oxidation of Cu might be insignificant as compared to Cu^{2+} reduction.

In this chapter, it is the first time to study and verify the potential of simultaneous Cu^{2+} removal and H_2 production over highly efficient TNT. Effect of Cu^{2+} concentration on photocatalytic reaction, competition of Cu^{2+} reduction over H_2 generation, and re-oxidation of deposited Cu were investigated and discussed. In addition, presence of cation/anion in solution may also show influence on photocatalytic reaction over TNT, which was studied in this chapter as well. This study may offer a potential and meritorious solution for treatment of metal containing wastewater with concurrent H_2 production.

6.2 Experimental

6.2.1 Synthesis and characterization of TNT

Detailed synthesis procedure of TNT was given in Chapter 5, and its characterization measures were identical to that in Chapter 5 as well.

6.2.2 Photocatalytic reaction

Experimental setup of photocatalytic reaction utilized in this chapter was similar to that in Chapter 5, and the only difference was the reaction solution. In this chapter, Cu precursor was first dissolved in 10 volume% methanol water mixture with certain concentration, and TNT was then dispersed into the above solution at a dosage of 1 g L^{-1} to form the reaction solution. Unless stated otherwise, Cu precursor employed in this chapter was $Cu(NO_3)_2$.

To investigate the applicable concentration range of Cu^{2+} by photocatalytic reduction over TNT, Cu^{2+} concentrations of 8, 80, 400 and 800 ppm were investigated in this chapter, and the Cu/Ti atom ratio in solution was controlled at 1:100, 10:100, 50:100, 100:100 respectively. To simplify, Cu/Ti ratio is described as 1%, 10%, 50%, 100% in the text, and the corresponding results were respectively denoted as TNT-1%, TNT-10%, TNT-50% and TNT-100%.

To evaluate the competition of Cu^{2+} reduction and effect of re-oxidation of reduced Cu species on H_2 generation, control experiments were carried out as follows: after normal TNT-10% reaction for 2 h, the fabricated Cu-TNT was collected and washed thoroughly with DI water, and then dispersed in fresh methanol solution with (or without) presence of Cu^{2+} (Cu^{2+}/Ti=10 atom%) to conduct photocatalytic reaction.

Effect of co-existing anion (NO_3^-, Cl^- or SO_4^{2-}) on Cu^{2+} removal and H_2 production was studied by employing different Cu^{2+} precursor ($Cu(NO_3)_2$, $CuCl_2$, or $CuSO_4$); effect of cation (Na^+, Ca^{2+} or Al^{3+}) was evaluated by adding $NaNO_3$, $Ca(NO_3)_2$, or $Al(NO_3)_3$ into reaction solution before addition of photocatalyst, with $Cu(NO_3)_2$ as Cu^{2+} precursor. Amount of cation was determined by equalizing the charges with initial Cu^{2+} in solution.

To analyse the effect of additional ions on photocatalytic reaction, point of zero charge of TNT was determined by measuring zeta potential of TNT under different pH conditions. $NaNO_3$ with concentration of 1 mM and 10 mM was used to adjust the ion strength of solution (1~10 mM) during zeta potential test, to equalize the ion strength of Cu^{2+} with other additional anions and cations (3.75~8.75 mM).

To evaluate the activity of TNT, P25, with an initial Cu^{2+}/Ti ratio of 10%, was chosen as a benchmark, and denoted as P25-10%. Control experiment for H_2 production over bare TNT was also conducted without addition of Cu precursor.

6.3 Results and Discussion

6.3.1 Reactions under various initial Cu^{2+} concentrations

6.3.1.1 Cu^{2+} removal in photocatalytic reactions

Figure 6.2 shows the changes of Cu^{2+} concentration in solution during photocatalytic reactions over TNT and P25; removal efficiency of Cu^{2+} is summarized in Figure 6.3.

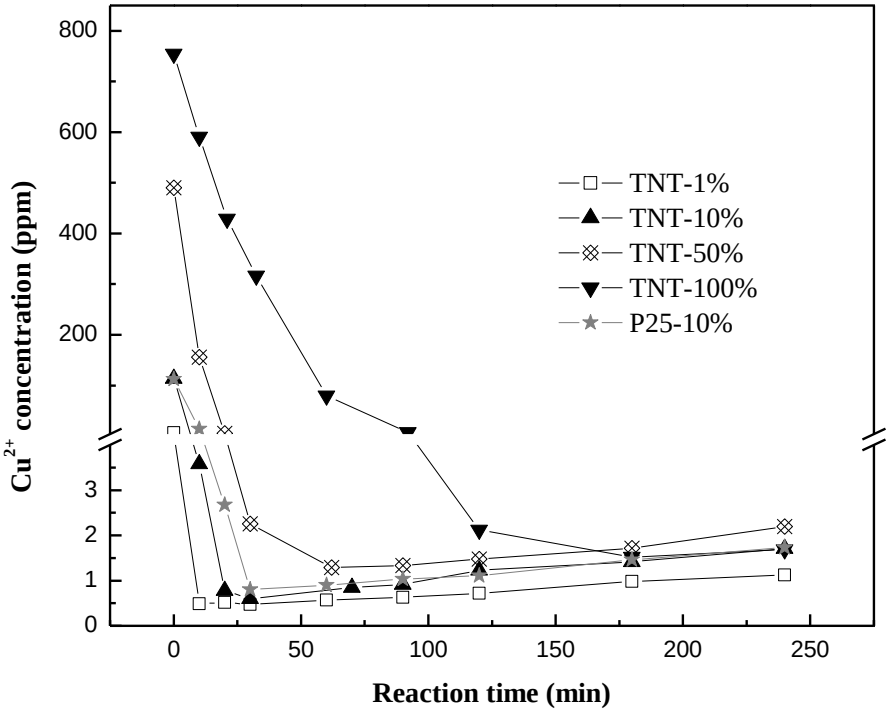

Figure 6.2 Variation of Cu^{2+} concentration during photocatalytic reaction.

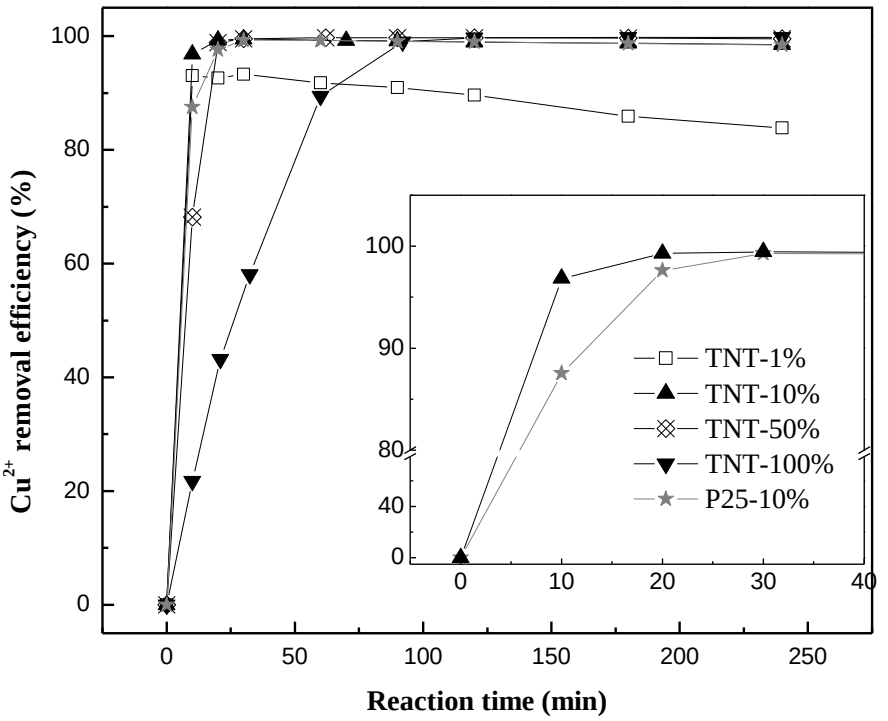

Figure 6.3 Changes of Cu^{2+} removal efficiency across 4 h reaction.

It reveals that photocatalytic Cu^{2+} reduction commenced immediately under irradiation, and TNT exhibited excellent removal efficiency of Cu^{2+}. For TNT-1% and TNT-10%, more than 90% of Cu^{2+} was eliminated in the first 10 min. Higher Cu^{2+} concentrations, for example, 400 and 800 ppm over TNT-50% and TNT-100%, required longer reaction time, but removal efficiency of 90% was respectively achieved after 20 and 60 min.

It is noteworthy that Cu^{2+} could not be completely eliminated via a photocatalytic reaction; a small amount of remaining Cu^{2+} (0.5-2.2 ppm) was detected in solution even after the 4 h reaction. In addition, Cu^{2+} concentration in solution increased slightly after majority of Cu^{2+} was reduced and separated from the liquid phase. This can be explained by the redox deposition-dissolution cycle of Cu (Barakat et al., 2004; Xu et al., 2010): Cu^{2+} was reduced by electrons under irradiation and deposited on TNT; some reduced Cu species could be re-oxidized back to Cu oxide by photo-generated holes and dissolved back into solution, closing the Cu transformation cycle. The redox transformation of Cu progressed throughout the entire photocatalytic reaction. As the reaction proceeded, Cu deposition was reduced due to decline in Cu^{2+} concentration, but Cu dissolution on the other hand, increased since accumulation of H_2 production by-products, CO_2 and HCOOH, facilitated Cu oxide dissolution. This led to a slight increase in Cu^{2+} concentration after the majority of Cu^{2+} had been reduced. However, concentration of Cu^{2+} in the cycle remained minuscule. Considering its fast elimination rate and broad application concentration range (8-800 ppm tested in this study), photocatalytic removal and recovery of Cu over TNT holds big potential in treatment of wastewater containing Cu^{2+}.

In comparison to P25, TNT clearly exhibited greater Cu^{2+} removal ability. In cases of initial Cu^{2+}/Ti ratio at 10%, 96.8% of Cu^{2+} was eliminated in the first 10 min

over TNT, and 87.5% of Cu^{2+} removal was recorded for P25. High activity of TNT mainly rooted from its large BET surface area and unique 1-D tubular structure, since large surface area provided more active sites for reaction, and 1-D tubular structure facilitated rapid electron transfer, and improved charge separation in TiO_2 (Khan et al., 2009).

6.3.1.2 Photocatalytic H_2 production

Figure 6.4 shows the time courses of H_2 evolution simultaneous with Cu^{2+} reduction, and the H_2 evolution rates are summarized in Figure 6.5. It can be found that noticeable amount of H_2 was generated as soon as Cu^{2+} reduction commenced. Reduced Cu species deposited on TNT and yielded Cu-TNT photocatalyst, which was highly active for H_2 production. Depending on initial Cu^{2+}/Ti ratios, average H_2 evolution rates over 4 h reactions ranged from 15.7-40.2 mmol h^{-1} $g^{-1}_{catalyst}$, which were even superior to some noble metal (Pt/Au) loaded TiO_2 (Sreethawong et al., 2005; Sreethawong et al., 2007). Control experiment performed over pure TNT without Cu^{2+} in solution, exhibited negligible H_2 evolution. The high H_2 productivity of Cu-TNT can be attributed to efficient charge separation in TNT, where excess electrons were accumulated on Cu species, which in turn provided reduction sites for H_2 formation (Bandara et al., 2005).

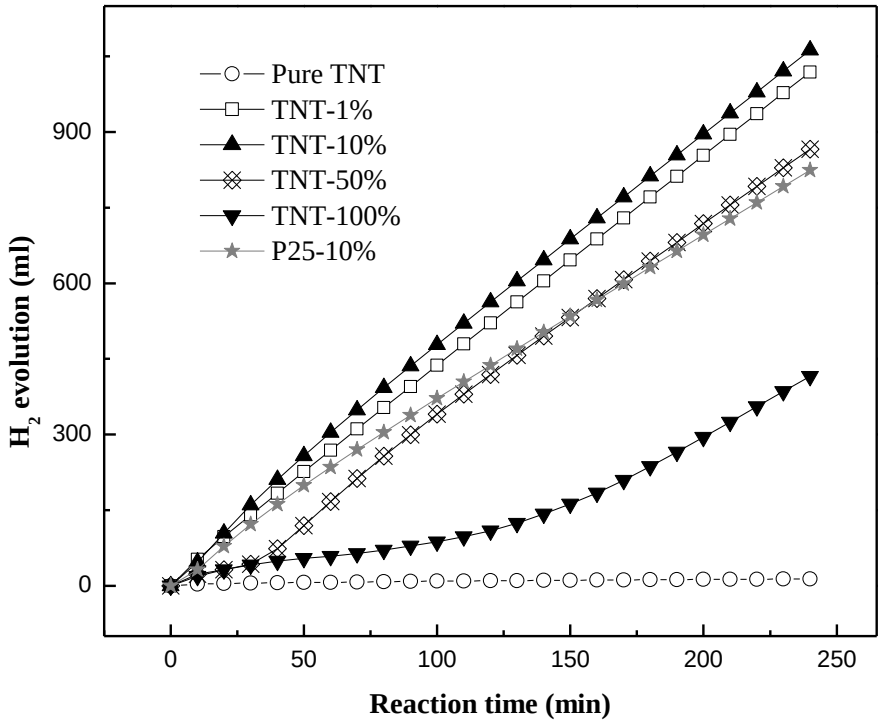

Figure 6.4 Time courses of H_2 evolution simultaneous with Cu^{2+} removal.

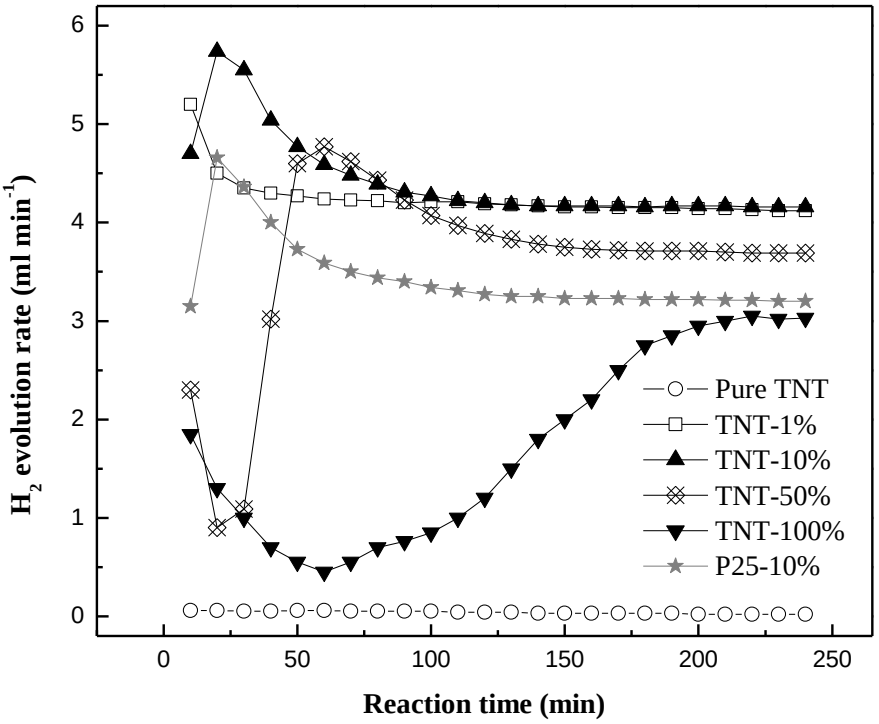

Figure 6.5 Changes of H_2 evolution rate during photocatalytic reaction.

From the time courses of H_2 evolution (Figure 6.4), it is readily observed that initial Cu^{2+}/Ti ratio had an important influence on H_2 generation activity. TNT-10% exhibited the greatest activity, followed by TNT-1%, TNT-50%, and TNT-100%, which was consistent with results presented in Chapter 3. Higher Cu^{2+}/Ti ratio increased Cu content in the fabricated Cu-TNT, which provided more active sites for H_2 formation, but at the same time, deposited Cu species on TNT surface increased UV light blockage to the photocatalyst. Henceforth, based on experimental results, a Cu^{2+}/Ti atom ratio of 10% provided the optimized balance between the effects of active sites and UV light interception, which resulted in the highest activity.

Changes in H_2 evolution rates (Figure 6.5) revealed that H_2 generation was heavily controlled by reduction of Cu^{2+}, and the control mode was dependent on initial Cu^{2+}/Ti ratio. Higher Cu^{2+}/Ti ratios compelled larger changes to H_2 evolution rates due to greater Cu^{2+} reduction.

For TNT-50% and TNT-100% with Cu^{2+}/Ti ratio greater than the optimized 10%, changes to H_2 generation rate can be divided into three distinctive stages: H_2 generation rate initially decreased with time and later ascended to a maximum, before finally declining slightly to a stable state. These changes were closely related to Cu transformation during the photocatalytic reaction. Take TNT-50% as example, 98.9% of the Cu^{2+} was reduced and deposited on TNT in the first 20 min, therefore capturing most of the photo-generated electrons from TNT and gradually blocking UV light access to TNT, which led to its low and decreasing H_2 generation rate during this period. Subsequently, with deceleration of Cu^{2+} reduction, protons began to successfully compete with Cu^{2+} for electrons and reduced to H_2, therefore increasing H_2 generation rate. In addition, the redox deposition-dissolution transformation of Cu over TNT enhanced dispersion of Cu

species within the photocatalyst (Xu et al., 2010), thus promoting H_2 generation further. The third stage started when maximum Cu^{2+} reduction was achieved (60 min for TNT-50%). During this period, Cu dissolution was more dominant over the deposition phenomenon in the redox transformation; hence more Cu on TNT dissolved in the solution, disrupting the optimum Cu condition achieved from the second stage and suppressing H_2 generation activity to a certain extent. Thereafter, H_2 generation rate became steady owing to dynamic functioning of Cu redox transformation. The described three-stage reaction was also manifested in TNT-100%.

In contrast to TNT-50% and TNT-100%, the first stage was not characteristic in the case of TNT-10% (optimal Cu^{2+}/Ti ratio). H_2 generation rate initially increased with Cu^{2+} reduction, since the increase in H_2 formation active sites was predominant over UV light scattering effect under this condition. However, when Cu dissolution exceeded deposition (20 min for TNT-10%), H_2 generation rate began to decline before stabilizing at a relatively high value. This was similar to the third stage of TNT-50% and TNT-100%.

In the case of TNT-1%, since initial Cu^{2+} concentration was considerably low, maximum Cu^{2+} reduction was achieved in less than 10 min under irradiation; therefore, H_2 evolution rate declined with time and stabilized later, exhibiting only the last stage in higher Cu^{2+}/Ti ratio cases.

Control experiments were conducted by applying Cu-TNT (TNT-10%) to fresh reaction solution with (or without) presence of Cu^{2+} to delineate the effect of Cu^{2+} reduction on H_2 generation. The results are summarized in Figure 6.6.

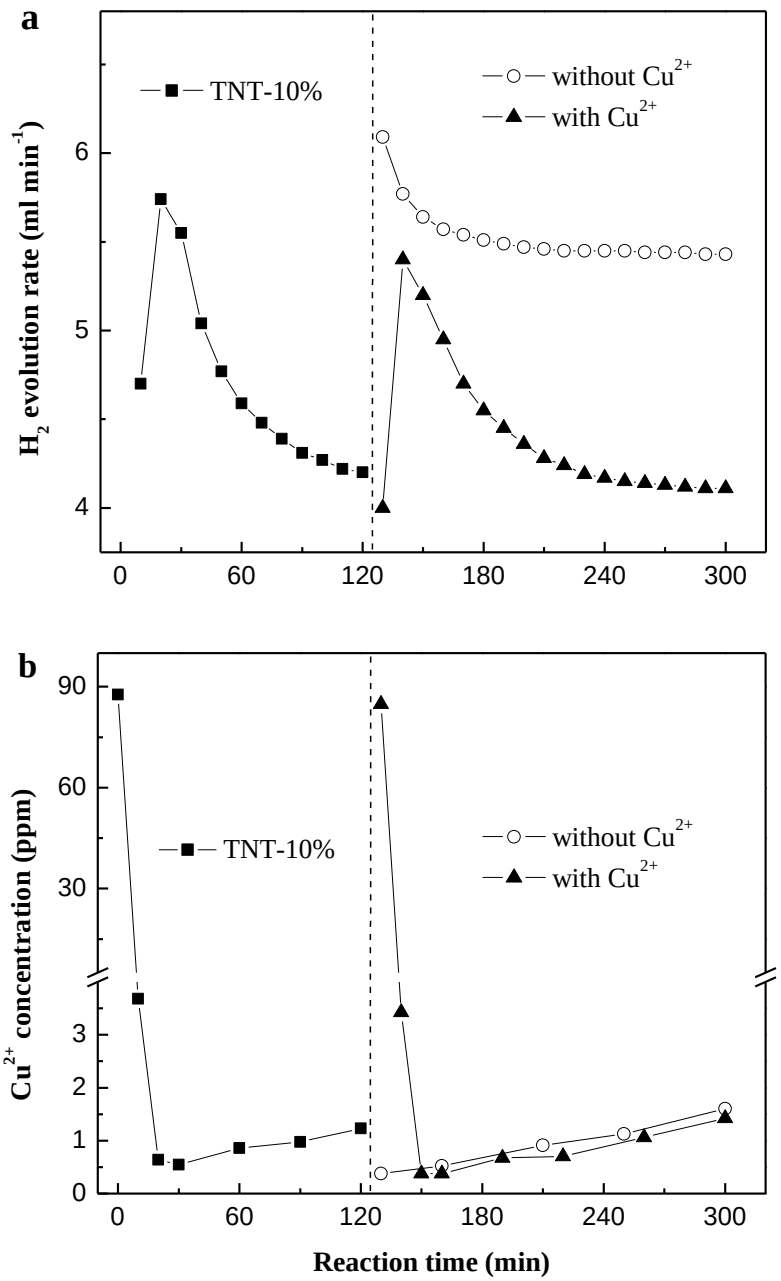

Figure 6.6 Changes of (a) H_2 evolution rate and (b) Cu^{2+} concentration when Cu-TNT (TNT-10%) is applied to fresh reaction solution with (or without) presence of Cu^{2+} (Cu^{2+}/Ti=10 atom%).

With addition of Cu^{2+}, H_2 evolution rate declined immediately since Cu^{2+} reduction took precedence due to its more positive redox potential ($E^{Ø}_{Cu^{2+}/Cu}$=0.34

V), and thus imposing a competition effect on proton reduction; the impact was more pronounced when more Cu^{2+} was added (data not shown). This supported the initial low H_2 generation rate in the three-stage reaction. As the reaction progressed, protons could successfully compete with Cu^{2+} for electrons when majority of the Cu^{2+} was reduced, hence H_2 evolution rate was noted to recover quickly. This observation mirrored the ascendant period in TNT-50% and TNT-100%.

On the other hand, the absence of Cu^{2+} in the fresh reaction solution would evoke a slight decline of H_2 evolution rate, as observed in the last phase of the three-stage reaction. This related with re-oxidation and dissolution of deposited Cu species (illustrated in Figure 6.6b), and has been investigated in Chapter 4 in detail.

In comparison with Cu-P25, in-situ synthesis of Cu-TNT was much faster, and Cu-TNT exhibited greater H_2 generation activity. Average H_2 generation rate over Cu-TNT in the 4 h reaction was 28.9% higher than that of Cu-P25 (40.2 vs. 31.2 mmol h^{-1} $g^{-1}_{catalyst}$), under same Cu^{2+}/Ti=10 atom% conditions. Superiority of TNT was credited to its large BET surface area and unique 1-D tubular structure, which was discussed earlier in photocatalytic Cu^{2+} removal.

In addition, it was observed that without agitation, more than 90% of Cu-TNT would settle down at the bottom of the reactor within 5 min, resulting in a supernatant of high clarity. The high settling ability of Cu-TNT facilitates its recovery from the liquid phase.

6.3.2 Effect of co-existing ions on photocatalytic reactions

Photocatalytic reactions were carried out with various inorganic ions in solution (anions: NO_3^-, Cl^- or SO_4^{2-}; cations: Na^+, Ca^{2+}, or Al^{3+}) to investigate the effect of

co-existing ions on photocatalytic reactions. Herein, initial Cu^{2+}/Ti ratio was controlled at 10%. The results of Cu^{2+} removal and H_2 generation are shown in Figures 6.7 and 6.8, respectively.

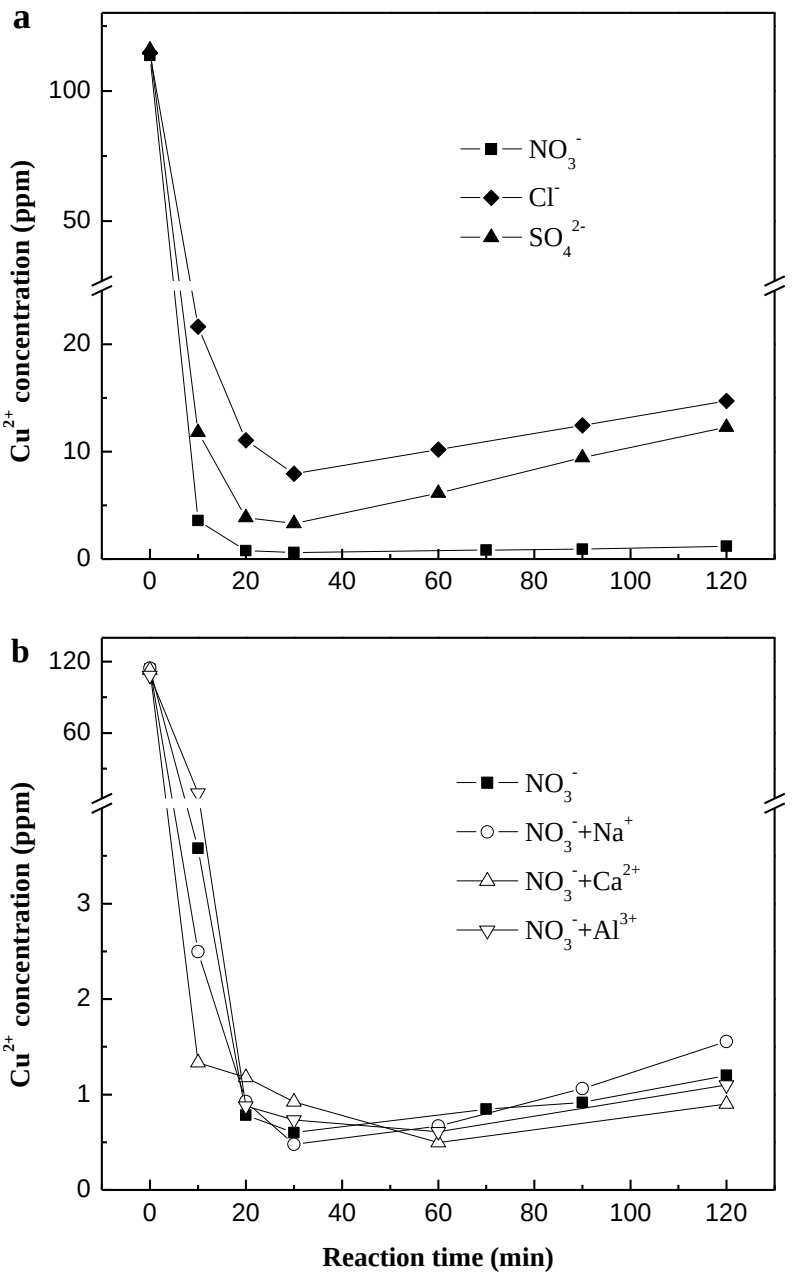

Figure 6.7 Variation of Cu^{2+} concentration during photocatalytic reaction with presence of co-existing (a) anions and (b) cations.

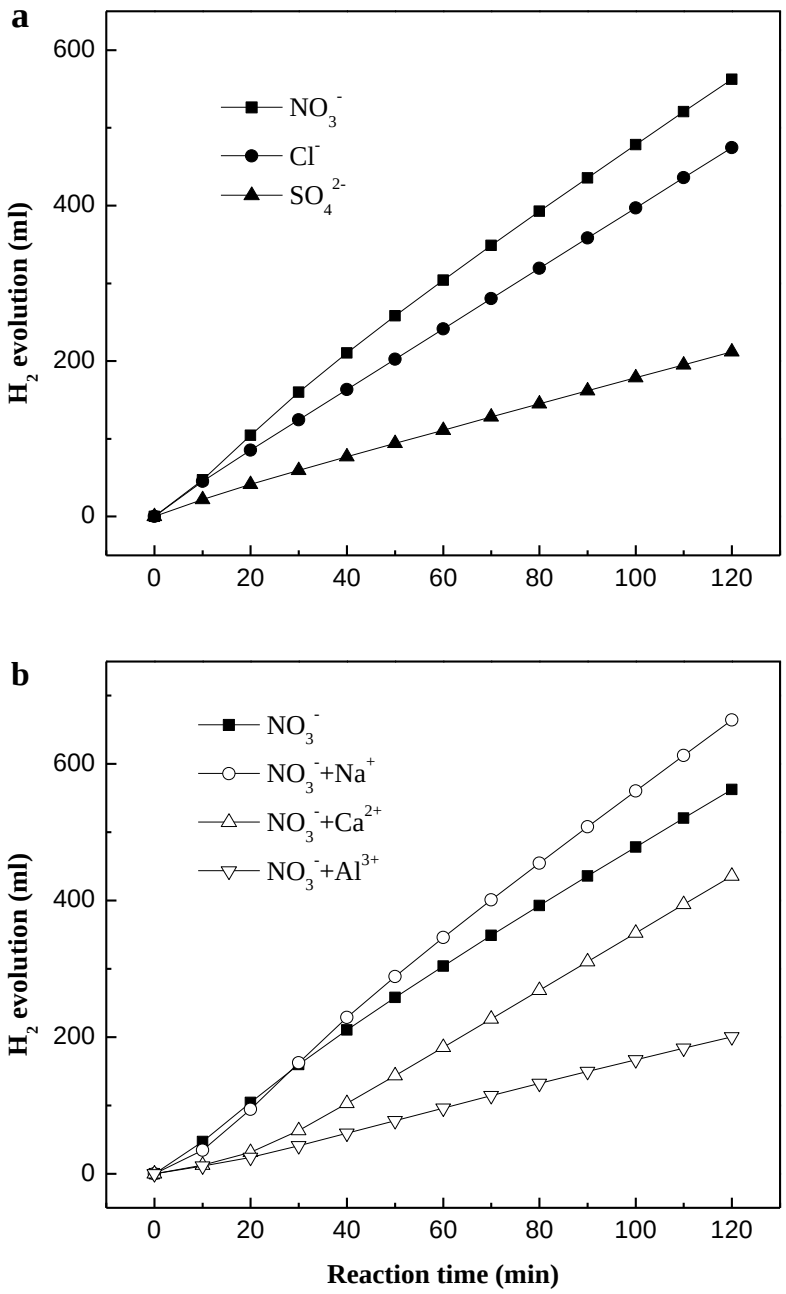

Figure 6.8 Time courses of H_2 evolution during photocatalytic reaction with presence of co-existing (a) anions and (b) cations.

From Figure 6.7, it can be found that, Cu^{2+} removal with presence of various ions still progressed very fast; removal efficiency in all cases exceeded 80% in the first 10 min. As counter anion, NO_3^- was more beneficial for Cu^{2+} reduction, compared

to Cl^- and SO_4^{2-}. Maximum Cu^{2+} removal efficiency with presence of NO_3^-, Cl^- and SO_4^{2-} was 99%, 93% and 97%, respectively. Inferiority of Cl^- and SO_4^{2-} might be mainly due to significant pH drop during photocatalytic reaction. After reaction for 2 h, solution pH with Cl^- and SO_4^{2-} dropped from 5.3, 5.4 to 2.9, 3.2, respectively, which was much lower than NO_3^- case (from 5.4 to 4.8). Lower pH facilitated re-dissolution of reduced Cu, and increased Cu^{2+} concentration in Cu transformation cycle, exhibiting inhibition to Cu^{2+} reduction.

In addition, from Figure 6.9, it can be found that pH_{pzc} of TNT with solution ion strength at 1 mM and 10 mM (represented by $NaNO_3$), was 5.3 and 5.4, respectively.

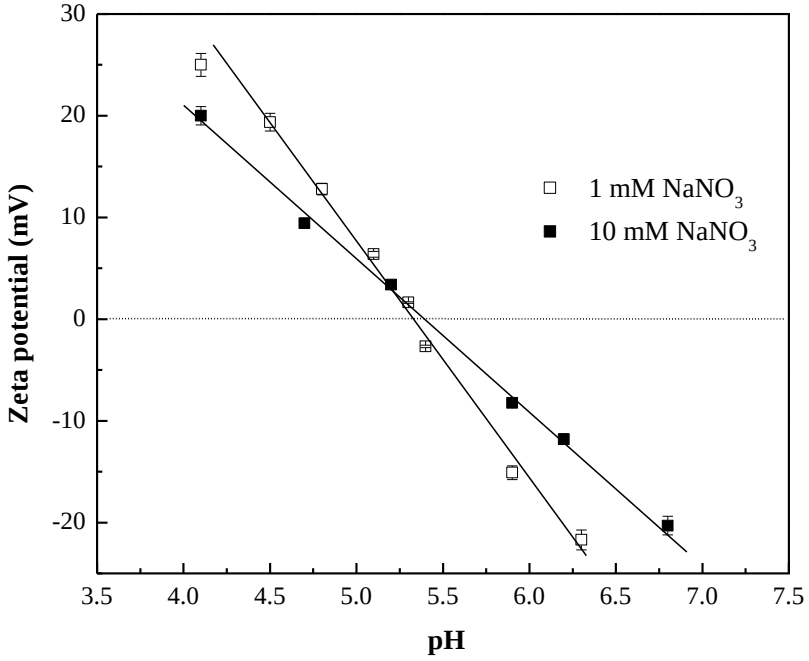

Figure 6.9 Zeta potential of TNT under various pH conditions.

As the photocatalytic reaction proceeded, solution pH decreased and TNT became positively charged, especially when Cl^- and SO_4^{2-} served as counter anions for Cu^{2+}. Cl^- and SO_4^{2-} could be easily adsorbed on TNT surface (stronger than NO_3^-)

(Abdullah et al., 1990; Wang et al., 2004), and block adsorption of methanol (long-pair electron donor) (Sreethawong et al., 2007). This might also limit Cu^{2+} reduction, since methanol adsorption was crucial for scavenging holes in TiO_2.

Different from anions, additional cations (Na^+, Ca^{2+} and Al^{3+}), showed no obvious inhibition to Cu^{2+} removal. This might be due to more negative redox potential of these cations, which could not compete with Cu^{2+} for electrons from TNT ($E^{Ø}_{Na^+/Na}$ = -2.714 V, $E^{Ø}_{Ca^{2+}/Ca}$ = -2.87 V, $E^{Ø}_{Al^{3+}/Al}$ = -1.66 V). In addition, with addition of Na^+, Ca^{2+} or Al^{3+}, pH of reaction solution was 5.4, 5.4 and 4.3 respectively, thus, surface of TNT was neutral or positively charged, and additional cations were not inclined to be adsorbed on TNT surface to restrain holes scavenging, owing to the electrostatic repulsion.

However, H_2 generation (Figure 6.8) was obviously influenced by the co-existing ions. H_2 evolution rate dropped when Cl^- or SO_4^{2-} served as counter anion for Cu^{2+}, instead of NO_3^-. SO_4^{2-} adsorbed stronger on TiO_2 than Cl^- (Wang et al., 2004), and exhibited higher inhibition to H_2 generation. It indicated that disadvantage of Cl^- and SO_4^{2-} might be mainly due to depression of holes scavenging, which has been discussed above.

Presence of Ca^{2+} or Al^{3+} confined H_2 generation to a certain extent. This might result from coverage of Cu-TNT by $CaCO_3$ or $Al(OH)_3$ precipitate. After 2 h reaction, solution pH with presence of Ca^{2+} or Al^{3+} increased to 6.8 and 6.9, respectively. Under these nearly neutral pH conditions, methanol decomposition product, CO_2, was inclined to precipitate Ca^{2+}, and hydrolysis of Al^{3+} was also promoted to produce $Al(OH)_3$. $CaCO_3$ and $Al(OH)_3$ precipitates might aggravate light blockage to TNT, and limit methanol adsorption over TNT surface, leading to depression of H_2 generation activity. It is interesting that presence of Na^+ promoted

H_2 generation. This might be credited to electrostatic repulsion between Na^+ and Cu^{2+} on TNT surface, where solution pH decreased slightly from 5.4 to 5.0 after 2 h reaction. The repulsion facilitated formation of more highly dispersed Cu species over TNT, and produced more active Cu-TNT photocatalyst. For real wastewater, influence from inorganic components was complicated. Further investigation should be carried out to optimize the reaction conditions for efficient H_2 production.

6.3.3 Characterization of photocatalyst after reaction

Characterizations of in-situ synthesized Cu-TNT with different initial Cu^{2+}/Ti ratio were carried out after photocatalytic reaction, to investigate Cu distribution and its chemical states.

From the EDS results (Figure 6.10), Cu/Ti atom ratios in the final photocatalysts were similar but slightly higher than initial Cu^{2+}/Ti ratios in solution before irradiation. It indicated that the leached Cu^{2+} from solution was transferred to the solid phase and combined with TNT; Cu species were prone to accumulate on surface of TNT rather than interstitially dissolved into the crystal lattice. Deposition of Cu on TNT surface, especially at higher Cu content, would cause interception of UV light access to TNT, which supported the hypothesis of initial decrease of H_2 generation rate in the three-stage reaction. In addition, elemental mapping images (data not shown) revealed that, all elements were well distributed throughout the bulk of the final photocatalysts.

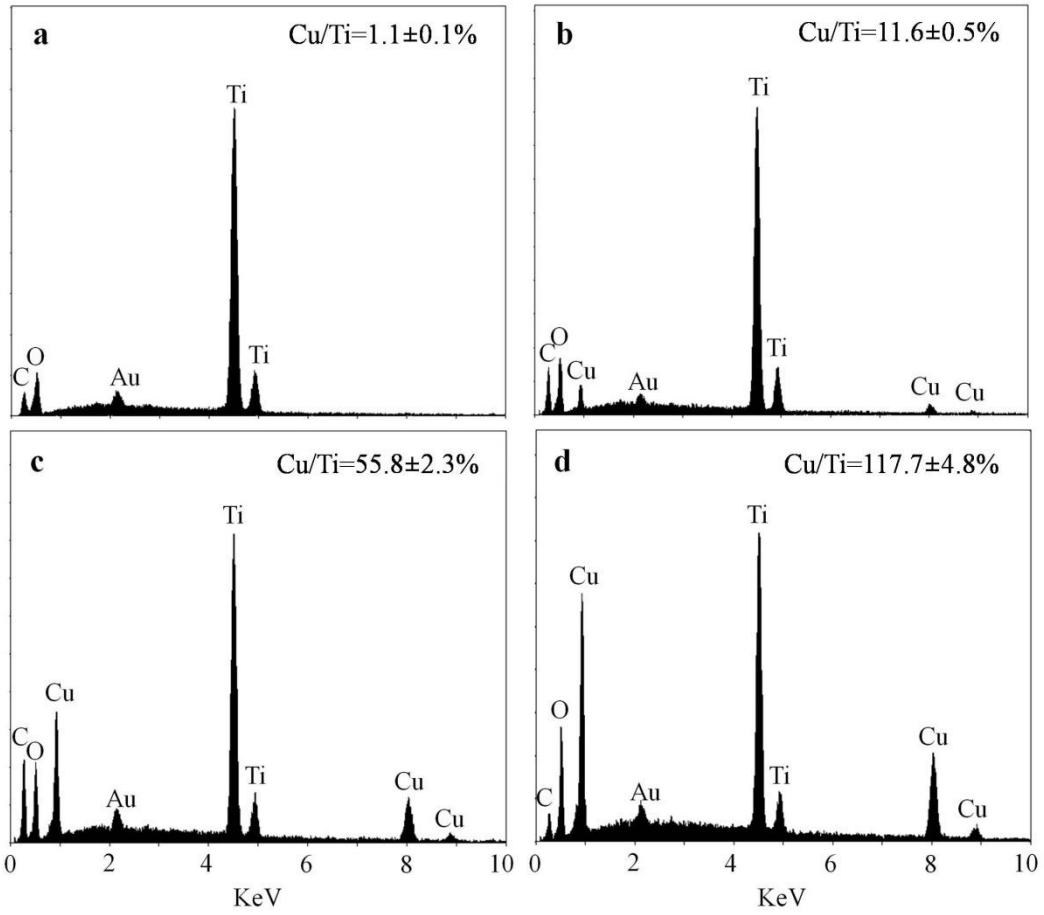

Figure 6.10 EDS spectra of Cu-TNT (a: TNT-1%; b: TNT-10%; c: TNT-50%; d: TNT-100%).

Chemical state of Cu in solid phase after photocatalytic reduction has been intensively investigated, but controversial results were reported. Complete reduction of Cu^{2+} to metallic Cu was observed in some studies (Reiche et al., 1979; Canterino et al., 2008); while some researchers concluded that the reduced Cu species was a mixture of metallic Cu and Cu_2O (Jacobs et al., 1989; Bideau et al., 1990). Foster et al. (Khan et al., 2009) reported that Cu^{2+} could only be reduced to Cu^{+}, and complete reduction to metallic Cu was not observed. To verify the chemical state of Cu, XRD and XPS analyses of Cu-TNT were carried out in this study.

XRD spectra from Figure 6.11 present the changes in chemical state of Cu over TNT after photocatalytic reduction. XRD patterns corresponding to Cu species varied according to initial Cu^{2+}/Ti ratios. For TNT-1% and TNT-10%, no obvious Cu phases were detected. Since EDS results confirmed the existence of Cu, it is believed that the dimensions of Cu species in both samples were below XRD detection limit, evidencing high Cu dispersion in the samples (Xu et al., 1998). In contrast, diffraction peaks of CuO (JCPDS 48-1548) and metallic Cu (JCPDS 4-836) were respectively identified in TNT-50% and TNT-100%.

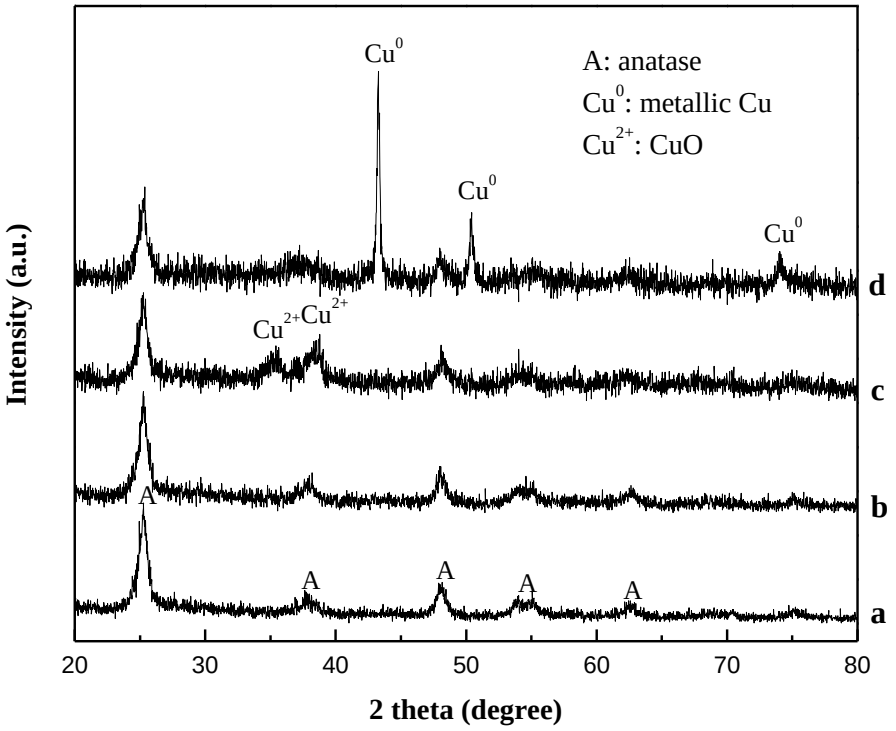

Figure 6.11 XRD patterns of Cu-TNT (a: TNT-1%; b: TNT-10%; c: TNT-50%; d: TNT-100%).

Different chemical states of Cu were also observed in XPS analysis (Figure 6.12). In the spectra of TNT-1%, TNT-10% and TNT-50%, Cu 2p were centered at c.a. 933.5 eV and 953.4 eV along with obvious shake-up satellite peaks, indicating

existence of CuO (Chusuei et al., 1999). While for TNT-100%, reduced Cu species with Cu 2p located at c.a. 932.2 eV and 952.1 eV was predominant, along with minor CuO peaks. Based on the obtained XRD pattern, the reduced Cu species in TNT-100% was confirmed to be metallic Cu.

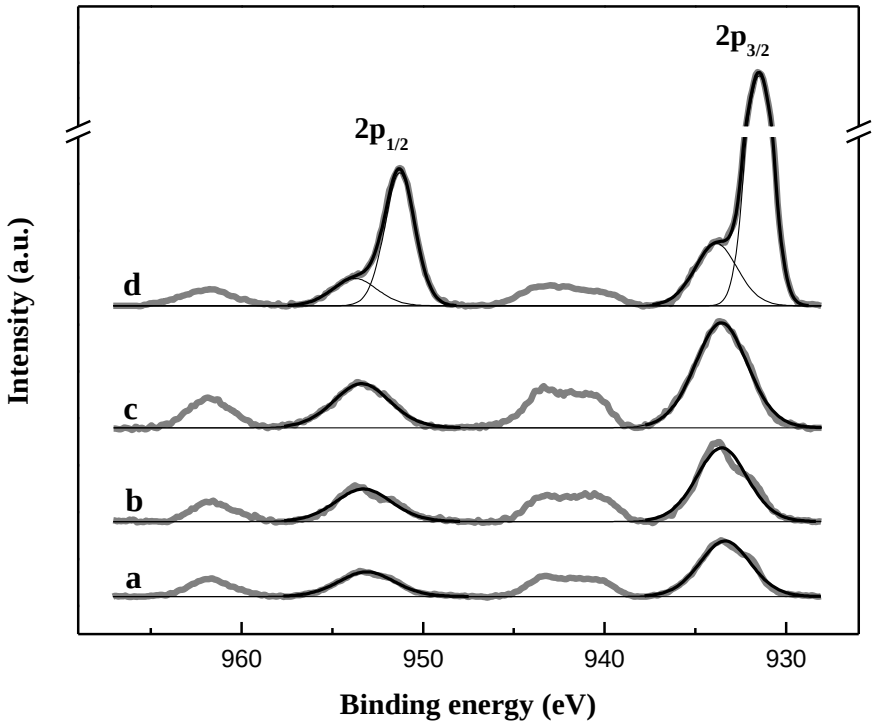

Figure 6.12 High resolution XPS spectra of Cu 2p in Cu-TNT (a: TNT-1%; b: TNT-10%; c: TNT-50%; d: TNT-100%).

Since photocatalytic reduction was carried out under same conditions, chemical state of Cu should be identical regardless of initial Cu^{2+} concentration. This hypothesis was in good agreement with the similar reddish colour appearance of the final photocatalysts. However, certain Cu species in the photocatalysts might be re-oxidized during sample preparation for XRD and XPS analyses, thus producing dissimilar results. In summary, we postulate that CuO in Cu-TNT was induced by air oxidation due to high dispersion of Cu species and great activity of

Cu-TNT, and the chemical state of Cu in mature Cu-TNT was metallic Cu, as deduced from XRD and XPS results of TNT-100%.

EDS, XRD and XPS results revealed that Cu^{2+} in solution was reduced to metallic Cu and highly dispersed on the surface of TNT after the photocatalytic reaction.

All the experiments presented in this chapter were carried out for 2-4 times, and good repeatability of the results, within ±5% variation, was observed.

6.4 Conclusion

Simultaneous Cu^{2+} removal and H_2 production were proved to be feasible over 1-D TNT photocatalyst.

Under irradiation, Cu^{2+} across a wide concentration range could be rapidly reduced to metallic Cu by photo-generated electrons, and deposited on TNT surface, serving as an excellent promoter for H_2 formation. However, minuscule Cu^{2+} still remained in solution after prolonged reaction, especially when Cl^- or SO_4^{2-} served as counter anion for Cu^{2+}. This is caused by redox deposition-dissolution transformation of Cu during photocatalytic reactions. In addition, co-existing cations in solution showed slight influence on Cu^{2+} removal.

For H_2 generation, the initial Cu^{2+}/Ti ratio in solution was a main factor influencing H_2 generation activity of the in-situ fabricated Cu-TNT, and an optimized ratio of 10 atom% was observed in this study. H_2 evolution during photocatalytic reaction was largely governed by Cu^{2+} reduction process, as protons competed with Cu^{2+} for electrons, and the reduced Cu species over TNT provided active sites for H_2 formation, albeit intercepting UV light to the photocatalyst. Influence of these factors on H_2 evolution became more complicated under higher

initial Cu^{2+}/Ti ratio conditions. In addition, co-existing inorganic ions in solution depressed H_2 evolution to a certain extent.

As compared to P25, TNT exhibited greater photocatalytic activity, due to its large surface area and 1-D tubular structure. This affirms the big potential of TNT in both metal ions removal and H_2 production.

CHAPTER 7

CONCLUSIONS AND RECOMMENDATIONS

7.1 Conclusions

In this study, Cu-TiO_2 photocatalyst was synthesized and proved to be highly efficient for photocatalytic H_2 production from water. Effects of operation conditions, fabrication methods and different forms of TiO_2 supports on H_2 generation were investigated to further enhance the activity of Cu-TiO_2 photocatalyst.

Firstly, optimal operation conditions of Cu-TiO_2 for H_2 generation were evaluated; herein Cu-TiO_2 was prepared by impregnation method, with P25 as support. It was found that Cu content in the photocatalyst was crucial for photocatalytic activity, and an optimum Cu content of 9.1 mol% (Cu/Ti=10 atom%) existed, which resulted in maximum active sites and limited blockage of light to TiO_2. H_2 generation rate could be enhanced further by increasing the sacrificial reagent concentration according to Freundlich adsorption isotherm, indicating that photocatalytic H_2 production was based on adsorption of sacrificial reagent on photocatalyst. For pH range of 5.8-10, H_2 generation over Cu-TiO_2 was not affected by pH changes; but under strong acidic or basic conditions, the H_2 generation activities were found to be depressed. In addition, optimum dosage of photocatalyst was found to be 1 g L^{-1}.

Based on the optimal operation conditions obtained above, effect of fabrication methods of Cu-TiO_2 on H_2 generation activity was investigated. For TiO_2 nanoparticle based Cu-TiO_2, four methods, namely, in-situ sol-gel (SG), wet

impregnation (WI), chemical reduction of Cu salt (NR), and in-situ photo-deposition (PD) were evaluated. All four methods endowed the products with good dispersion of Cu component and excellent light absorption ability. While different methods also led to various Cu chemical states, as well as different Cu distribution ratios in the surface and bulk phases of photocatalysts. Both factors were proven to influence photocatalytic activities. Cu_2O in NR sample exhibited the greatest enhancement in terms of initial H_2 generation, followed by CuO in SG and WI samples, while metallic Cu in PD was relatively inferior. Cu components distributed on the surface of TiO_2 facilitated charge transfer more efficiently than that dissolved in TiO_2 lattice, thus leading to a higher H_2 generation rate. Nevertheless, Cu component dissolved in TiO_2 lattice restricted the Cu leaching into liquid phase during reaction, hence resulting in better stability of H_2 generation activity. For TiO_2 nanotube (TNT) based Cu-TiO_2 photocatalyst, compared with wet impregnation method, adsorption-calcination process was superior to produce active photocatalyst, since it was prone to produce photocatalyst with more highly dispersed Cu components.

To further improve the activity of Cu-TiO_2, pure anatase TNT with large BET surface area of 279.9 m^2 g^{-1} was employed as TiO_2 support, in comparison with P25. The fabricated Cu-TNT exhibited excellent H_2 generation activity; H_2 evolution rate during 5 h reaction was above 7 ml min^{-1}, which was 70% higher than P25 based Cu-TiO_2, even superior to some Pt/Ni incorporated TNT. Compared to P25 based Cu-TiO_2, Cu-TNT was characterized by the 1-D tubular structure, and possessed large specific surface area and high Cu component dispersion, all of which were proved to be advantageous for high H_2 generation activity.

Good stability is significantly important for photocatalyst as well as high activity.

This study revealed that, during photocatalytic reaction, Cu component in all samples underwent kinetic transformations in terms of both chemical state and distribution on TiO_2 support. This is related with the redox deposition-dissolution transformation cycle of Cu^{2+}/metallic Cu/Cu_xO during photocatalytic reactions. For TiO_2 nanoparticle (P25) based Cu-TiO_2, H_2 generation activity decreased to a certain extent with the reaction progress, mainly due to the more reduction of Cu_xO to metallic Cu, and Cu leaching into the liquid phase. While, for TNT based Cu-TNT sample, H_2 generation rate kept vigorous during 5 h reaction, and no deactivation occurred. This might be attributed to the high activity and large surface area of TNT which accelerated the re-deposition of Cu^{2+} back to TiO_2 support, and the transformation cycle further promoting high distribution of Cu components in TNT. Considering its high activity, Cu-TNT possessed big potential for H_2 production in practical applications.

Fast H_2 generation could also be achieved with simultaneous Cu^{2+} removal from water over highly efficient TNT photocatalyst, which was an excellent attempt to combine Cu^{2+} contaminated wastewater treatment with energy production. Under irradiation, Cu^{2+} across a wide concentration range (8-800 ppm) could be rapidly reduced to metallic Cu by photo-generated electrons, and deposited on TNT surface, serving as an excellent promoter for H_2 formation. The initial Cu^{2+}/Ti ratio in solution was a main factor influencing H_2 generation activity of the in-situ fabricated Cu-TNT, and an optimized ratio of 10 atom% was observed, which was consistent with result of first phase study. In addition, H_2 evolution during photocatalytic reaction was largely governed by Cu^{2+} reduction process, as protons competed with Cu^{2+} for electrons, and the reduced Cu species over TNT provided active sites for H_2 formation, albeit intercepting UV light to the photocatalyst. Influence of these factors on H_2 evolution became more complicated under higher initial Cu^{2+}/Ti ratio conditions.

High activity, cost-effective property, flexible fabrication methods, moderate reaction conditions and versatile applications affirm the potential of Cu-TiO_2, especially Cu-TNT, in photocatalytic H_2 production.

7.2 Recommendations

In this study, Cu components in all Cu-TiO_2 samples underwent kinetic transformations during H_2 production. A redox deposition-dissolution cycle was confirmed based on the changes of Cu chemical states, Cu distribution on TiO_2, and Cu^{2+} concentration in solution during the reaction. For the future study, detailed mechanisms of the transformation and influencing factors should be investigated and controlled with greater precisions, in order to maintain the high activity of Cu-TiO_2. In addition, for TiO_2 nanoparticle (P25) based Cu-TiO_2, besides the effect of Cu transformation, there are still some unidentified factors that depressed H_2 generation activity during intensive reaction, which should be studied in the future as well.

For efficient H_2 production over Cu-TiO_2, sacrificial reagents are required to suppress the electron/hole recombination in TiO_2 by reacting irreversibly with photo-induced holes. It would be environment-friendly and economically advantageous if organic pollutants in water could be used as sacrificial reagents, and polluted wastewater could be utilized directly for H_2 production by serving as source of protons and electron donors concurrently. By this means, cost induced by the consumption of the sacrificial reagent can be saved, and organic pollutants can also be degraded simultaneously into harmless products. This study holds great potential in practical applications. Nevertheless, for such practical applications to come true, many efforts should be put in, since compositions of wastewaters from various sources are complex, and many factors would affect photocatalytic H_2

generation activity.

In this study, simultaneous H_2 production and Cu^{2+} removal was proved to be feasible over TNT, which is interesting to achieve water treatment with H_2 production simultaneously. However, from an engineering point of view, it is difficult and costly to separate the suspended photocatalyst from water. It is proposed to assembly the TiO_2 nanotubes to form a novel nonwoven membrane, hence there is no need to separate the photocatalyst from treated water, and it further enhances the water treatment ability by filtration. In addition, fouling of this membrane could be less than other traditional membranes since pollutants on the membrane surface would be degraded by the photocatalytic reaction. The outcome of this study would achieve efficient H_2 production and water purification simultaneously without the need to separate the photocatalyst from water.

REFERENCES

Abdullah, M., Low, G. K. C. and Matthews, R. W. (1990). "Effects of common inorganic anions on rates of photocatalytic oxidation of organic carbon over illuminated titanium dioxide." Journal of Physical Chemistry 94(17): 6820-6825.

Abe, R. (2010). "Recent progress on photocatalytic and photoelectrochemical water splitting under visible light irradiation." Journal of Photochemistry and Photobiology C-Photochemistry Reviews 11(4): 179-209.

Abe, R., Hara, K., Sayama, K., Domen, K. and Arakawa, H. (2000). "Steady hydrogen evolution from water on Eosin Y-fixed TiO_2 photocatalyst using a silane-coupling reagent under visible light irradiation." Journal of Photochemistry and Photobiology a-Chemistry 137(1): 63-69.

Abe, R., Sayama, K. and Arakawa, H. (2003). "Significant effect of iodide addition on water splitting into H_2 and O_2 over Pt-loaded TiO_2 photocatalyst: suppression of backward reaction." Chemical Physics Letters 371(3-4): 360-364.

Abe, R., Sayama, K. and Arakawa, H. (2004). "Dye-sensitized photocatalysts for efficient hydrogen production from aqueous I^- solution under visible light irradiation." Journal of Photochemistry and Photobiology a-Chemistry 166: 115-122.

Abe, R., Sayama, K., Domen, K. and Arakawa, H. (2001). "A new type of water splitting system composed of two different TiO_2 photocatalysts (anatase, rutile) and a IO_3^-/I^- shuttle redox mediator." Chemical Physics Letters 344(3-4): 339-344.

Abe, R., Sayama, K. and Sugihara, H. (2005). "Development of new photocatalytic water splitting into H_2 and O_2 using two different semiconductor photocatalysts and a shuttle redox mediator IO_3^-/I^-." Journal of Physical Chemistry B 109(33): 16052-16061.

Al-Mazroai, L. S., Bowker, M., Davies, P., Dickinson, A., Greaves, J., James, D. and Millard, L. (2007). "The photocatalytic reforming of methanol." Catalysis Today 122(1-2): 46-50.

Anpo, M. and Takeuchi, M. (2003). "The design and development of highly reactive titanium oxide photocatalysts operating under visible light irradiation." Journal of Catalysis 216(1-2): 505-516.

Arakawa, H. and Sayama, K. (2000). "Solar hydrogen production. Significant effect of Na_2CO_3 addition on water splitting using simple oxide semiconductor photocatalysts." Catalysis Surveys from Japan 4(1): 75-80.

Aritani, H., Akasaka, N., Tanaka, T., Funabiki, T., Yoshida, S., Gotoh, H. and Okamoto, Y. (1996). "Reduction of NO over TiO_2-supported Cu catalysts." Journal of the Chemical Society-Faraday Transactions 92(14): 2625-2630.

Armstrong, G., Armstrong, A. R., Canales, J. and Bruce, P. G. (2005). "Nanotubes with the TiO_2-B structure." Chemical Communications(19): 2454-2456.

Asahi, R., Morikawa, T., Ohwaki, T., Aoki, K. and Taga, Y. (2001). "Visible-light photocatalysis in nitrogen-doped titanium oxides." Science 293(5528): 269-271.

Bae, E. and Choi, W. (2003). "Highly enhanced photoreductive degradation of perchlorinated compounds on dye-sensitized metal/TiO_2 under visible light." Environmental Science & Technology 37(1): 147-152.

Bak, T., Nowotny, J., Rekas, M. and Sorrell, C. C. (2002). "Photo-electrochemical hydrogen generation from water using solar energy. Materials-related aspects." International Journal of Hydrogen Energy 27(10): 991-1022.

Bamwenda, G. R., Tsubota, S., Nakamura, T. and Haruta, M. (1995). "Photoassisted hydrogen production from a water-ethanol solution: a comparison of activities of Au-TiO_2 and Pt-TiO_2." Journal of Photochemistry and Photobiology a-Chemistry 89(2): 177-189.

Bandara, J., Udawatta, C. P. K. and Rajapakse, C. S. K. (2005). "Highly stable CuO incorporated TiO_2 catalyst for photocatalytic hydrogen production from H_2O." Photochemical & Photobiological Sciences 4(11): 857-861.

Bando, K. K., Sayama, K., Kusama, H., Okabe, K. and Arakawa, H. (1997). "In-situ FT-IR study on CO_2 hydrogenation over Cu catalysts supported on SiO_2, Al_2O_3, and TiO_2." Applied Catalysis a-General 165(1-2): 391-409.

Barakat, M. A., Chen, Y. T. and Huang, C. P. (2004). "Removal of toxic cyanide and Cu(II) Ions from water by illuminated TiO_2 catalyst." Applied Catalysis B-Environmental 53(1): 13-20.

Bard, A. J. and Fox, M. A. (1995). "Artificial photosynthesis: solar splitting of water to hydrogen and oxygen." Accounts of Chemical Research 28(3): 141-145.

Bavykin, D. V., Parmon, V. N., Lapkin, A. A. and Walsh, F. C. (2004). "The effect of hydrothermal conditions on the mesoporous structure of TiO_2 nanotubes." Journal of Materials Chemistry 14(22): 3370-3377.

Bavykin, D. V. and Walsh, F. C. (2009). "Elongated titanate nanostructures and their applications." European Journal of Inorganic Chemistry(8): 977-997.

Bideau, M., Claudel, B., Faure, L. and Rachimoellah, M. (1990). "Photooxidation of formic-acid by oxygen in the presence of titanium-dioxide and dissolved copper ions-oxygen-transfer and reaction-kinetics." Chemical Engineering Communications 93: 167-179.

Blake, D. M., Maness, P. C., Huang, Z., Wolfrum, E. J., Huang, J. and Jacoby, W. A. (1999). "Application of the photocatalytic chemistry of titanium dioxide to disinfection and the killing of cancer cells." Separation and Purification Methods 28(1): 1-50.

Boccuzzi, F., Chiorino, A., Manzoli, M., Andreeva, D., Tabakova, T., Ilieva, L. and Iadakiev, V. (2001). "Gold, silver and copper catalysts supported on TiO_2 for pure hydrogen production." Catalysis Today 75: 169-175.

Boccuzzi, F., Chiorino, A., Martra, G., Gargano, M., Ravasio, N. and Carrozzini, B. (1997). "Preparation, characterization, and activity of Cu/TiO_2 catalysts 1. Influence of the preparation method on the dispersion of copper in Cu/TiO_2." Journal of Catalysis 165(2): 129-139.

Boccuzzi, F., Guglielminotti, E., Martra, G. and Cerrato, G. (1994). "Nitric oxide reduction by CO on Cu/TiO_2 catalysts." Journal of Catalysis 146(2): 449-459.

Bokhimi, X., Morales, A., Novaro, O., Lopez, T., Chimal, O., Asomoza, M. and Gomez, R. (1997). "Effect of copper precursor on the stabilization of titania phases, and the optical properties of Cu/TiO_2 prepared with the sol-gel technique." Chemistry of Materials 9(11): 2616-2620.

Borgarello, E., Kiwi, J., Gratzel, M., Pelizzetti, E. and Visca, M. (1982). "Visible light induced water cleavage in colloidal solutions of chromium-doped titanium dioxide particles." Journal of the American Chemical Society 104(11): 2996-3002.

Bowker, M., James, D., Stone, P., Bennett, R., Perkins, N., Millard, L., Greaves, J. and Dickinson, A. (2003). "Catalysis at the metal-support interface: exemplified by the photocatalytic reforming of methanol on Pd/TiO_2." Journal of Catalysis 217(2):

427-433.

Burda, C., Lou, Y. B., Chen, X. B., Samia, A. C. S., Stout, J. and Gole, J. L. (2003). "Enhanced nitrogen doping in TiO_2 nanoparticles." Nano Letters 3(8): 1049-1051.

Canterino, M., Di Somma, I., Marotta, R. and Andreozzi, R. (2008). "Kinetic investigation of Cu(II) ions photoreduction in presence of titanium dioxide and formic acid." Water Research 42(17): 4498-4506.

Carraway, E. R., Hoffman, A. J. and Hoffmann, M. R. (1994). "Photocatalytic oxidation of organic acids on quantum-sized semiconductor colloids." Environmental Science & Technology 28(5): 786-793.

Chen, C. C., Li, X. Z., Ma, W. H., Zhao, J. C., Hidaka, H. and Serpone, N. (2002a). "Effect of transition metal ions on the TiO_2-assisted photodegradation of dyes under visible irradiation: A probe for the interfacial electron transfer process and reaction mechanism." Journal of Physical Chemistry B 106(2): 318-324.

Chen, D. and Ray, A. K. (2001). "Removal of toxic metal ions from wastewater by semiconductor photocatalysis." Chemical Engineering Science 56: 1561-1570.

Chen, J., Ollis, D. F., Rulkens, W. H. and Bruning, H. (1999). "Photocatalyzed oxidation of alcohols and organochlorides in the presence of native TiO_2 and metallized TiO_2 suspensions. Part (II): photocatalytic mechanisms." Water Research 33(3): 669-676.

Chen, Q., Zhou, W. Z., Du, G. H. and Peng, L. M. (2002b). "Trititanate nanotubes made via a single alkali treatment." Advanced Materials 14(17): 1208-1211.

Chen, X. B., Shen, S. H., Guo, L. J. and Mao, S. S. (2010). "Semiconductor-based photocatalytic hydrogen generation." Chemical Reviews 110(11): 6503-6570.

Chiang, K., Amal, R. and Tran, T. (2002). "Photocatalytic degradation of cyanide using titanium dioxide modified with copper oxide." Advances in Environmental Research 6(4): 471-485.

Chiou, C. H., Wu, C. Y. and Juang, R. S. (2008). "Influence of operating parameters on photocatalytic degradation of phenol in UV/TiO_2 process." Chemical Engineering Journal 139(2): 322-329.

Choi, H. J. and Kang, M. (2007). "Hydrogen production from methanol/water

decomposition in a liquid photosystem using the anatase structure of Cu loaded TiO_2." International Journal of Hydrogen Energy 32(16): 3841-3848.

Choi, W. Y., Termin, A. and Hoffmann, M. R. (1994). "The role of metal-ion dopants in quantum-sized TiO_2 - correlation between photoreactivity and charge-carrier recombination dynamics." Journal of Physical Chemistry 98(51): 13669-13679.

Chusuei, C. C., Brookshier, M. A. and Goodman, D. W. (1999). "Correlation of relative X-ray photoelectron spectroscopy shake-up intensity with CuO particle size." Langmuir 15(8): 2806-2808.

Colon, G., Maicu, M., Hidalgo, M. C. and Navio, J. A. (2006). "Cu-doped TiO_2 systems with improved photocatalytic activity." Applied Catalysis B-Environmental 67(1-2): 41-51.

Dang, M. C., Nguyen, N. V., Nguyen, T. K. V. and Nguyen, T. P. P. (2009). "Characteristics modification of TiO_2 thin films by doping with silica and alumina for self-cleaning application." Journal of Experimental Nanoscience 4(3): 221-232.

Dhanalakshmi, K. B., Latha, S., Anandan, S. and Maruthamuthu, P. (2001). "Dye sensitized hydrogen evolution from water." International Journal of Hydrogen Energy 26(7): 669-674.

Di Paola, A., Marci, G., Palmisano, L., Schiavello, M., Uosaki, K., Ikeda, S. and Ohtani, B. (2002). "Preparation of polycrystalline TiO_2 photocatalysts impregnated with various transition metal ions: Characterization and photocatalytic activity for the degradation of 4-nitrophenol." Journal of Physical Chemistry B 106(3): 637-645.

Draper, R. B. and Fox, M. A. (1990). "Titanium dioxide photosensitized reactions studied by diffuse reflectance flash photolysis in aqueous suspensions of TiO_2 powder." Langmuir 6(8): 1396-1402.

Dvoranova, D., Brezova, V., Mazur, M. and Malati, M. A. (2002). "Investigations of metal-doped titanium dioxide photocatalysts." Applied Catalysis B-Environmental 37(2): 91-105.

El Zayat, M. Y., Saed, A. O. and El-Dessouki, M. S. (1998). "Photoelectrochemical properties of dye sensitized Zr-doped $SrTiO_3$ electrodes." International Journal of Hydrogen Energy 23(4): 259-266.

Fox, M. A. and Dulay, M. T. (1993). "Heterogeneous photocatalysis." Chemical Reviews 93(1): 341-357.

Fujihara, B., Ohno, T. and Matsumura, M. (1998). "Splitting of water by electrochemical combination of two photocatalytic reactions on TiO_2 particles." Journal of the Chemical Society-Faraday Transactions 94(24): 3705-3709.

Fujishima, A. and Honda, K. (1972). "Electrochemical photolysis of water at a semiconductor electrode." Nature 238(5358): 37-38.

Galinska, A. and Walendziewski, J. (2005). "Photocatalytic water splitting over Pt-TiO_2 in the presence of sacrificial reagents." Energy & Fuels 19(3): 1143-1147.

Gerischer, H. and Heller, A. (1991). "The role of oxygen in photoxidation of organic molecules on semiconductor particles." Journal of Physical Chemistry 95(13): 5261-5267.

Gerischer, H. and Heller, A. (1992). "Photocatalytic oxidation of organic molecules at TiO_2 particles by sunlight in aerated water." Journal of the Electrochemical Society 139(1): 113-118.

Gombac, V., Sordelli, L., Montini, T., Delgado, J. J., Adamski, A., Adami, G., Cargnello, M., Bernal, S. and Fornasiero, P. (2010). "CuO_x-TiO_2 photocatalysts for H_2 production from ethanol and glycerol solutions." Journal of Physical Chemistry A 114(11): 3916-3925.

Gratzel, M. and Howe, R. F. (1990). "Electron paramagnetic resonance studies of doped TiO_2 colloids." Journal of Physical Chemistry 94(6): 2566-2572.

Gregg, S. J. and Sing, K. S. W. (1982). Adsorption, Surface Area and Porosity. London, Academic Press.

Hameed, A. and Gondal, M. A. (2005). "Production of hydrogen-rich syngas using p-type NiO catalyst: a laser-based photocatalytic approach." Journal of Molecular Catalysis a-Chemical 233(1-2): 35-41.

Hara, M., Kondo, T., Komoda, M., Ikeda, S., Shinohara, K., Tanaka, A., Kondo, J. N. and Domen, K. (1998). "Cu_2O as a photocatalyst for overall water splitting under visible light irradiation." Chemical Communications(3): 357-358.

Hashimoto, K., Kawai, T. and Sakata, T. (1984). "Photocatalytic reactions of

hydrocarbons and fossil fuels with water. Hydrogen production and oxidation." Journal of Physical Chemistry 88(18): 4083-4088.

He, C., Li, X. Z., Xiong, Y., Zhu, X. H. and Liu, S. R. (2005). "The enhanced PC and PEC oxidation of formic acid in aqueous solution using a Cu-TiO_2/ITO film." Chemosphere 58(4): 381-389.

Herrmann, J. M. (1999). "Heterogeneous photocatalysis: fundamentals and applications to the removal of various types of aqueous pollutants." Catalysis Today 53(1): 115-129.

Hirano, K., Suzuki, E., Ishikawa, A., Moroi, T., Shiroishi, H. and Kaneko, M. (2000). "Sensitization of TiO_2 particles by dyes to achieve H_2 evolution by visible light." Journal of Photochemistry and Photobiology a-Chemistry 136(3): 157-161.

Hodes, G., Cahen, D. and Manassen, J. (1976). "Tungsten trioxide as a photoanode for a photoelectrochemical cell (PEC)." Nature 260: 312-313.

Hoffmann, M. R., Martin, S. T., Choi, W. Y. and Bahnemann, D. W. (1995). "Environmental applications of semiconductor photocatalysis." Chemical Reviews 95(1): 69-96.

Jacobs, J. W. M., Kampers, F. W. H., Rikken, J. M. G., Bullelieuwma, C. W. T. and Koningsberger, D. C. (1989). "Copper photodeposition on TiO_2 studied with HREM and EXAFS." Journal of the Electrochemical Society 136(10): 2914-2923.

Jana, A. K. (2000). "Solar cells based on dyes." Journal of Photochemistry and Photobiology a-Chemistry 132(1-2): 1-17.

Jang, J. S., Choi, S. H., Kim, D. H., Jang, J. W., Lee, K. S. and Lee, J. S. (2009). "Enhanced photocatalytic hydrogen production from water-methanol solution by nickel intercalated into titanate nanotube." Journal of Physical Chemistry C 113(20): 8990-8996.

Jang, J. S., Ji, S. M., Bae, S. W., Son, H. C. and Lee, J. S. (2007). "Optimization of CdS/TiO_2 nano-bulk composite photocatalysts for hydrogen production from Na_2S/Na_2SO_3 aqueous electrolyte solution under visible light ($\lambda \geqslant 420$ nm)." Journal of Photochemistry and Photobiology a-Chemistry 188(1): 112-119.

Jang, J. S., Li, W., Oh, S. H. and Lee, J. S. (2006). "Fabrication of CdS/TiO_2 nano-bulk composite photocatalysts for hydrogen production from aqueous H_2S

solution under visible light." Chemical Physics Letters 425(4-6): 278-282.

Jeon, M. K., Park, J. W. and Kang, M. (2007). "Hydrogen production from methanol/water decomposition in a liquid photosystem using the anatase and rutile forms of Cu-TiO_2." Journal of Industrial and Engineering Chemistry 13(1): 84-91.

Jin, Z. L., Zhang, X. J., Li, Y. X., Li, S. B. and Lu, G. X. (2007). "5.1% Apparent quantum efficiency for stable hydrogen generation over eosin-sensitized CuO/TiO_2 photocatalyst under visible light irradiation." Catalysis Communications 8(8): 1267-1273.

Kasuga, T., Hiramatsu, M., Hoson, A., Sekino, T. and Niihara, K. (1998). "Formation of titanium oxide nanotube." Langmuir 14(12): 3160-3163.

Khan, M. A., Akhtar, M. S., Woo, S. I. and Yang, O. B. (2008). "Enhanced photoresponse under visible light in Pt ionized TiO_2 nanotube for the photocatalytic splitting of water." Catalysis Communications 10(1): 1-5.

Khan, M. A. and Yang, O. B. (2009). "Photocatalytic water splitting for hydrogen production under visible light on Ir and Co ionized titania nanotube." Catalysis Today 146(1-2): 177-182.

Khan, S. U. M., Al-Shahry, M. and Ingler, W. B. (2002). "Efficient photochemical water splitting by a chemically modified n-TiO_2." Science 297(5590): 2243-2245.

Kida, T., Guan, G. Q., Yamada, N., Ma, T. L., Kimura, K. and Yoshida, A. (2004). "Hydrogen production from sewage sludge solubilized in hot-compressed water using photocatalyst under light irradiation." International Journal of Hydrogen Energy 29(3): 269-274.

Kikuchi, Y., Sunada, K., Iyoda, T., Hashimoto, K. and Fujishima, A. (1997). "Photocatalytic bactericidal effect of TiO_2 thin films: dynamic view of the active oxygen species responsible for the effect." Journal of Photochemistry and Photobiology a-Chemistry 106: 51-56.

Kim, H. J., Lu, L. H., Kim, J. H., Lee, C. H., Hyeon, T., Choi, W. Y. and Lee, H. I. (2001). "UV light induced photocatalytic degradation of cyanides in aqueous solution over modified TiO_2." Bulletin of the Korean Chemical Society 22(12): 1371-1374.

Kim, K. H. and Ihm, S. K. (2007). "Characteristics of titania supported copper

oxide catalysts for wet air oxidation of phenol." journal of Hazardous Materials 146: 610-616.

Kim, S. and Choi, W. (2002). "Dual photocatalytic pathways of trichloroacetate degradation on TiO_2: effects of nanosized platinum deposits on kinetics and mechanism." Journal of Physical Chemistry B 106(51): 13311-13317.

Kondarides, D. I., Daskalaki, V. M., Patsoura, A. and Verykios, X. E. (2008). "Hydrogen production by photo-induced reforming of biomass components and derivatives at ambient conditions." Catalysis Letters 122(1-2): 26-32.

Kormann, C., Bahnemann, D. W. and Hoffmann, M. R. (1991). "Photolysis of chloroform and other organic molecules in aqueous TiO_2 suspensions." Environmental Science & Technology 25(3): 494-500.

Korzhak, A. V., Ermokhina, N. I., Stroyuk, A. L., Bukhtiyarov, V. K., Raevskaya, A. E., Litvin, V. I., Kuchmiy, S. Y., Ilyin, V. G. and Manorik, P. A. (2008). "Photocatalytic hydrogen evolution over mesoporous TiO_2/metal nanocomposites." Journal of Photochemistry and Photobiology a-Chemistry 198(2-3): 126-134.

Kudo, A. and Miseki, Y. (2009). "Heterogeneous photocatalyst materials for water splitting." Chemical Society Reviews 38(1): 253-278.

Lachheb, H., Puzenat, E., Houas, A., Ksibi, M., Elaloui, E., Guillard, C. and Herrmann, J. M. (2002). "Photocatalytic degradation of various types of dyes (Alizarin S, Crocein Orange G, Methyl Red, Congo Red, Methylene Blue) in water by UV-irradiated titania." Applied Catalysis B-Environmental 39(1): 75-90.

Lalitha, K., Sadanandam, G., Kumari, V. D., Subrahmanyam, M., Sreedhar, B. and Hebalkar, N. Y. (2010). "Highly stabilized and finely dispersed Cu_2O/TiO_2: A promising visible sensitive photocatalyst for continuous production of hydrogen from glycerol:water mixtures." Journal of Physical Chemistry C 114(50): 22181-22189.

Larsson, P. O. and Andersson, A. (1998). "Complete oxidation of CO, ethanol, and ethyl acetate over copper oxide supported on titania and ceria modified titania." Journal of Catalysis 179(1): 72-89.

Lee, S. G., Lee, S. and Lee, H. I. (2001). "Photocatalytic production of hydrogen from aqueous solution containing CN^- as a hole scavenger." Applied Catalysis a-General 207(1-2): 173-181.

Lehn, J. M., Sauvage, J. P. and Ziessel, R. (1980). "Photochemical water splitting continuous generation of hydrogen and oxygen by irradiation of aqueous suspensions of metal loaded strontium-titanate." Nouveau Journal De Chimie-New Journal of Chemistry 4(11): 623-627.

Leung, D. Y. C., Fu, X. L., Wang, C. F., Ni, M., Leung, M. K. H., Wang, X. X. and Fu, X. Z. (2010). "Hydrogen production over titania-based photocatalysts." Chemsuschem 3(6): 681-694.

Li, C. L., Yuan, J. A., Han, B. Y., Jiang, L. and Shangguan, W. F. (2010). "TiO_2 nanotubes incorporated with CdS for photocatalytic hydrogen production from splitting water under visible light irradiation." International Journal of Hydrogen Energy 35(13): 7073-7079.

Li, Q. Y., Jin, Z. L., Peng, Z. G., Li, Y. X., Li, S. B. and Lu, G. X. (2007). "High-efficient photocatalytic hydrogen evolution on Eosin Y-sensitized Ti-MCM41 zeolite under visible-light irradiation." Journal of Physical Chemistry C 111(23): 8237-8241.

Li, Y. X., Lu, G. X. and Li, S. B. (2001). "Photocatalytic hydrogen generation and decomposition of oxalic acid over platinized TiO_2." Applied Catalysis a-General 214(2): 179-185.

Li, Y. X., Lu, G. X. and Li, S. B. (2003). "Photocatalytic production of hydrogen in single component and mixture systems of electron donors and monitoring adsorption of donors by in situ infrared spectroscopy." Chemosphere 52(5): 843-850.

Li, Y. X., Xie, Y. Z., Peng, S. Q., Lu, G. X. and Li, S. B. (2006). "Photocatalytic hydrogen generation in the presence of chloroacetic acids over Pt/TiO_2." Chemosphere 63(8): 1312-1318.

Lin, C. H., Lee, C. H., Chao, J. H., Kuo, C. Y., Cheng, Y. C., Huang, W. N., Chang, H. W., Huang, Y. M. and Shih, M. K. (2004). "Photocatalytic generation of H_2 gas from neat ethanol over Pt/TiO_2 nanotube catalysts." Catalysis Letters 98(1): 61-66.

Linsebigler, A. L., Lu, G. Q. and Yates, J. T. (1995). "Photocatalysis on TiO_2 surfaces: principles, mechanisms, and selected results." Chemical Reviews 95(3): 735-758.

Liu, Z. Y., Zhang, X. T., Nishimoto, S., Murakami, T. and Fujishima, A. (2008).

"Efficient Photocatalytic Degradation of Gaseous Acetaldehyde by Highly Ordered TiO_2 Nanotube Arrays." Environmental Science & Technology 42(22): 8547-8551.

Manivel, A., Naveenraj, S., Kumar, P. S. S. and Anandan, S. (2010). "CuO-TiO_2 nanocatalyst for photodegradation of acid red 88 in aqueous solution." Science of Advanced Materials 2: 51-57.

Mao, Y., Schoneich, C. and Asmus, K. D. (1991). "Identification of organic acids and other intermediates in oxidative degradation of chlorinated ethanes on TiO_2 surfaces en route to mineralization: a combined photocatalytic and radiation chemical study." Journal of Physical Chemistry 95(24): 10080-10089.

Martin, S. T., Herrmann, H., Choi, W. Y. and Hoffmann, M. R. (1994a). "Time-resolved microwave conductivity Part 1. - TiO_2 photoreactivity and size quantization." Journal of the Chemical Society-Faraday Transactions 90(21): 3315-3322.

Martin, S. T., Herrmann, H. and Hoffmann, M. R. (1994b). "Time-resolved microwave conductivity Part 2. - quantum-sized TiO_2 and the effect of adsorbates and light intensity on charge-carrier dynamics " Journal of the Chemical Society-Faraday Transactions 90(21): 3323-3330.

Melis, A., Zhang, L. P., Forestier, M., Ghirardi, M. L. and Seibert, M. (2000). "Sustained photobiological hydrogen gas production upon reversible inactivation of oxygen evolution in the green alga Chlamydomonas reinhardtii." Plant Physiology 122(1): 127-135.

Menzel, R., Peiro, A. M., Durrant, J. R. and Shaffer, M. S. P. (2006). "Impact of hydrothermal processing conditions on high aspect ratio titanate nanostructures." Chemistry of Materials 18(25): 6059-6068.

Michalow, K. A., Logvinovich, D., Weidenkaff, A., Amberg, M., Fortunato, G., Heel, A., Graule, T. and Rekas, M. (2009). "Synthesis, characterization and electronic structure of nitrogen-doped TiO_2 nanopowder." Catalysis Today 144(1-2): 7-12.

Miyake, J. and Kawamura, S. (1987). "Efficiency of light energy conversion to hydrogen by the photosynthetic bacterium *Rhodobacter sphaeroides*." International Journal of Hydrogen Energy 12(3): 147-149.

Mor, G. K., Carvalho, M. A., Varghese, O. K., Pishko, M. V. and Grimes, C. A.

(2004). "A room-temperature TiO_2-nanotube hydrogen sensor able to self-clean photoactively from environmental contamination." Journal of Materials Research 19(2): 628-634.

Moser, J., Gratzel, M. and Gallay, R. (1987). "Inhibition of electron-hole recombination in substitutionally doped colloidal semiconductor crystallites." Helvetica Chimica Acta 70(6): 1596-1604.

Nada, A. A., Hamed, H. A., Barakat, M. H., Mohamed, N. R. and Veziroglu, T. N. (2008). "Enhancement of photocatalytic hydrogen production rate using photosensitized TiO_2/RuO_2-MV^{2+}." International Journal of Hydrogen Energy 33(13): 3264-3269.

Nagaveni, K., Hegde, M. S. and Madras, G. (2004). "Structure and photocatalytic activity of $Ti_{1-x}M_xO_{2\pm\delta}$ (M = W, V, Ce, Zr, Fe, and Cu) synthesized by solution combustion method." Journal of Physical Chemistry B 108(52): 20204-20212.

Nguyen, T. V. and Wu, J. C. S. (2008). "Photoreduction of CO_2 in an optical-fiber photoreactor: Effects of metals addition and catalyst carrier." Applied Catalysis a-General 335(1): 112-120.

Ni, M., Leung, M. K. H., Leung, D. Y. C. and Sumathy, K. (2007). "A review and recent developments in photocatalytic water-splitting using TiO_2 for hydrogen production." Renewable & Sustainable Energy Reviews 11(3): 401-425.

Nozik, A. J. (1975). "Photoelectrolysis of water using semiconducting TiO_2 crystals." Nature 257: 383-386.

O'Regan, B. and Gratzel, M. (1991). "A low-cost, high-efficiency solar cell based on dye-sensitized colloidal TiO_2 films." Nature 353(24): 737-740.

Patsoura, A., Kondarides, D. I. and Verykios, X. E. (2006). "Enhancement of photoinduced hydrogen production from irradiated Pt/TiO_2 suspensions with simultaneous degradation of azo-dyes." Applied Catalysis B-Environmental 64(3-4): 171-179.

Patsoura, A., Kondarides, D. I. and Verykios, X. E. (2007). "Photocatalytic degradation of organic pollutants with simultaneous production of hydrogen." Catalysis Today 124: 94-102.

Peng, S. Q., Xie, D., Li, Y. X., Lu, G. X. and Li, S. B. (2008). "Preparation of

SiO_2-Pt-CdS composite photocatalyst and its photocatalytic activity for hydrogen evolution under visible light." Reaction Kinetics and Catalysis Letters 95(1): 185-192.

Pichat, P., Mozzanega, M. N., Disdier, J. and Herrmann, J. M. (1982). "Pt content and temperature effects on the photocatalytic H_2 production from aliphatic alcohols over Pt TiO_2." Nouveau Journal De Chimie-New Journal of Chemistry 6(11): 559-564.

Poulston, S., Parlett, P. M., Stone, P. and Bowker, M. (1996). "Surface oxidation and reduction of CuO and Cu_2O studied using XPS and XAES." Surface and Interface Analysis 24(12): 811-820.

Praliaud, H., Mikhailenko, S., Chajar, Z. and Primet, M. (1998). "Surface and bulk properties of Cu-ZSM-5 and Cu/Al_2O_3 solids during redox treatments. Correlation with the selective reduction of nitric oxide by hydrocarbons." Applied Catalysis B-Environmental 16(4): 359-374.

Puangpetch, T., Sreethawong, T., Yoshikawa, S. and Chavadej, S. (2009). "Hydrogen production from photocatalytic water splitting over mesoporous-assembled $SrTiO_3$ nanocrystal-based photocatalysts." Journal of Molecular Catalysis a-Chemical 312(1-2): 97-106.

Randeniya, L. K., Murphy, A. B. and Plumb, I. C. (2008). "A study of S-doped TiO_2 for photoelectrochemical hydrogen generation from water." Journal of Materials Science 43(4): 1389-1399.

Reiche, H., Dunn, W. W. and Bard, A. J. (1979). "Heterogeneous photocatalytic and photosynthetic deposition of copper on TiO_2 and WO_3 powders." Journal of Physical Chemistry 83(17): 2248-2251.

Reutergardh, L. B. and Iangphasuk, M. (1997). "Photocatalytic decolourization of reactive azo dye: A comparison between TiO_2 and CdS photocatalysis." Chemosphere 35(3): 585-596.

Rhoderick, E. H. and Williams, R. H. (1988). Metal-semiconductor contacts. New York, Oxford University Press.

Richard, C. (1993). "Regioselectivity of oxidation by positive holes (h^+) in photocatalytic aqueous transformations." Journal of Photochemistry and Photobiology a-Chemistry 72(2): 179-182.

Rosseler, O., Shankar, M. V., Du, M. K. L., Schmidlin, L., Keller, N. and Keller, V. (2010). "Solar light photocatalytic hydrogen production from water over Pt and Au/TiO_2 (anatase/rutile) photocatalysts: influence of noble metal and porogen promotion." Journal of Catalysis 269(1): 179-190.

Sakata, Y., Yamamoto, T., Okazaki, T., Imamura, H. and Tsuchiya, S. (1998). "Generation of visible light response on the photocatalyst of a copper ion containing TiO_2." Chemistry Letters(12): 1253-1254.

Sakthivel, S., Shankar, M., Palanichamy, M., Arabindoo, B., Bahnemann, D. and Murugesan, V. (2004). "Enhancement of photocatalytic activity by metal deposition: characterisation and photonic efficiency of Pt, Au and Pd deposited on TiO_2 catalyst." Water Research 38(13): 3001-3008.

Sato, S. and White, J. M. (1980). "Photodecomposition of water over Pt/TiO_2 catalysts." Chemical Physics Letters 72(1): 83-86.

Sayama, K., Abe, R., Arakawa, H. and Sugihara, H. (2006). "Decomposition of water into H_2 and O_2 by a two-step photoexcitation reaction over a Pt-TiO_2 photocatalyst in $NaNO_2$ and Na_2CO_3 aqueous solution." Catalysis Communications 7(2): 96-99.

Sayama, K. and Arakawa, H. (1992). "Significant effect of carbonate addition on stoichiometric photodecomposition of liquid water into hydrogen and oxygen from platinum-titanium oxide suspension." Journal of the Chemical Society-Chemical Communications(2): 150-152.

Sayama, K. and Arakawa, H. (1996). "Effect of carbonate addition on the photocatalytic decomposition of liquid water over a ZrO_2 catalyst." Journal of Photochemistry and Photobiology a-Chemistry 94(1): 67-76.

Sayama, K. and Arakawa, H. (1997). "Effect of carbonate salt addition on the photocatalytic decomposition of liquid water over Pt-TiO_2 catalyst." Journal of the Chemical Society-Faraday Transactions 93(8): 1647-1654.

Sayama, K., Mukasa, K., Abe, R., Abe, Y. and Arakawa, H. (2001). "Stoichiometric water splitting into H_2 and O_2 using a mixture of two different photocatalysts and an IO_3^-/I^- shuttle redox mediator under visible light irradiation." Chemical Communications(23): 2416-2417.

Sennik, E., Colak, Z., Kilinc, N. and Ozturk, Z. Z. (2010). "Synthesis of

highly-ordered TiO_2 nanotubes for a hydrogen sensor." International Journal of Hydrogen Energy 35(9): 4420-4427.

Shchukin, D. G., Kulak, A. I. and Sviridov, D. V. (2002). "Magnetic photocatalysts of the core-shell type." Photochemical & Photobiological Sciences 1(10): 742-744.

Shchukin, D. G., Ustinovich, E. A., Kulak, A. I. and Sviridov, D. V. (2004). "Heterogeneous photocatalysis in titania-containing liquid foam." Photochemical & Photobiological Sciences 3(2): 157-159.

Shimura, K. and Yoshida, H. (2011). "Heterogeneous photocatalytic hydrogen production from water and biomass derivatives." Energy & Environmental Science 4(7): 2467-2481.

Singh, S. P., Srivastava, S. C. and Pandey, K. D. (1990). "Photoproduction of hydrogen by a non-sulphur bacterium isolated from root zones of water fern *Azolla pinnata*." International Journal of Hydrogen Energy 15(6): 403-406.

Sjogren, J. C. and Sierka, R. A. (1994). "Inactivation of phage MS2 by iron-aided titanium dioxide photocatalysis." Applied and Environmental Microbiology 60(1): 344-347.

Skorb, E. V., Antonouskaya, L. I., Belyasova, N. A., Shchukin, D. G., Mohwald, H. and Sviridov, D. V. (2008). "Antibacterial activity of thin-film photocatalysts based on metal-modified TiO_2 and TiO_2:In_2O_3 nanocomposite." Applied Catalysis B-Environmental 84(1-2): 94-99.

So, W. W., Kim, K. J. and Moon, S. J. (2004). "Photo-production of hydrogen over the CdS-TiO_2 nano-composite particulate films treated with $TiCl_4$." International Journal of Hydrogen Energy 29(3): 229-234.

Sreethawong, T., Puangpetch, T., Chavadej, S. and Yoshikawa, S. (2007). "Quantifying influence of operational parameters on photocatalytic H_2 evolution over Pt-loaded nanocrystalline mesoporous TiO_2 prepared by single-step sol-gel process with surfactant template." Journal of Power Sources 165(2): 861-869.

Sreethawong, T. and Yoshikawa, S. (2005). "Comparative investigation on photocatalytic hydrogen evolution over Cu-, Pd-, and Au-loaded mesoporous TiO_2 photocatalysts." Catalysis Communications 6(10): 661-668.

Stanley, A., Verity, B. and Matthews, D. (1998). "Minimizing the dark current at

the dye-sensitized TiO_2 electrode." Solar Energy Materials and Solar Cells 52(1-2): 141-154.

Strataki, N., Bekiari, V., Kondarides, D. I. and Lianos, P. (2007). "Hydrogen production by photocatalytic alcohol reforming employing highly efficient nanocrystalline titania films." Applied Catalysis B-Environmental 77(1-2): 184-189.

Stumm, W. (1992). Chemistry of the solid-water interface: processes at the mineral-water and particle-water interface in natural systems. New York, John Wiley & Sons.

Subrahmanyam, M., Supriya, V. T. and Reddy, P. R. (1996). "Photocatalytic H_2 production with CdS-based catalysts from a sulphide/sulphite substrate: An effort to develop MgO-supported catalysts." International Journal of Hydrogen Energy 21(2): 99-106.

Subramanian, V., Wolf, E. E. and Kamat, P. V. (2004). "Catalysis with TiO_2/gold nanocomposites. Effect of metal particle size on the Fermi level equilibration." Journal of the American Chemical Society 126(15): 4943-4950.

Sun, X. M. and Li, Y. D. (2003). "Synthesis and characterization of ion-exchangeable titanate nanotubes." Chemistry-a European Journal 9(10): 2229-2238.

Tambwekar, S. V., Venugopal, D. and Subrahmanyam, M. (1999). "H_2 production of (CdS-ZnS)-TiO_2 supported photocatalytic system." International Journal of Hydrogen Energy 24(10): 957-963.

Thorne, A., Kruth, A., Tunstall, D., Irvine, J. T. S. and Zhou, W. Z. (2005). "Formation, structure, and stability of titanate nanotubes and their proton conductivity." Journal of Physical Chemistry B 109(12): 5439-5444.

Troupis, A., Hiskia, A. and Papaconstantinou, E. (2002). "Photocatalytic reduction and recovery of copper by polyoxometalates." Environmental Science & Technology 36(24): 5355-5362.

Tseng, I. H., Wu, J. C. S. and Chou, H. Y. (2004). "Effects of sol-gel procedures on the photocatalysis of Cu/TiO_2 in CO_2 photoreduction." Journal of Catalysis 221(2): 432-440.

Wang, C. M., Heller, A. and Gerischer, H. (1992). "Palladium catalysis of O_2 reduction by electrons accumulated on TiO_2 particles during photoassited oxidation of organic compounds." Journal of the American Chemical Society 114(13): 5230-5234.

Wang, K., Zhang, J. Y., Lou, L. P., Yang, S. Y. and Chen, Y. X. (2004). "UV or visible light induced photodegradation of AO7 on TiO_2 particles: the influence of inorganic anions." Journal of Photochemistry and Photobiology a-Chemistry 165(1-3): 201-207.

Ward, M. D., White, J. R. and Bard, A. J. (1983). "Electrochemical investigation of the energetics of particulate titanium dioxide photocatalysts. The methyl viologen-acetate system." Journal of the American Chemical Society 105(1): 27-31.

Weaver, P. F., Lien, S. and Seibert, M. (1980). "Photobiological production of hydrogen." Solar Energy 24(1): 3-45.

Wilke, K. and Breuer, H. D. (1999). "The influence of transition metal doping on the physical and photocatalytic properties of titania." Journal of Photochemistry and Photobiology a-Chemistry 121(1): 49-53.

Wiszniowski, J., Robert, D., Surmacz-Gorska, J., Miksch, K., Malato, S. and Weber, J. V. (2004). "Solar photocatalytic degradation of humic acids as a model of organic compounds of landfill leachate in pilot-plant experiments: Influence of inorganic salts." Applied Catalysis B-Environmental 53(2): 127-137.

Wu, N. L. and Lee, M. S. (2004). "Enhanced TiO_2 photocatalysis by Cu in hydrogen production from aqueous methanol solution." International Journal of Hydrogen Energy 29(15): 1601-1605.

Wu, Y. Q., Lu, G. X. and Li, S. B. (2009). "The role of Cu(I) species for photocatalytic hydrogen generation over CuO_x/TiO_2." Catalysis Letters 133(1-2): 97-105.

Wu, Z. F. (2005). The effects of reaction temperature and humidity on the gas-phase photocatalytic degradation of volatile organic compounds. Institute of Environmental Engineering. Kaohsiung, National Sun Yat-sen University. **doctor:** 2-13.

Xing, C. J., Jing, D. W., Liu, M. C. and Guo, L. J. (2009). "Photocatalytic

hydrogen production over $Na_2Ti_2O_4(OH)_2$ nanotube sensitized by CdS nanoparticles." Materials Research Bulletin 44(2): 442-445.

Xu, A. W., Gao, Y. and Liu, H. Q. (2002). "The preparation, characterization, and their photocatalytic activities of rare-earth-doped TiO_2 nanoparticles." Journal of Catalysis 207(2): 151-157.

Xu, B., Dong, L. and Chen, Y. (1998). "Influence of CuO loading on dispersion and reduction behavior of CuO/TiO_2 (anatase) system." Journal of the Chemical Society-Faraday Transactions 94(13): 1905-1909.

Xu, C., Killmeyer, R., Gray, M. L. and Khan, S. U. M. (2006). "Photocatalytic effect of carbon-modified n-TiO_2 nanoparticles under visible light illumination." Applied Catalysis B-Environmental 64(3-4): 312-317.

Xu, C. K., Shaban, Y. A., Ingler, W. B. and Khan, S. U. M. (2007). "Nanotube enhanced photoresponse of carbon modified (CM)-n-TiO_2 for efficient water splitting." Solar Energy Materials and Solar Cells 91(10): 938-943.

Xu, S. P., Ng, J. W., Zhang, X. W., Bai, H. W. and Sun, D. D. (2010). "Fabrication and comparison of highly efficient Cu incorporated TiO_2 photocatalyst for hydrogen generation from water." International Journal of Hydrogen Energy 35(11): 5254-5261.

Xu, S. P. and Sun, D. D. (2009). "Significant improvement of photocatalytic hydrogen generation rate over TiO_2 with deposited CuO." International Journal of Hydrogen Energy 34(15): 6096-6104.

Yamashita, H., Nishiguchi, H., Kamada, N., Anpo, M., Teraoka, Y., Hatano, H., Ehara, S., Kikui, K., Palmisano, L., Sclafani, A., Schiavello, M. and Fox, M. A. (1994). "Photocatalytic reduction of CO_2 with H_2O on TiO_2 and Cu/TiO_2 catalysts." Research on Chemical Intermediates 20(8): 815-823.

Yamazaki, S., Iwai, S., Yano, J. and Taniguchi, H. (2001). "Kinetic studies of reductive deposition of copper(II) ions photoassisted by titanium dioxide." Journal of Physical Chemistry A 105(50): 11285-11290.

Yang, H. H., Guo, L. J., Yan, W. and Liu, H. T. (2006). "A novel composite photocatalyst for water splitting hydrogen production." Journal of Power Sources 159(2): 1305-1309.

Yi, H. B., Peng, T. Y., Ke, D. N., Ke, D., Zan, L. and Yan, C. H. (2008). "Photocatalytic H_2 production from methanol aqueous solution over titania nanoparticles with mesostructures." International Journal of Hydrogen Energy 33(2): 672-678.

Yuan, J., Chen, M. X., Shi, J. W. and Shangguan, W. F. (2006). "Preparations and photocatalytic hydrogen evolution of N-doped TiO_2 from urea and titanium tetrachloride." International Journal of Hydrogen Energy 31(10): 1326-1331.

Yuan, Z. Y. and Su, B. L. (2004). "Titanium oxide nanotubes, nanofibers and nanowires." Colloids and Surfaces a-Physicochemical and Engineering Aspects 241(1-3): 173-183.

Zhang, S. L., Zhou, J. F., Zhang, Z. J., Du, Z. L., Vorontsov, A. V. and Jin, Z. S. (2000). "Morphological structure and physicochemical properties of nanotube TiO_2." Chinese Science Bulletin 45(16): 1533-1536.

Zhang, X., Pan, J. H., Fu, W., Du, A. J. and Sun, D. D. (2009). "TiO_2 nanotube photocatalytic oxidation for water treatment." Water Science and Technology: Water supply 9(1): 45-49.

Zhang, Y. X., Gao, B., Puma, G. L., Ray, A. K. and Zeng, H. C. (2010). "Self-assembled Au/TiO_2/CNTs ternary nanocomposites for photocatalytic applications." Science of Advanced Materials 2: 503-513.

Zhou, J. K., Zhang, Y. X., Zhao, X. S. and Ray, A. K. (2006). "Photodegradation of benzoic acid over metal-doped TiO_2." Industrial & Engineering Chemistry Research 45(10): 3503-3511.

Zhu, J. F. and Zach, M. (2009). "Nanostructured materials for photocatalytic hydrogen production." Current Opinion in Colloid & Interface Science 14(4): 260-269.

Zou, Z. G., Ye, J. H., Sayama, K. and Arakawa, H. (2001). "Direct splitting of water under visible light irradiation with an oxide semiconductor photocatalyst." Nature 414(6864): 625-627.